# Using Pressure Retarded Osmosis Technology to Generate Salinity Gradient Energy (Osmotic Power) as a New Renewable Energy Source: Pretreatment to Reduce PRO Membrane Fouling

Elham Abbasi-Garravand

A Thesis

In

The Department of

Building, Civil, and Environmental Engineering

Presented in Partial Fulfillment of the Requirements for the Degree of

Doctor of Philosophy (Civil Engineering)

at Faculty of Engineering and Computer Science

Concordia University

Montreal, Quebec, Canada

September 2016

**CONCORDIA UNIVERSITY**
**SCHOOL OF GRADUATE STUDIES**

This is to certify that the thesis prepared

By: Elham Abbasi-Garravand

Entitled: Using Pressure Retarded Osmosis Technology to Generate Salinity Gradient Energy (Osmotic Power) as a New Renewable Energy Source: Pretreatment to Reduce PRO Membrane Fouling

and submitted in partial fulfillment of the requirements for the degree of

Doctor of Philosophy (Civil Engineering)

complies with the regulations of the University and meets the accepted standards with respect to originality and quality.

Signed by the final examining committee:

Dr. W. Zhu — Chair

Dr. P. Champagne — External Examiner

Dr. P. Pillay — External to Program

Dr. S. Rahaman — Examiner

Dr. Z. Chen — Examiner

Dr. C. Mulligan — Thesis Supervisor

Approved by

Chair of Department or Graduate Program Director

September 30, 2016

Dean of Faculty

# Abstract


## Using Pressure Retarded Osmosis Technology to Generate Salinity Gradient Energy (Osmotic Power) as a New Renewable Energy Source: Pretreatment to Reduce PRO Membrane Fouling

Elham Abbasi-Garravand, Ph.D.

Concordia University, 2016

As the population increases, the demand for electricity has also increased. Most of the required electricity is produced by burning fossil fuels at power stations all over the world which has dangerous influences on climate. Therefore, it is important to produce new renewable and maintainable energy sources to decrease the use of fossil fuels. Osmotic power is a renewable source of energy that is generated by using salt and fresh waters. Pressure retarded osmosis (PRO) is a membrane based technology that can produce osmotic power. One of the main challenges for generating osmotic power by using PRO technology is the membrane fouling which reduces the permeate flux and consequently increases the cost and decreases the osmotic power generation. In this research, various pretreatment methods such as different types of ultrafiltration systems and a sand filter were used for removing total organic carbon (TOC), turbidity, and hardness from raw water. Moreover, different feed waters with various qualities were used to investigate the effect of fouling on a commercial membrane in PRO mode in continuous conditions. In addition, two physical and chemical cleaning methods were used to investigate and determine the desirable cleaning methods in PRO processes in order to control and reduce the membrane fouling. Most of the tests were performed at LTE Hydro Québec

located at Shawinigan and the rest were performed at Concordia University. Based on the results, highest removal efficiency of turbidity occurred at 3.72 NTU and was 100% and 68.6% for ultrafiltration and the multimedia sand filter, respectively. Maximum TOC removal in ultrafiltration multimedia sand filter was 41% and 1.5% at 6.62 mg/L TOC initial concentration respectively. According to the results, the fouling rate when the draw solution was synthetic salt water followed the order of: untreated river water > multimedia sand filter > microfiltration > ultrafiltration effluents. It was observed that complete blocking, cake filtration and cake enhanced osmotic pressure were the main fouling mechanisms that governed the membrane fouling. The main inorganic foulants using synthetic salt water were iron, aluminum, calcium, sodium, and silica and when sea water was used as the draw solution, iron, aluminum, silica, magnesium, calcium, sodium and potassium were detected as inorganic foulants. The organic foulants were humic substances, polysaccharides and proteins from use of both synthetic salt water and sea water as draw solutions. The successful cleaning method was chemical cleaning using a combination of acidic and basic cleaners. This research indicates that using appropriate pretreatment and membrane cleaning methods can decrease the membrane fouling in PRO processes and consequently can improve the osmotic power generation.

# Acknowledgements

First and foremost, I would like to express my deepest appreciation and thanks to my advisor Professor Catherine Mulligan for encouraging my research and for supporting me to grow as a researcher, for her endless kindness, guidance, continuous support, motivation, and immense knowledge. She has been a tremendous mentor for me. Her advice on both research as well as on my career have been priceless. I am also thankful for the excellent example she has provided as a successful scientist and professor.

My sincere thanks also goes to Dr. François Allaire, and Dr. Claude Laflamme, who provided me an opportunity to join Research Institute of Hydro-Quebec as intern, and who gave me access to the laboratory and research facilities. Without their precious support it would not be possible to conduct this research. It was a great privilege to work with Dr. Claude Laflamme. This opportunity gave me the chance to learn a lot from such a passionate scientist.

I am also very appreciative to Mr. Guillaume Clairet from H2O Innovation, especially for sharing his invaluable expertise, and for his brilliant comments and suggestions to my research.

I would also like to thank my committee members for their guidance through my study and research.

I would especially like to thank Mr. Pascal Champagne, Mr. Guy. Lavallee and Mr. Yancee Bourassa for their valuable help in the Hydro-Quebec lab, as well as Mr. Erik Desormeaux from Porifera and Mr. Simon Barbeau from H2O Innovation.

I would also like to acknowledge the support of Mitacs, Hydro-Quebec, H2O Innovation, Centre National en Electrochimie et en Technologies Environnementales du College de Shawinigan and Concordia Institute for Water, Energy, and Sustainable Systems for my research.

Special thanks also to the faculty and staff in the Building Civil and Environmental Engineering department specially Mr. Joseph Hrib for his valuable help.

Last but not the least, I wish to express my love and gratitude to my beloved parents, and my husband for their understanding, support and endless love, through my studies. To my beloved daughter Anahita, I would like to express my thanks for being such a good girl always cheering me up. Thank you.

# Table of Contents

## List of Figures

## List of Tables

## List of Abbreviations

| | |
|---|---|
| ATR-FTIR | Attenuated Total Reflectance-Fourier Transform Infrared Spectroscopy |
| CFC | Chlorofluorocarbon |
| EDLC | Electrical Double Layer Capacitor |
| EDTA | Ethylene Diamine Tetra Acetic acid |
| FO | Forward Osmosis |
| GHG | Greenhouse Gases |
| IPCC | Intergovernmental Panel on Climate Change |
| IUPAC | International Union of Pure and Applied Chemistry |
| MWCO | Molecular Weight Cut Off |
| NOM | Natural Organic Matter |
| NMVOC | Non-Methane Volatile Organic Compounds |
| PRO | Pressure Retarded Osmosis |
| RED | Reverse Electro Dialysis |
| RO | Reverse Osmosis |
| SDI | Silt Density Index |
| SEM | Scanning Electron Microscopy |
| SGE | Salinity Gradient Energy |

| | |
|---|---|
| TOC | Total Organic Carbon |
| TOM | Total Organic Matter |
| TMP | Transmembrane Pressure |
| USEPA | U.S. Environmental Protection Agency |
| VPD | Vapour Pressure Difference |

# 1 Introduction

## 1.1 Greenhouse Gases (GHGs)

The highest part of the earth's atmosphere receives 1,370 Watts per second energy for one square meter of this surface which is facing the Sun daily and only one quarter of it reaches the entire planet on average (Le Treut *et al.*, 2007). Approximately 30% of the sunlight (reached the highest of the atmosphere) is sent back to space and two thirds of this amount of reflection is caused by clouds and aerosols which are small particles existing in the atmosphere. Snow, ice and deserts as areas of the earth that have proportionately small amounts of colors, reflect the rest of the sunlight (about one-third which is 240 W/$m^2$).

The surface of the earth and atmosphere absorb that part of the energy that is not sent back to space. The earth radiates approximately the same amount of the incoming energy to space due to the balance and this happens based on the emitted outgoing long wave radiation of the earth. Emission of the long wave radiation is done by everything on earth. It is the radiated heat energy coming out of a fire that any person can feel. Everything that is warmer emits more heat energy. A surface with a temperature about -19 ℃ can emit 240 W/$m^2$, but the average temperature of the earth's surface is around 14 ℃ which is much higher than this. At a height of 5 km above the earth's surface, 19 ℃ can be reached.

The reflected long wave radiation from the surface is covered by the greenhouse gases which creates an effect known as the natural greenhouse effect (Le Treut *et al.*, 2007).

Earth is a suitable human habitation due to the position of the earth proportional to the sun and the natural greenhouse effect of the earth's atmosphere.

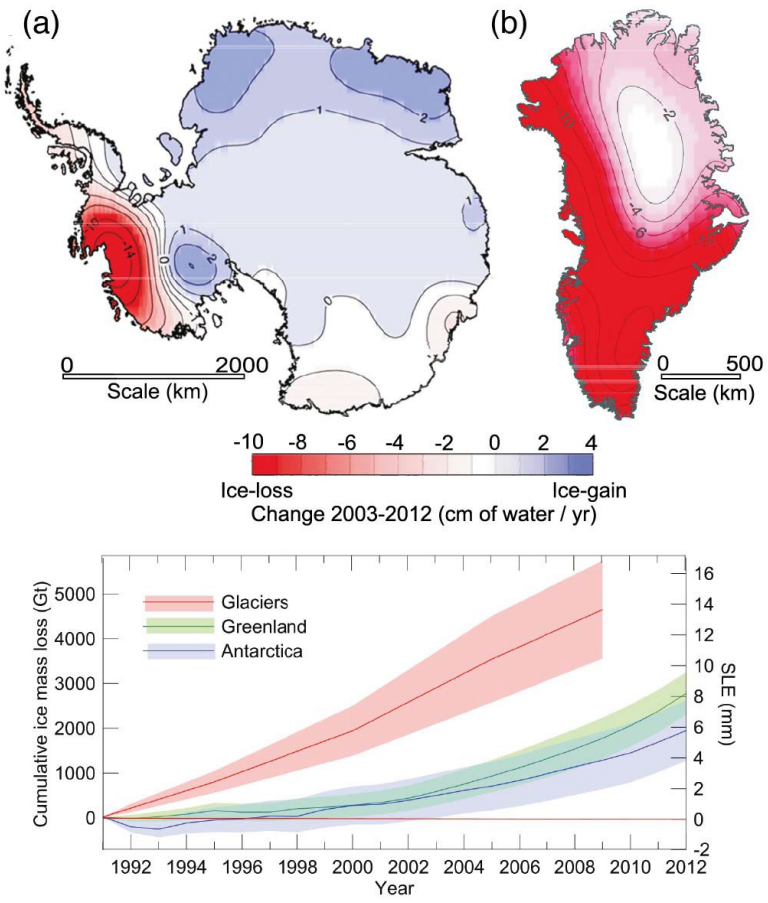


**Figure 1-1: Increase in the ice loss in glaciers of Greenland, and Antarctica (IPCC Report, 2013).**

Worldwide surface temperature has had a linear increase in the last fifty years that is nearly double in comparison with one hundred years ago based on the 2007 IPCC report (Fei, 2010). This increase in the average temperature of the earth can cause some adverse influences such as global warming, rising sea level, and higher frequency in some weather events. These climate changes expose the ecosystems (Ding and Somani, 2010). The universal average rise of sea level is 1.8 mm every year. The ice surface area

on average is reducing about 2.7% every decade and in the summer, this increases even to 7.4% at the North Pole (Figure 1-1) (Fei, 2010).

There is a reason that explains why the Earth's surface is so warm and it is the existence of greenhouse gases (Le Treut *et al.*, 2007). This fact has been demonstrated by significant scientific evidence (Hajibabai Dizaji and Feniosky, 2009). Greenhouse gases are a combination of different gases in the atmosphere such as water vapor (60%), carbon dioxide (25%), ozone (8%), and methane and nitrous oxide (Karl and Trenberth, 2003). Table 1-1 shows the most important greenhouse gases and their contributions.

**Table 1-1: Most important greenhouse gases (Kiehl and Trenberth, 1997).**

| Compound | Formula | Contribution (%) |
|---|---|---|
| Water Vapour and Clouds | $H_2O$ | 36 – 72% |
| Carbon Dioxide | $CO_2$ | 9 – 26% |
| Methane | $CH_4$ | 4 – 9% |
| Ozone | $O_3$ | 3 – 7% |

Emissions of the four main greenhouse gases (carbon dioxide, methane, nitrous oxide, and halocarbons) due to the human activities, especially in the industrial era have increased the concentration of these gases in the atmosphere over time (Figure 1-2) (Forster *et al.*, 2007). The most important sources in the increase of carbon dioxide from human activities are fossil fuel use in electricity, transportation, building heating and cooling, and production of cement and other goods, and deforestation. It also is released from natural processes like the decay of plant matter.

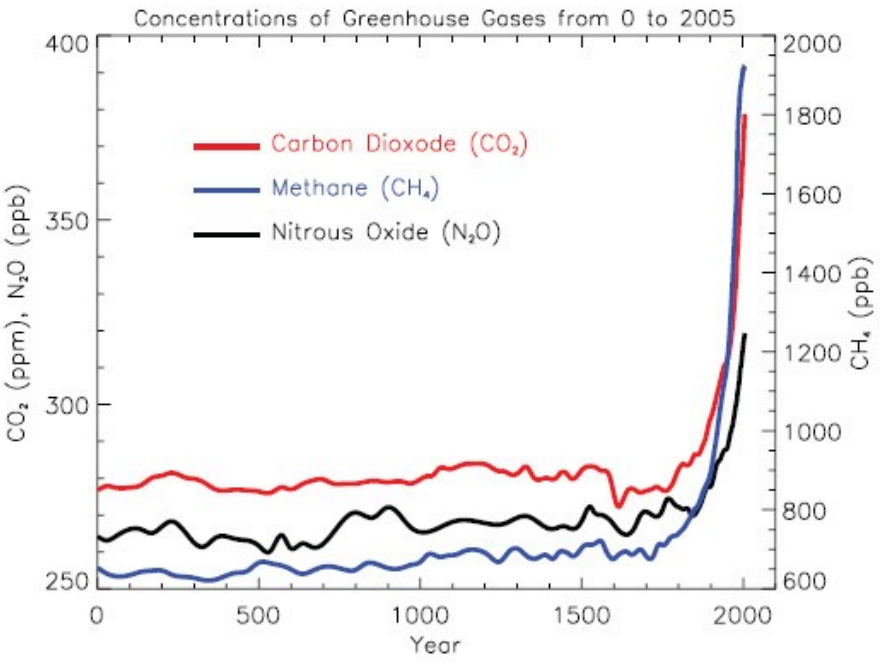


**Figure 1-2: Atmospheric concentrations of important greenhouse gases over 2000 years (Forster *et al.*, 2007).**

Methane has increased from human agricultural actions, natural gas distribution, landfills, and natural processes in wetlands. As methane growth rates have decreased over the last two decades, its concentration has not increased in the atmosphere. Nitrous oxide as another type of greenhouse gas enters the environment from fertilizer use, fossil fuel burning, and natural processes in soils and oceans. Halocarbon gas is mainly emitted by human activities and much less by natural processes. The main halocarbons include the chlorofluorocarbons such as CFC-11 and CFC-12 which deplete the ozone layer in the atmosphere. Based on the international regulations that have been designed for protection of the ozone layer, their concentrations have been reduced. Ozone is also a greenhouse gas that is emitted by the release and reaction of gases from human activities such as carbon monoxide, hydrocarbons and nitrogen oxide. Chemical reactions constantly produce and destroy the ozone in the atmosphere. The most important and

plentiful greenhouse gas is water vapour in the atmosphere. Human activities affect its concentration less directly and more indirectly by changing the climate. Producing water vapour from a warm atmosphere, and through methane emissions are some examples of the indirect effect of human activities on water vapour (Forster *et al.*, 2007).

The impact of various greenhouse gases is a function of their different concentrations and warming potential. As the proportional relation of carbon dioxide to all greenhouse gases is more than 50%, this gas is known as the main greenhouse gas and has the main influence on global warming (Fei, 2010).

The effects of global warming are not very easy to understand. Besides the fact that global warming has advantages like making sub polar area suitable for habitation and hastening the growth of plants due to increase of carbon dioxide concentration, it should be improved and restrained because of its drawbacks such as flood increasing, food shortage, illness spreading, coastal erosion and eco-system destruction (Fei, 2010). Using more efficient technologies for producing, processing, and distributing energy as well as people changing their life styles and the way that they use energy play an important role in decreasing greenhouse gases emissions at local and global levels (Huang and Lo, 2011). For example, emission of some contaminants such as carbon monoxide (CO), mono-nitrogen oxides (NOx) and non-methane volatile organic compounds (NMVOC) has decreased over the last decades due to the technological improvements in vehicles (López *et al.*, 2009).

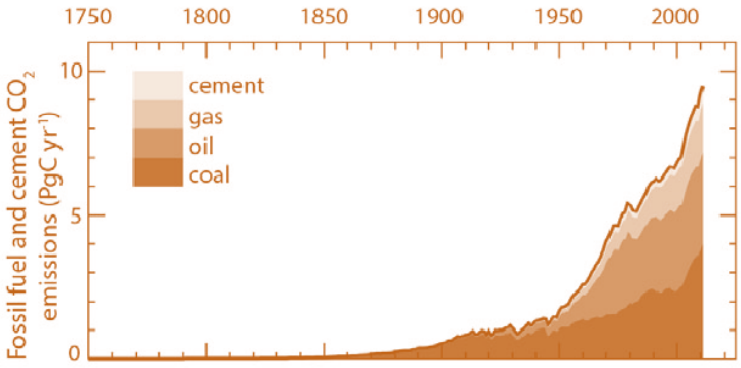


**Figure 1-3: Annual anthropogenic $CO_2$ emissions and their partitioning among the atmosphere, land and ocean from 1750 to 2011 (IPCC Report, 2013).**

Conversion of organic carbon, which exists in solid coal, into carbon monoxide (CO), carbon dioxide ($CO_2$) and hydrocarbons like methane ($CH_4$) by gasification and pyrolysis reactions to produce synthesis gas in power generation is one example of human activities that intensify the greenhouse effect (Esmaili *et al.*, 2013).

As mentioned above, the use of fossil fuels has an important role in increasing the greenhouse effect and raising the earth's temperature (Figure 1-3). Based on the assessment of Energy Information Administration of Department of Energy in U.S.A. in 2006, the initial sources of energy were petroleum (36.8%), coal (26.6%) and natural gas (22.9%). This indicates that 86.3% of the total required sources for producing the energy in the world are harvested from fossil fuels (Ding and Somani, 2010).

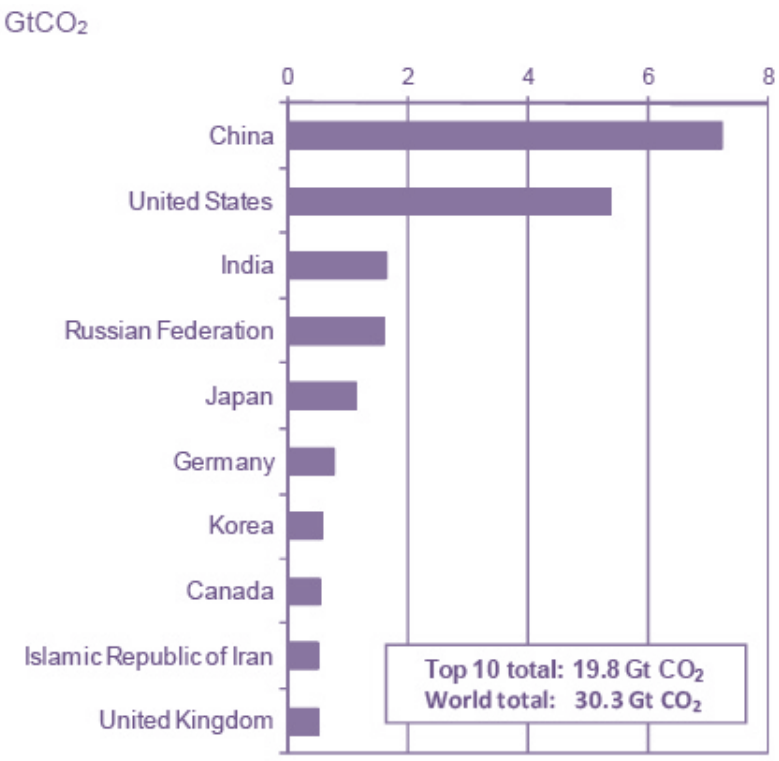


**Figure 1-4: Top 10 emitting countries in 2010 (IEA, 2012).**

Canada is one of the top 10 countries that generates almost two-thirds of the global carbon dioxide emissions (Figure 1-4). Canada produces about 2% of all universal greenhouse gases emissions. Canada emitted around 23t of greenhouse gases per capita in 2005 and this demonstrates an increase of 8% since 1990 (Figure 1-5) (Environment Canada, 2007). Excessive increases in temperature and precipitation, fluctuating lake levels, winter storms, hurricanes, tornadoes, droughts, floods, smog, sea ice conditions, road icing, melting permafrost, shrinking sea ice cover and aircraft turbulence are some examples of the influences of the environmental and weather conditions that effect the health, safety, economy and environment of Canadians (Environment Canada, 2008).

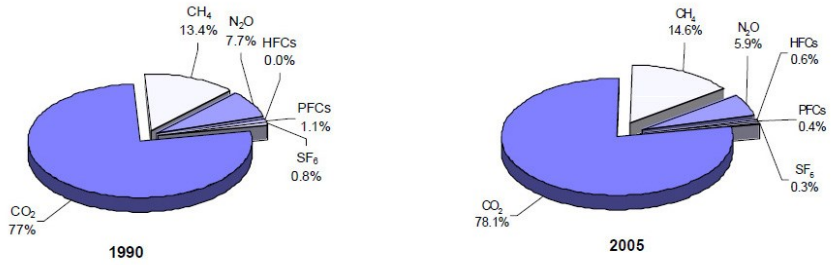


**Figure 1-5: Comparison of emitting GHGs from Canada between 1990 and 2005 (Environment Canada, 2007).**

The amount of greenhouse gas emissions caused by human activities in Quebec changed from 85300 to 89400 kton of carbon dioxide equivalent between 1990 and 2005 (Environment Canada, 2007). Also, the average temperatures in southern Quebec have increased from 0.2°C to 0.4°C per decade. Although Quebec has abundant resources of hydro-power, Quebec's society and life depend considerably on fossil fuels specially oil in several ways such as work related travel, leisure activities, production and transportation of food to consumption sites, mechanized agricultural production, etc. Also, Quebec's industrialization has imposed a significant consumption of fossil fuels (Quebec Government, 2012).

## 1.2 Problem Statement

In order to decrease the drawbacks of global warming due to greenhouse gases, it is necessary to take action to control and reduce the amount of the GHGs. As mentioned in the previous section, by increasing the population, demands for electricity from different sectors such as residential, industry, transport, and agriculture have increased. Most of the required electricity is produced by using fossil fuels at power stations all over the world. Continuously burning fossil fuels has dangerous influences on the climate.

Therefore, it is very important to produce new renewable and maintainable sources of energy to decrease the use of fossil fuels (Achilli and Childress, 2010). Solar, wind, biomass, geothermal, and hydro are the most advanced sources of renewable energies. There is another renewable source of energy that is called osmotic power or salinity gradient energy and is generated by the salt difference of fresh water with salt water. However, one of the main challenges for producing salinity gradient energy by using pressure retarded osmosis (PRO) technology is membrane fouling which causes problems such as a decrease in the permeate flux, increase of the pressure drop and energy consumption, and decrease in the membrane filtration efficiency. In order to overcome this problem, an appropriate pretreatment method and a good membrane cleaning method should be employed.

## 1.3 Scope and Applications

The three geographical locations with the greatest potential for setting up an osmotic power station in Québec province are along the Saint Lawrence River in the east, Hudson Bay and James Bay in the west, and finally Ungava Bay in the north of Québec according to the research that has been done by Hydro-Québec (Figure 1-6) (Laflamme, 2013).

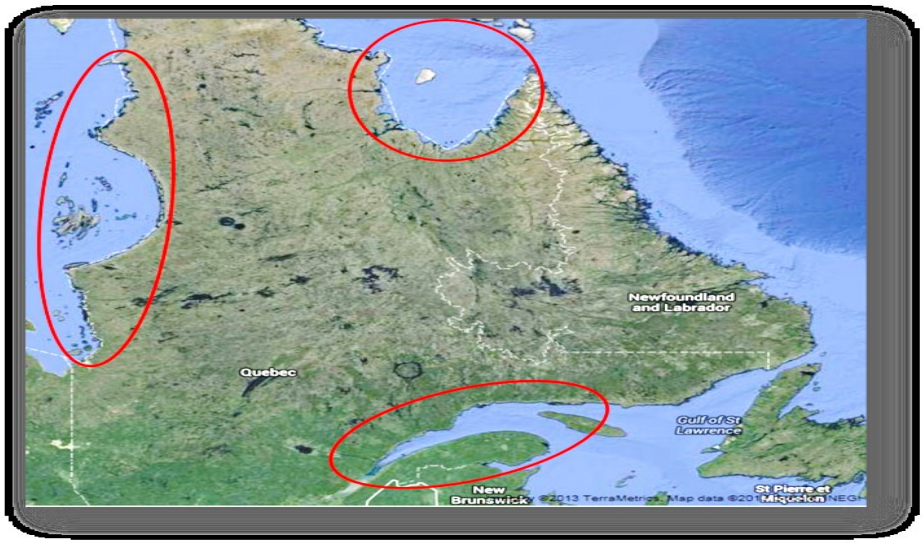


**Figure 1-6: Map of Quebec showing the areas circled in red for potential osmotic power (Source: Google map).**

There are two main applications for osmotic power: first, salinity gradient energy from fresh and salt water where a river meets a sea or an ocean and the second one is energy recovery from desalination of brine concentrates. It can also be used for small off grid communities in order to produce their required electricity.

## 1.4 Objectives

Pressure retarded osmosis is a membrane based technology that produces osmotic power as a sustainable energy by using salt and fresh waters. Pretreatment and membrane cleaning can reduce membrane fouling as the main challenge in PRO. This research will consist of the evaluation and determination of a pretreatment method for the PRO membrane, studying the effect of different pretreatment methods on PRO power plant efficiency, investigation of the membrane fouling and its mechanisms in PRO mode, identification of the types of foulants, examination of membrane cleaning methods, and studying the effect of operating conditions on PRO membrane performance. In this

research, ultrafiltration and a sand filter were used for removing total organic matter (TOC), turbidity, and hardness. In addition, four different feed waters including untreated river water, filtered water from multimedia sand filter, and permeate from ultrafiltration and microfiltration and two various draw solutions such as synthetic salt water and sea water were used to study the membrane fouling in PRO processes.

The objectives of this study are as follows:

- To investigate the physiochemical characteristics of the river water (St. Maurice River) and sea water
- To examine the performance of the different pretreatment methods (various ultrafiltration systems and multimedia sand filter) for removal of TOC, turbidity, and hardness
- To determine the effect of transmembrane pressure (TMP), and water pressure and fouling on permeate and filter fluxes in mentioned pretreatment methods as well as to study the effect of different pretreatment methods on PRO power plant efficiency
- To evaluate the effect of operating conditions such as temperature, pressure and salt concentration on permeate flux for FO (forward osmosis) and PRO modes
- To examine the membrane fouling, physio-chemical characterization of foulants, and membrane fouling mechanisms in PRO mode as well as investigate a method for cleaning the PRO membrane using both physical and chemical cleaning methods

## 1.5 Organization of the Research Study

There are five chapters in this thesis. In chapter one, the introduction and purpose of the research are presented. Chapter two describes the literature review on salinity gradient energy (osmotic power), and PRO technology. Chapter three includes materials, instruments, and methods which were used in the experiments. In chapter four, the results of different experiments are demonstrated and discussed. Chapter five summarizes the conclusions of this study and introduces the recommendations for future work. This thesis is completed by the list of references and an appendix.

# 2 Literature Review

## 2.1 Renewable Energy

Using the renewable energies is a well-known way for reducing the amount of greenhouse gases in the world (Manzini *et al.*, 2001). The principal component of this plentiful and well- founded technology is free (Bilgen and Kaygusuz, 2004). Natural resources produce the renewable energy. Sunlight, wind, biomass, tides, water and geothermal heat are some examples of these natural resources (Shi, 2010).

Renewable energies are able to succeed in facing up to the gradual decrease of traditional fossil energies and their connected environmental effects. They also can solve the problems such as energy sustainability, economic evolvement and environmental safety (Kim *et al.*, 2012).

Each type of renewable energy system is suited to specific applications based on its own unique benefit such as a decrease in external energy dependence, reduction in transmission and transformation losses, not releasing gaseous or liquid contaminants and favorable power producing sources. Their only disadvantage is the uncertain nature and dependency on weather and climatic situations (Erdinc and Uzunoglu, 2012).

As mentioned above, solar, wind, hydro, biomass, geothermal, and marine are the most advanced sources of the renewable energies. For generating marine energy, different sources such as tides, ocean currents, and salinity gradient are utilized and among them, a salinity gradient represents a high energy density (Berrouche and Pillay, 2012). The

renewable source of energy that is called osmotic power or salinity gradient energy is generated by fresh and salt water salt differences (Achilli and Childress, 2010).

Osmotic power and hydropower are similar because both of them produce the electricity by using hydroturbines. However, the water type and energy conversion that are used in both of them (osmotic power and hydropower) are different. In a hydropower plant, the energy is generated by exploiting river water and a dam, but in an osmotic power plant, the energy is produced by using river water and sea water separated by a semi permeable membrane (Kim and Elimelech, 2013).

## 2.2 Salinity Gradient Energy (SGE)

Osmotic power or salinity gradient energy as a renewable source of energy has attracted a lot of attention recently (Brauns, 2008; Labrecque, 2009; Achilli and Childress, 2010; Ramon *et al.*, 2011; Berrouche and Pillay, 2012; Burheim *et al.*, 2012). The worldwide potential for producing the power from mixing of sea and river water is more than 2 TW (Burheim *et al.*, 2012). Parameters such as percent recovery, averaged river flow rates, source salinities, and temperature influence the salinity gradient energy generation (Ramon *et al.*, 2011).

The difference of the chemical potential which is related to the difference of osmotic pressure between two solutions with various concentrations of salt causes the salinity gradient energy. The concentration of salt and osmotic pressure are proportional. This means when a solution has a high concentration of salt, its osmotic pressure is high as well and includes a significant amount of energy (Brauns, 2008). Salinity gradient can create the difference in the chemical potential and this gradient can be discovered in an

estuary which is a partially surrounded coastal area where fresh water from streams or rivers meets salt water from an ocean, gulf or salt lake (Labrecque, 2009).

## 2.3 Available Technologies

Different technologies such as pressure retarded osmosis (PRO), Reversed electrodialysis (RED), electrical double layer capacitor (EDLC), and power production by vapour pressure difference (VPD) are under development for production of the electric power based on salinity gradient energy (Kim *et al.*, 2013).

### 2.3.1 Reverse Electro dialysis (RED)

Reverse electrodialysis (RED) is a clean and maintainable technology that can generate electrical energy by mixing fresh and salt water in a direct manner (Dlugolecki *et al.*, 2009). The feasibility of this technology was demonstrated by Pattle in 1953 (Veerman *et al.*, 2008). Reverse electro dialysis is the opposite of desalination process which is a well-known method. In electrodialysis, there are many cells formed by cation and anion exchange membranes placed interchangeably in parallel between two electrodes. Applying a voltage to the solution streaming through the compartments, causes the salt to move from alternating cells to the neighbor cell which its consequence is a desalination of one flow in order to enrich the other one. In reverse electrodialysis, as its name explains, the process is reversed (Figure 2-1). By exposing salt water and fresh water through an ion exchange membrane a voltage is produced (Lacey, 1980).

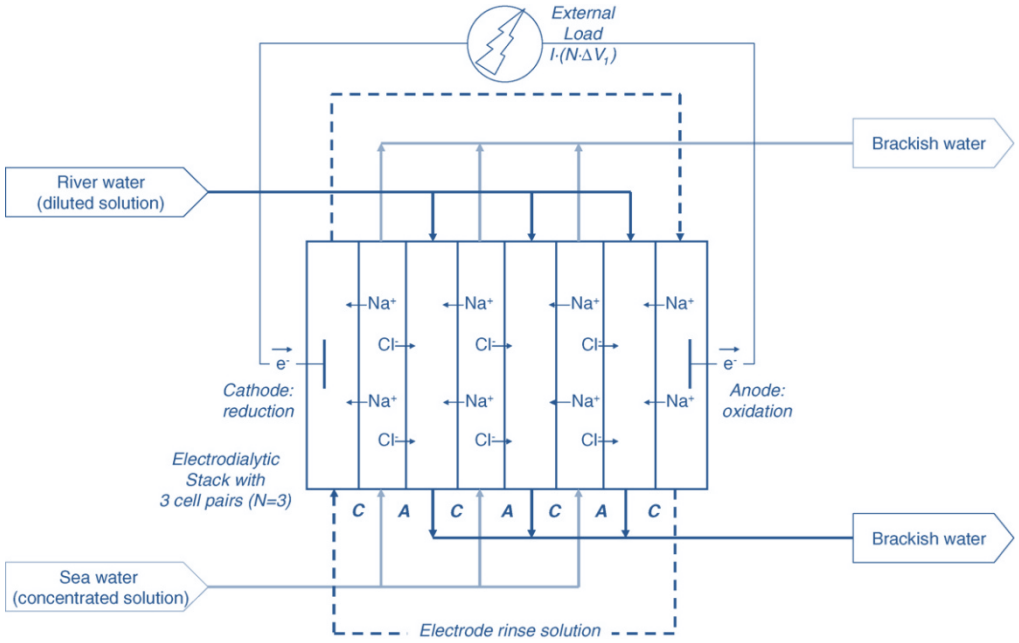


**Figure 2-1: Schematic of reverse electrodialysis (Post *et al.*, 2007).**

### 2.3.2 Electrical Double Layer Capacitor (EDLC)

Electric double layer capacitor (EDLC) is a new technology that produces the clean energy (Hiroyuki *et al.*, 2011). This technology has a high power rate and long cycling life which makes it a necessity to overcome deficiencies of batteries or fuel cells (Huang *et al.*, 2012). EDLC is formed by activated carbon electrodes which are submerged in sea water. The charge is stored in the EDLC based on opposite distributions of ions that are close to the electrode surfaces. By mixing the salt water and fresh water, salt ions move away from the electrodes because of the electrostatic force and it causes an increase in the electrostatic energy of the whole system (Brogioli, 2009). Figure 2-2 shows a schematic of the electric double layer capacitor.

Some of the reasons for using activated carbon as an electrode in EDLC technology are their electrical conductivity, surface functional groups, pore size, pore shape,

electrochemically inert character, and high surface area (Nishihara *et al.*, 2009). EDLCs work on the basis of the physisorption of ions (Tanaka *et al.*, 2012).

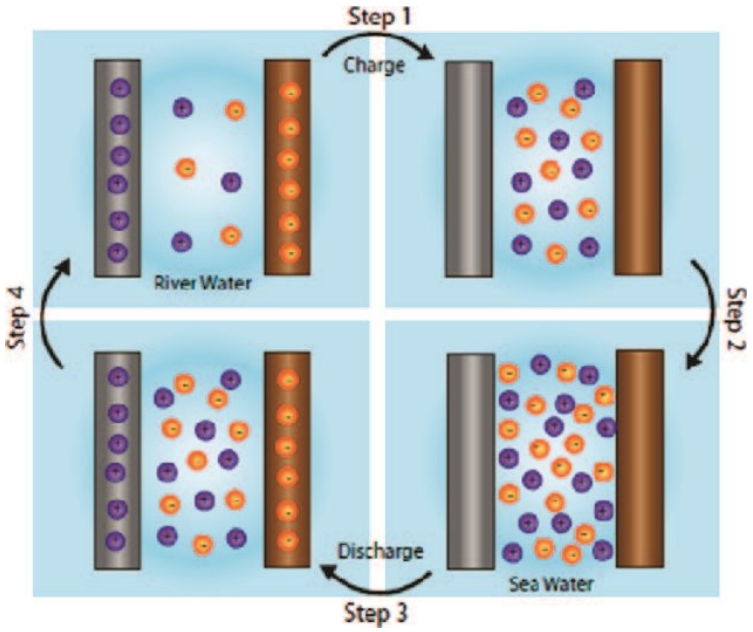


**Figure 2-2: Schematic of electric double layer capacitor (La Mantia *et al.*, 2011).**

### 2.3.3 Power Production by Vapour Pressure Difference (VPD)

Power can be generated from the difference of vapour pressure between fresh water and salt water, this technology is called a vapour pressure difference (VPD). In this method, membranes are not required as compared to PRO and RED. The fresh water converts to vapour under a vacuum condition, and then the vapour in a natural manner converts to liquid in the brine. The generated vapour flow can run the turbine and produce power (Figure 2-3) (Olsson *et al.*, 1979).

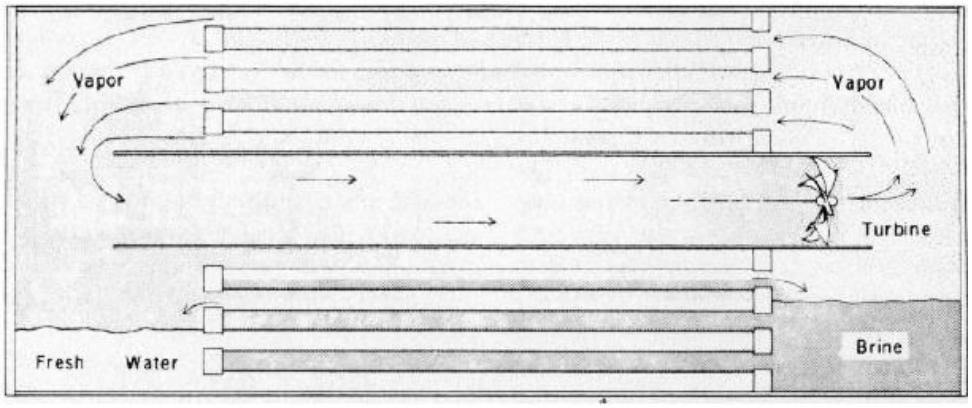


**Figure 2-3: Power production by vapour pressure difference (Olsson *et al.*, 1979).**

### 2.3.4 Pressure Retarded Osmosis (PRO)

Pressure retarded osmosis (PRO) has attracted significant attention in recent years (Xu *et al.*, 2010; Álvarez-Silva *et al.*, 2011; Thelin *et al.*, 2013; Abbasi-Garravand *et al.*, 2015; Kim *et al.*, 2015; Lee *et al.*, 2015; Abbasi-Garravand *et al.*, 2016; Chen *et al.*, 2016; Choi *et al.*, 2016; Hayashi and Okumura, 2016; Kim *et al.*, 2016; Wan and Chung, 2016). Pressure retarded osmosis technology was suggested in the 1970s by Prof. Sidney Leob. The membrane is a key parameter in this technology (Achilli *et al.*, 2009; Alsvik and Hägg, 2013; Le *et al.*, 2016; O'Toole *et al.*, 2016; Sarp *et al.*, 2016; She *et al.*, 2016; Touati *et al.*, 2016; Xiong *et al.*, 2016). Theory shows that a salinity gradient energy production is possible by PRO technology, but it was practically and economically impossible due to a lack of effective and appropriate PRO membranes in the past and research in this field ceased because of this issue. Introduction and improvement of forward osmosis membranes (FO) have made many developments in PRO processes (Li and Chung, 2014). Achilli and Childress (2010) have published an extensive review of PRO technology recently. The PRO technology, invented by Prof. Sidney Leob, has attracted increasing attention. Kim et al. (2013b), Kim and Lee (2012), She et al. (2012), Álvarez-

Silva et al. (2011), Xu et al. (2010), and Post et al. (2007) have published their research on PRO technology in recent years. In the preliminary studies on PRO, asymmetric reverse osmosis (RO) membranes were used and the power density was very low because of the thick support layers of RO membranes. However, it has been indicated that encouraging advances based on the developments that have been done recently in osmotic membranes and processes. The first PRO osmotic power plant in the world was built by Statkraft Company in Norway in 2009 (Figure 2-4). As Statkraft has previsioned, the generated power by PRO technology will reach 5 $^{W}/_{m^2}$ or above. Also, WETSUS in the Netherlands is working on the process of osmotic power. In Japan, Kyowakiden Industry Co. in collaboration with Kyushu University, Nagasaki University, Tokyo Institute of Technology and Mega-ton Water System are studying and developing their PRO prototype plant which produces 9 $^{W}/_{m^2}$ (Tanioka *et al.*, 2012).

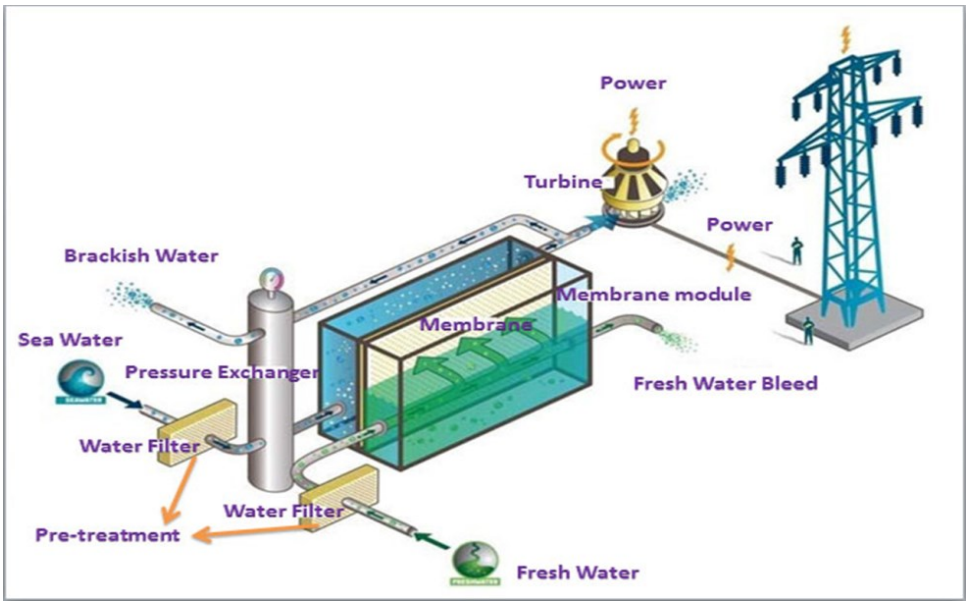


**Figure 2-4: Schematic of PRO power plant (Statkraft, 2011).**

The one of the main obstacles of osmotic power is the availability of a membrane with a low fouling effect. Figure 2-5 indicates a comparison between different experimental studies that have been done in terms of PRO power density during four decades. Blue symbols demonstrate power densities that reached their maximum experimental levels when draw water with salinity close to sea water was used and orange symbols show maximum power density obtained by experimental work based on a draw solution with salinity higher than sea water (Achilli and Childress, 2010).

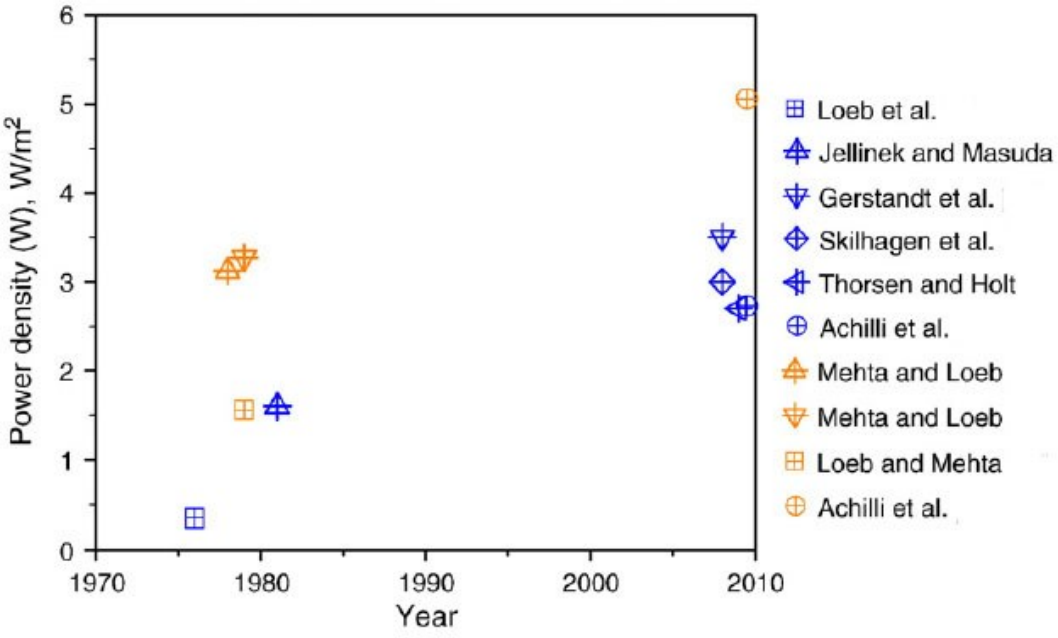


**Figure 2-5: Comparison between different experimental studies that have been done in terms of PRO power density over four decades (Achilli and Childress, 2010).**

## 2.4 Membranes

Membrane technology is used in many separation processes. It is a cost effective and safe separation technique from an environmental standpoint (Beolchini *et al.*, 2006). Membrane technology like every other treatment method has some advantages and

disadvantages. Some of the benefits are: continuous separation, low energy consumption, combination with other membrane separation processes, easy scale-up, variable and adjustable properties, and additives are not required. Also, membrane technology has some drawbacks such as concentration polarization, membrane fouling, low membrane lifetime, and low selectivity (Mulder, 1991).

Semipermeable membranes work as a barrier between two phases and separate metals by limiting the movement of ions and molecules as illustrated in Figure 2-6. Size exclusion, differences in diffusion coefficients, electrical charge, and solubility are the factors that affect these movements. Driving forces control the membrane separation processes such as micro-, ultra-, and nanofiltration, reverse osmosis (RO) by hydrostatic pressure, dialysis by concentration gradient; and gas permeation by membrane separation processes pressure and concentration gradients (Malaviya and Singh, 2011).

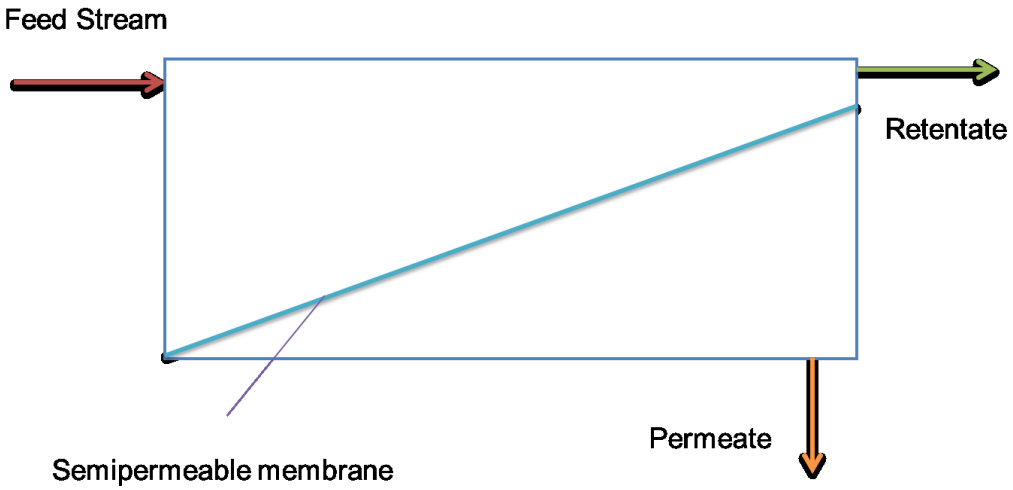


**Figure 2-6: Schematic of a separation process through a semipermeable membrane (MWH, 2005).**

The structure of membranes is homogeneous or heterogeneous and can have different thicknesses. Classification of membranes can also be done based on the pore diameter.

The International Union of Pure and Applied Chemistry (IUPAC) has classified three different types of pore diameter size (dp): microporous (dp < 2 nm), mesoporous (2 nm < dp < 50 nm), and macroporous (dp> 50 nm). The status of membranes is either neutral or charged, and that of particle transport is active or passive (Ambashta and Sillanpää, 2012). Based on the type of driving forces, the membrane processes are classified and shown in Table 2-1.

**Table 2-1: Classification of membrane processes (Belfort, 1984).**

| Process | Driving potential | Constituents removed from feed water | Constituents remaining in the product (other than water) | Possible size ranges of permeable species (nm) |
|---|---|---|---|---|
| **Hyperfiltration (Reverse osmosis)** | Pressure (as high as 3948 kPa) | Water without dissolved and undissolved inorganic and organic constituents | Little salt (owing to membrane leakage $BO_3^-$, $NO_3^-$, urea, low MW organics | 0.4 – 30 |
| **Ultrafiltration** | Pressure (usually below 987 kPa) | Water without dissolved and undissolved organic constituents | All salt and low molecular weight organics | 2- 10000 |
| **Electrodialysis** | Electrical | Dissolved inorganic ions | Little salt, all organics (dissolved and undissolved) including viruses, bacteria, etc. | 0.4 – 30 |
| **Transport depletion** | Electrical | Dissolved inorganic ions | More than a little salt, all organics (dissolved and undissolved) including viruses, bacteria, etc. | 1- 100 |

### 2.4.1 Reverse Osmosis Membrane

Reverse osmosis (RO) is defined as a membrane permeation process which is applied for separation of the pure solvent from a solution with less purity. In this process the solution is passed over a semipermeable membrane when the pressure is more than osmotic pressure of the feed solution (Lonsdale and Podall, 1972). Particles as small as $10^{-3}$ to $10^{-4}$ nm are rejected by RO (Malaviya and Singh, 2011). RO can be used over a wide range of pH from 3 to 11 and at 450-1500 kPa of pressure and this occurs based on the membrane characteristics such as the porosity, hydrophilicity, thickness, roughness, and charge of the membrane (Kurniawan *et al.*, 2006). In Table 2-2, properties of some RO membranes are shown.

**Table 2-2: Properties of some commercial reverse osmosis membranes (Fell *et al.*, 1995).**

| Type | Manufacturer | Form in which used | pH range | Chlorine tolerance | Oxidation tolerance |
|---|---|---|---|---|---|
| Cellulose acetate blend | Various | Spiral wound | 3–8 | Fair | Fair |
| Cellulose triacetate | Dow/Toyota | Capillary fiber | 4–9 | Fair | Good |
| Aromatic Polyamide | Du Pont | Hollow fiber | 4–11 | Poor | Fair |
| Crosslinked polyether TFC | Toray | Spiral wound | 1–12 | Poor | Fair |
| Aryl–Alkyl polyetherurea TFC | Fluid Systems/UOP | Spiral wound | 3.5–12 | Poor | Fair |
| Cross-linked fully aromatic polyamide TFC | Filmtec/Dow | Spiral wound | 1–12 | Poor | Fair |

### 2.4.2 Forward Osmosis Membrane

Recently forward osmosis (FO) as one of the membrane processes which works by osmotic pressure has drawn considerable attention (Chou *et al.*, 2010; Mi and Elimelech, 2010; Ling and Chung, 2011; Chung *et al.*, 2012; Blandin *et al.*, 2013; Cath *et al.*, 2013) (Zhang *et al.*, 2010; Zhao *et al.*, 2012). Osmotic pressure difference across the semi-permeable membrane is used in forward osmosis process compared to high hydraulic pressure that is used in RO process. Table 2-3 shows some differences between FO and RO processes. The concentrated draw solution provides the required driving force in forward osmosis processes and due to this produced osmotic pressure, water permeates across the membrane from a low salt concentration feed solution to the concentrated draw solution. Forward osmosis membranes have attracted interest in different industries such as desalination, waste water treatment, liquid food processing, membrane bioreactors and biological processes because of their many benefits such as low operating cost, low fouling tendency, a wide range of feed solutions because of operation with low temperatures and pressures and achievable high recovery (Amini *et al.*, 2013).

### 2.4.3 Pressure Retarded Osmosis Membrane

Pressure Retarded Osmosis (PRO) is a technology that generates osmotic power based on the salinity gradients. This technology is a membrane based process with it's a driving force of osmotic pressure. Water moves from a feed solution with a low osmotic pressure towards a draw solution with a high osmotic pressure versus a hydraulic pressure (She *et al.*, 2013).

In comparison with forward osmosis (FO) process, an applied back pressure is needed on the high salinity draw solution side to retard the permeate water flow in the PRO process. Then the power is produced by releasing the pressure from the solution through a turbine (Kim and Elimelech, 2013).

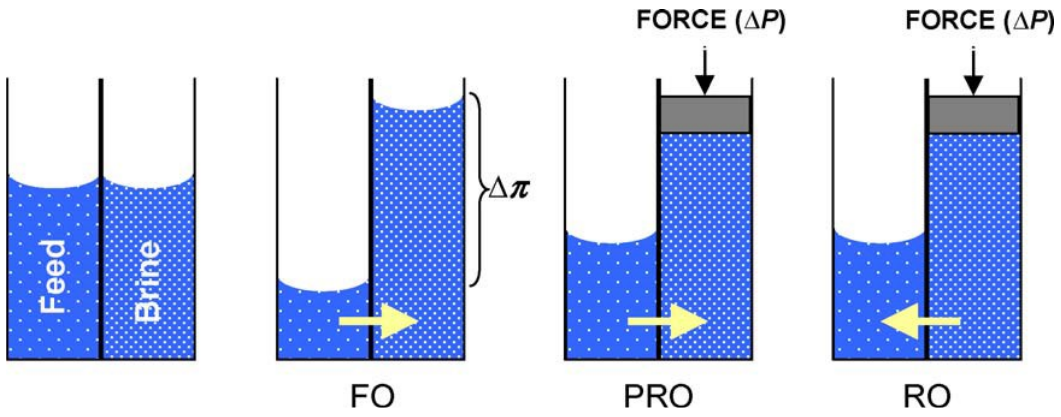


**Figure 2-7: Schematic of RO, FO, and PRO membranes (Cath *et al.*, 2006).**

Figure 2-7 indicates the differences between RO, FO, and PRO membranes. For FO, hydraulic pressure is nearly zero and water passes through the membrane from diluted side to the concentrated side. For PRO, water passes through the membrane from diluted salt side to the concentrated side which is under hydraulic pressure ($\Delta\pi > \Delta P$). For RO, water passes through the membrane from concentrated side to diluted side by applying hydraulic pressure ($\Delta P > \Delta\pi$) (Cath *et al.*, 2006).

**Table 2-3: Comparisons between FO and RO (Jia *et al.*, 2010).**

| Items | Reverse Osmosis | Forward Osmosis |
|---|---|---|
| Driven Pressure | High hydraulic pressure supplied by high pressure pump | Osmosis pressure difference between the feed solution and draw solution |
| Special membrane | Abundant in materials, module forms and specifications, brands, etc. | Limited commercial availability such as the FO product of Hydration Technologies Inc. |
| Process Configuration | 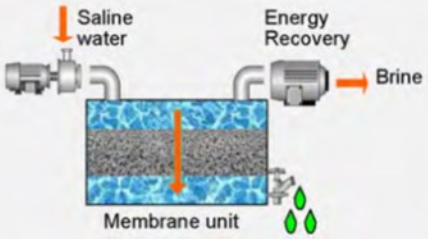 | 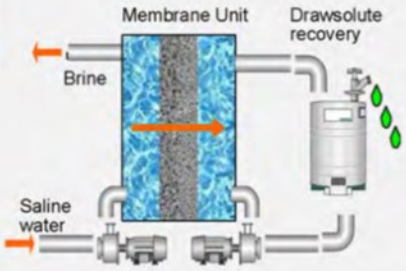 |
| Water Recovery | 30%～50% [1] | as much as around 85% [2] |
| Energy consumption | High energy requirement for overcoming osmosis pressure | Low energy demand for stirring or pumping of the solutions involved |
| Membrane fouling | Higher propensity, highly dependent on pretreatment | Lower propensity due to lesser cake layer compaction[3] |
| Equipments & Cost | High-pressure pumps；Energy recovery unit；Resistant high-pressure pipelines； High investment in equipments and high cost of Energy | General pumps, pipelines, and tanks. Low investment in equipment and low cost of energy |
| Environment effect | Harmful, the discharge of the concentrated salt water | Friendly, minimized brine discharge |
| Applications | Normal separation and purification of water systems | Besides the normal water systems, it can also play role in the temperature-sensitive systems, the pressure-sensitive systems, drug delivery, the production of electrical power and even the pretreatment for RO. |

### 2.4.4 Membrane Process Operation

#### 2.4.4.1 Concentration Polarization

Concentration polarization is defined as the accumulation of solutes nearby boundary layer. Concentration polarization is affected by operating parameters such as velocity, pressure, temperature and feed concentration (Ilias and Govind, 1993). Formation of concentration polarization boundary layer on the membrane surface affects the driving force efficiency through the membrane. In other words, when the concentration near the membrane surface increases, the driving force decreases (Zhang *et al.*, 2006).

In membranes which work based on pressure as their driving force, the concentration polarization in direction of gel formation usually occurs. These phenomena reduce permeability and transport characteristics. The diffusion layer and laid down gel include various particles which have different diffusivity characteristics. Hydrodynamic and mass transfer properties of membrane process are affected by a gel or cake layer which is accumulated on the membrane surface (Agashichev, 2006). Formation of concentration polarization on the membrane surface is shown in Figure 2-8.

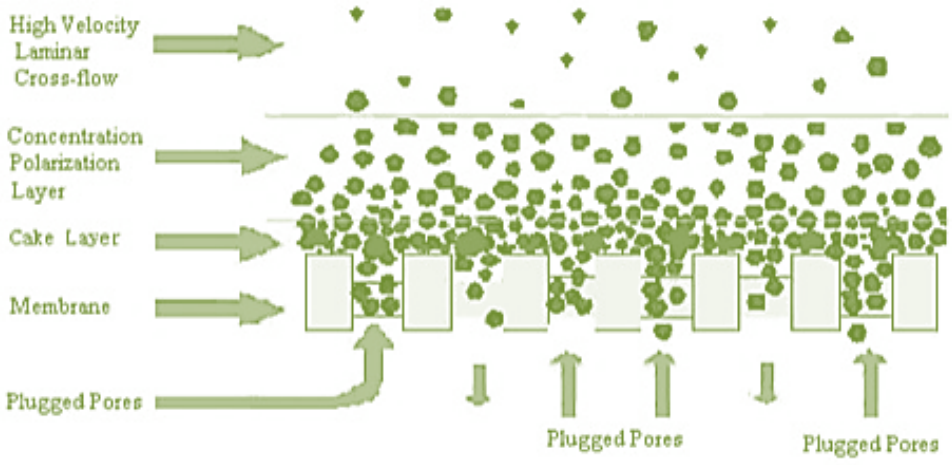


**Figure 2-8: Schematic diagram of formation of concentration polarization on membrane surface (Zhan *et al.*, 2004).**

#### 2.4.4.2 Membrane Fouling

Membrane fouling is the phenomena in which the membrane loses its permeability during the filtration and this happens because the impurities such as physico-, chemico- and bio-substances accumulate on or in the membrane matrices. Foulants play an important role in membrane fouling control, so recognition of them is very significant. Based on the type of foulants, fouling is classified as particle fouling, organic fouling, and bio-fouling. Particle fouling is defined according to two classical plugging laws. Firstly, larger particles which accumulate on the membrane surface and smaller ones go through the membrane pore. Secondly, the cake which is formed by increasing precipitation of particles on the initial layer, causes a high resistance of membrane flux. Organic fouling is created by natural organic matter (NOM) from the source waters, but this type of fouling is not well understood. Bio-fouling comes from 29 organisms which live or grow in water. Algae are a good example of aquatic organisms that create colonies which result in bio-fouling (Guo *et al.*, 2009). Fouling is generally known to be a time-dependent and irreversible

phenomenon (Ilias and Govind, 1993). Execution and efficient performance in the production of drinking water are restricted by fouling of the membranes (Peiris *et al.*, 2010). One of the most important problems of membrane technology is the membrane fouling which affects the process of commercialization of the membrane processes (Kwona *et al.*, 2008). Changing the operating conditions, chemical additions and pre-treatment are the parameters which can control the membrane fouling (Schafer, 2001). However, the fouling in the osmotically driven membranes depends on the membrane orientation compared to the pressure driven membranes. In FO mode, the active layer faces the feed water and as a result the particles deposit on the active layer. In PRO mode, the support layer faces the feed water and particle deposition occurs on/within the support layer (Seidel and Elimelech, 2002; Alsvik and Hägg, 2013). The type of fouling in FO and PRO membranes relies on various parameters such as water quality, temperature, system design, water flow, and membrane surface (Alsvik and Hägg, 2013).

#### 2.4.4.2.1 Membrane Fouling Mechanisms

Numerous studies have been done to investigate the fouling mechanisms in membrane processes (Kim *et al.*, 1992; Jarusutthirak, 2002; Jiang *et al.*, 2005; Nghiem and Hawkes, 2007; Mi and Elimelech, 2010; Mattaraj *et al.*, 2011; Brião and Tavares, 2012). Hermans and Bredée (1935) proposed four well-known and extensively used fouling models (cake filtration, adsorption or standard blocking, complete blocking and intermediate blocking) for investigation of the membrane fouling mechanisms (Hermia, 1982; Bolton *et al.*, 2006; Bolton *et al.*, 2006; Londono, 2011; Rezaei *et al.*, 2011). In complete blocking, particles block the pores and hinder flow. In intermediate blocking, part of the particles block the pores and the remainder are gathered on top of other deposited particles. In cake

filtration, particles accumulate on the surface of the membrane and create a penetrable cake that decreases the flow. In standard blocking, particles gather inside the membrane pores. Over time, the pores become smaller due to the deposition of the particles and consequently, flow decreases (Bolton *et al.*, 2006). A new mechanism for salt rejecting membranes has been introduced which is called cake enhanced osmotic pressure (CEOP) (Hoek *et al.*, 2002; Hoek and Elimelech, 2003; Lee *et al.*, 2004; Herzberg and Elimelech, 2007). In this mechanism, the back diffusion of salt is prevented by a cake layer and as a result, the osmotic pressure increases close to the membrane surface. In osmotically driven membranes such as FO and PRO, solutes can penetrate through the membrane from the high concentration draw solution to the feed solution. The reverse flux of solutes from the draw solution into the feed solution can increase and enhance the membrane fouling in FO and PRO processes (Hancock and Cath, 2009; Lee *et al.*, 2010; She *et al.*, 2012; Park *et al.*, 2013; She *et al.*, 2013).

### 2.4.5 Membrane Cleaning

Using an appropriate cleaning method is an unavoidable part of the membrane processes. Periodic cleaning of the membrane removes the foulant materials and restores the productivity of the membrane (Mi and Elimelech, 2010; Shi *et al.*, 2014). In the FO process, membrane fouling on the feed side is less and can be controlled simply by using hydrodynamic cleaning. However, in the PRO process, due to the deposition of the organic and inorganic species in the feed water inside the porous support layer, the efficiency of the PRO membrane reduces critically (Mi and Elimelech, 2010; Kim *et al.*, 2015). In order to reduce and control the membrane fouling in PRO mode, it is necessary

to determine the type of foulants. According to the type of foulants, an appropriate cleaning procedure can be used. Therefore, the membrane can be cleaned more efficiently and effectively and as a result, the performance of the PRO processes improves (She *et al.*, 2016). Physical cleaning which comprises surface flushing and membrane backwashing has been used widely to control the membrane fouling in osmotically driven membranes (Yip and Elimelech, 2013; She *et al.*, 2016). Chemical cleaning is also an efficient method to remove foulants from the membrane surface. Some important parameters that should be considered in chemical cleaning are cleaning agent type, cleaning agent concentration, temperature, pH, flow rate, and cleaning time. It is also necessary to choose a suitable cleaning agent that is compatible with the membrane because some cleaning agents damage the membrane surface and reduce its performance irreversibly (Zheng *et al.*, 2009; Wei *et al.*, 2010).

As it was mentioned above, fouling is a main challenge in membrane processes and imposes high cost to the system in terms of energy consumption. One way to decrease fouling and cost is using an appropriate pretreatment method. In this research, the physicochemical characteristics of the Saint Maurice River including silt density index (SDI) were investigated. By using SDI as an empirical parameter, the fouling potential of a feed water stream can be determined (Alhadidi *et al.*, 2011). Different ultrafiltration systems and a multimedia sand filter were used as two different pretreatment methods for reducing the amount of main foulants such as TOC, turbidity and hardness from raw water which are very effective in PRO membrane fouling and consequently improving the osmotic power generation.

Although much research has been done on PRO, the membrane fouling and its mechanisms have not been studied very well yet. In the few existing fouling studies on PRO membrane, artificial foulants and synthetic draw and feed solutions were mostly used (Kim and Elimelech, 2013; She *et al.*, 2013; Thelin *et al.*, 2013; Chen *et al.*, 2015). In this research, however, river water and sea water were used as the feed and draw waters, respectively, to observe the effect of fouling on a commercial semi permeable membrane in PRO mode in realistic conditions. Also various parameters were determined in raw sea water to examine the sea water characteristics. In addition, four classic fouling models such as complete blocking model (CBM), intermediate blocking model (IBM), standard blocking model (SBM) and cake filtration model (CFM) were used. Cake enhanced osmotic pressure as a new mechanism for osmotically driven membranes was studied as well. These models were used to study the fouling mechanisms in PRO processes in real conditions.

In the few available publications on PRO membrane fouling, artificial foulants were mainly used in order to study the fouling phenomena (Kim and Elimelech, 2013; She *et al.*, 2013; Thelin *et al.*, 2013). In this research, however, different feed waters including untreated river water were used in order to identify the physicochemical characterization of foulants on a commercial semi permeable membrane at realistic conditions in the PRO process. The tests were performed using synthetic salt water and sea water as the draw solutions. Also, two physical and chemical cleaning methods were used to study the effect of cleaning on control and decrease of fouling in PRO mode.

# 3 Materials and Methods

In this section, the required materials and methods for this research will be explained. Most of the experiments were done at LTE (Laboratoire des technologies de l'énergie), the Hydro-Québec Research Institute located at Shawinigan, Quebec, Canada. The experiments regarding crossflow ultrafiltration systems were done at Concordia University.

## 3.1 Water Sampling

In the experiments, fresh water was taken from Saint-Maurice River at the entrance of pressure channels in central Shawinigan-2 (Figure 3-1). The river water was transported to the Hydro-Québec LTE laboratory (Laboratoire des technologies de l'énergie) in a 2 $m^3$ polypropylene tank which was mounted on a trailer (Magnum Water Trailer – MWT500) rented from Hewitt Company (Figure 3-2). Sea water was taken from the Saint Lawrence River at the Station Aquicole (Figure 3-3) located in Rimouski, Québec in the estuary of the Saint Lawrence River and was sent to the Hydro-Québec laboratory in Shawinigan, Québec in a volume of 3 $m^3$.

**Figure 3-1: Water intake at the central Shawinigan 2.**


**Figure 3-2: Trailer and $2m^3$ tank.**

**Figure 3-3: Station Aquicole at ISMER (Institut des sciences de la mer de Rimouski) in Rimouski, Québec (Institut des Sciences de la Mer de Rimouski, 2012).**

## 3.2 Water Quality

In order to investigate the sea water and fresh waters (river water, filtered and permeate waters from the multimedia sand filter, ultrafiltration and microfiltration) characteristics, the amount of parameters such as color, iron, total organic carbon (TOC), silica,

suspended solids, alkalinity, hardness, pH, salinity, conductivity, turbidity, dissolved solids, sodium, calcium, magnesium, potassium and silt density index (SDI) were measured. The amount of iron, silica, sodium, potassium, calcium, and magnesium were measured by optima 4300 DV ICP-OES (Inductively Coupled Plasma Optical Emission Spectrometer) from Perkin Elmer Inc. For TOC analysis, a TOC-L (Laboratory Total Organic Carbon Analyzer) from Shimadzu Corporation was used. The amount of color, and suspended solids were measured by a DR 6000™ UV VIS Spectrophotometer from the Hach Company. Alkalinity and hardness were measured by titration of sulfuric acid (0.02 N) and titration of Titraver EDTA (0.02 N) respectively. Salinity, pH, conductivity, and dissolved solids were measured by an HQ440d Benchtop Dual Input Multi-Parameter Meter from the Hach Company. Turbidity was measured by a Ratio Turbidimeter/XR 115/230 V from the Hach Company. SDI was measured by using a Simple SDI: auto manufactured by SDI Solutions, a division of Procam Controls Inc.

The river water quality results for SDI, TOC, hardness and turbidity will be introduced and discussed in the results and discussion section. The rest of the results for river water quality during winter and spring can be found in the appendix. The results in Tables 3-1 and 3-2 demonstrate the average physiochemical characteristics of the different used feed waters and sea water used.

**Table 3-1: Physio-chemical characteristic of sea water.**

| Parameters | Sea Water |
|---|---|
| Apparent Color (mg/L PtCo) | 7.00 |
| Total Iron (mg/L Fe) | 0.00 |
| TOC (mg/L C) | 1.85 |
| Silica (mg/L $SiO_2$) | 0.7 |
| Suspended Solids (mg/L) | 0.00 |
| Total Alkalinity | 78.00 |
| Hardness (mg/L as $\boldsymbol{CaCO_3}$) | 4500.00 |
| pH | 7.75 |
| Salinity (‰) | 30 |
| Conductivity ($\boldsymbol{\mu}$S/cm) | 37000.0 |
| Turbidity (NTU) | 0.503 |
| Dissolved Solids (mg/L) | 22.6 |
| Sodium (mg/L) | 8750.00 |
| Calcium (mg/L) | 324.00 |
| Magnesium (mg/L) | 1100.00 |
| Potassium (mg/L) | 404.00 |

SDI is an empirical parameter that indicates the fouling potential of a feed water stream. SDI was specified by using the standard method D4189 of American Society for Testing and Measuring (ASTM). Due to the different shapes, sizes and nature of the particulates, the quality of particulates may not be measured absolutely (ASTM, 2007). In this method the rate of clogging was calculated by passing a fixed volume of the water (500 mL) through a 0.45 µm membrane filter for a specific time (15 min) at a constant pressure of 30 psi (207 kPa) (Wei *et al.*, 2012). The direct method (Method 10129) for a low range test (0.3 to 20 mg/L C) and USEPA ManVer Buret titration method (Method 8226) for the range of 0 to 25000 mg/L as $CaCO_3$ were used for TOC and hardness respectively (Hach Company, 2007). For color, and iron platinum-cobalt standard method (method 8025), and the USEPA FerroVer method (method 8008: 0.02 to 3 mg/L) were used respectively. The methods used for silica, and suspended solids were as follows respectively: the

silicomolybdate method (method 8185: 1.0 to 100 mg/L), and the photometric method (method 8006: 5.0 to 750 mg/L).

**Table 3-2: Physio-chemical characteristics of ultrafiltration, microfiltration, multimedia sand filter, and river water.**

| Parameters | Ultrafiltration | Microfiltration | Multimedia Sand Filter | River Water |
|---|---|---|---|---|
| $SDI_{15}$ (500ml) | 1.98 | 12.50 | 15.64 | 19.17 |
| Apparent Color (mg/L PtCo) | 11.57 | 63.00 | 68.47 | 98.00 |
| Total Iron (mg/L Fe) | 0.01 | 0.15 | 0.17 | 0.27 |
| TOC (mg/LC) | 3.49 | 6.03 | 6.72 | 7.17 |
| Silica (mg/L$SiO_2$) | 2.10 | 2.12 | 2.15 | 2.29 |
| Suspended Solids (mg/L) | 0.14 | 1.00 | 1.00 | 2.00 |
| Total Alkalinity | 4.57 | 5.00 | 5.00 | 5.00 |
| Hardness (mg/L as $\boldsymbol{CaCO_3}$) | 3.67 | 5.00 | 5.00 | 5.00 |
| pH | 7.14 | 7.39 | 7.49 | 7.64 |
| Salinity (‰) | 0.01 | 0.01 | 0.01 | 0.01 |
| Conductivity ($\boldsymbol{\mu}$S/cm) | 17.27 | 21.40 | 23.90 | 24.00 |
| Turbidity (NTU) | 0.01 | 0.63 | 0.72 | 1.37 |
| Dissolved Solids (mg/L) | 8.02 | 9.97 | 11.1 | 11.20 |
| Sodium (mg/L) | 1.26 | 1.40 | 1.50 | 1.51 |
| Calcium (mg/L) | 1.37 | 2.19 | 2.23 | 2.28 |
| Magnesium (mg/L) | 0.39 | 0.58 | 0.59 | 0.61 |
| Potassium (mg/L) | 0.29 | 0.34 | 0.36 | 0.41 |

These parameters were monitored during the winter and spring seasons. Some of these parameters such as iron, TOC, silica, sodium, potassium, calcium, and magnesium were measured at the CNETE (Centre National en Électrochimie et en Technologies Environnementales located at Shawinigan, Quebec, Canada) and the rest were measured at the Hydro-Québec Research Institute. Particle size distribution was measured at Concordia University using a Laser Scattering Particle Size Distribution Analyzer LA-950 from Horiba Scientific Company.

## 3.3 Experimental Design

### 3.3.1 Multimedia Sand Filter

Figure 3-4 shows the experimental setup for the sand filter at LTE Hydro-Québec. Materials and equipment that were used in the multimedia sand filter bench system are indicated in Table 3-3.

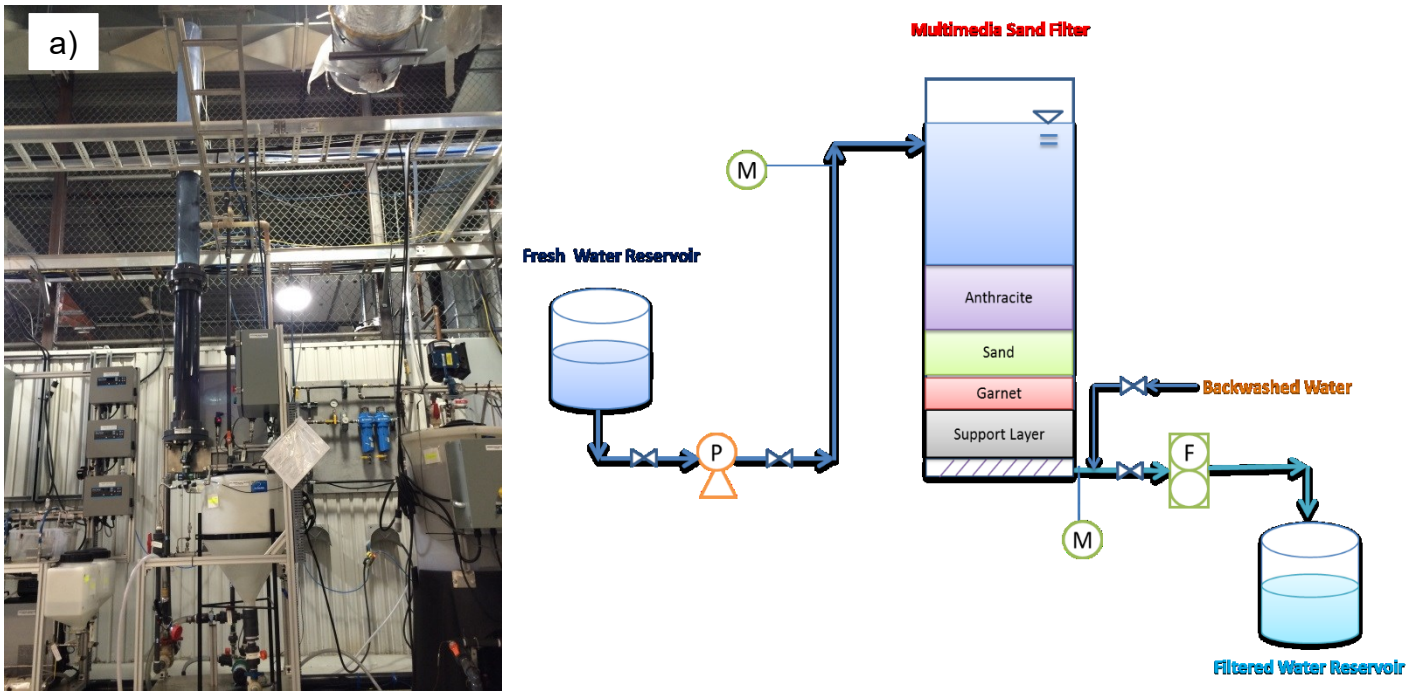


**Figure 3-4: a) Sand filter setup at LTE Hydro-Québec and b) schematic of multimedia sand filter.**

Water from the fresh water reservoir was pumped to the multimedia sand filter and then filtered water was collected at the end of the sand filter column while impurities and suspended particles were rejected by multimedia sand filter. The permeate was used for the fouling tests. The equation used to calculate the removal efficiency was Equation 3-1:

$$\text{Removal Efficiency (\%)} = [1- \left(\frac{C_P}{C_F}\right)] \times 100 \qquad \textbf{Equation 3-1}$$

Where,

$C_P$: Permeate or filtered concentration, $\frac{mg}{L}$

$C_F$: Feed concentration, $mg/L$

**Table 3-3: Materials and equipment in the multimedia sand filter bench system (Hydro-Québec, 2013).**

| Material | Quantity | Supplier | Code | Capacity |
|---|---|---|---|---|
| **Pumps** | | | | |
| Feed Pump | 1 | Cole Parmer | 72012-00 | 2 L/min -2 bar (200 kPa) |
| **Reservoir** | | | | |
| Reservoir of Filtered Water | 1 | Ace | AC-INFD1519 | 50 L |
| **Sensors** | | | | |
| Manometer | 1 | Swagelok | PGI-63B-PG30-LAQX | 0-30 psi (0-206.84 kPa) |
| Temperature Probe | 1 | Omega | PR-24-3-100-A-1/4-1/4-6 | RTD |
| Flow meter | 1 | Cole Parmer | NOE4-96 | - |
| **Multimedia Column** | | | | |
| Transparent PVC Pipe 6 in(15.24 cm) | 1 | Fabco Plastiques | PL-060 | - |
| Garnet | 0.1 m height | - | FMSND.45X.5550# - 0.45-0.55MM | |
| Sand | 0.3 m height | - | FMGNT50X50 (SIZE 0,25-0,35MM) | |
| Anthracite | 0.5 m height | - | FMANTH 1.5 | |

### 3.3.2 Ultrafiltration

#### 3.3.2.1 Dead-end Ultrafiltration

Figure 3-6 indicates the experimental setup for ultrafiltration at LTE Hydro-Québec. Materials and equipment that were used in ultrafiltration bench system are demonstrated in Table 3-4. The used membrane had a hollow fiber configuration with molecular weight cut off (MWCO) of 400 kDa (Mosqueda-Jimenez and Huck, 2006). This means that when dead-end ultrafiltration was used, all the particles that had an approximate molecular weight higher than 400 kDa were removed from the water. As Figure 3-6 part b shows,

water was pumped from the fresh water reservoir to the ultrafiltration cartridge and permeate water was collected in the permeate reservoir after passing fresh water through the ultrafiltration membrane (Figure 3-5). The permeate was used for the fouling tests. Permeate and filter fluxes were calculated by using Equation 3-2.

$$\boldsymbol{Flux}\ \left(\frac{\boldsymbol{L}}{\boldsymbol{m^2.h}}\right) = \left[\boldsymbol{permeate\ or\ filtered\ flow}\ \left(\frac{\boldsymbol{mL}}{\boldsymbol{min}}\right) \Big/ \boldsymbol{Cartridge\ or\ cross\ sectional\ area}\ (\boldsymbol{m^2})\right] \times \mathbf{0.06}$$

**Equation 3-2**

The cartridge and cross sectional areas were 470 and 180 $cm^2$ for ultrafiltration and the multimedia sand filter, respectively. As it is known, the specific energy is defined as the power per volume and the power is energy divided by time. By replacing energy per volume with pressure, the required energy per volume of produced water can be calculated as shown in Equation 3-3.

$$\textit{Required Energy } (Wh/m^3) = {Pressure\ (Pa)}/{3600}$$

**Equation 3-3**

**Figure 3-5: Module ZeeWeed ZW-1.**

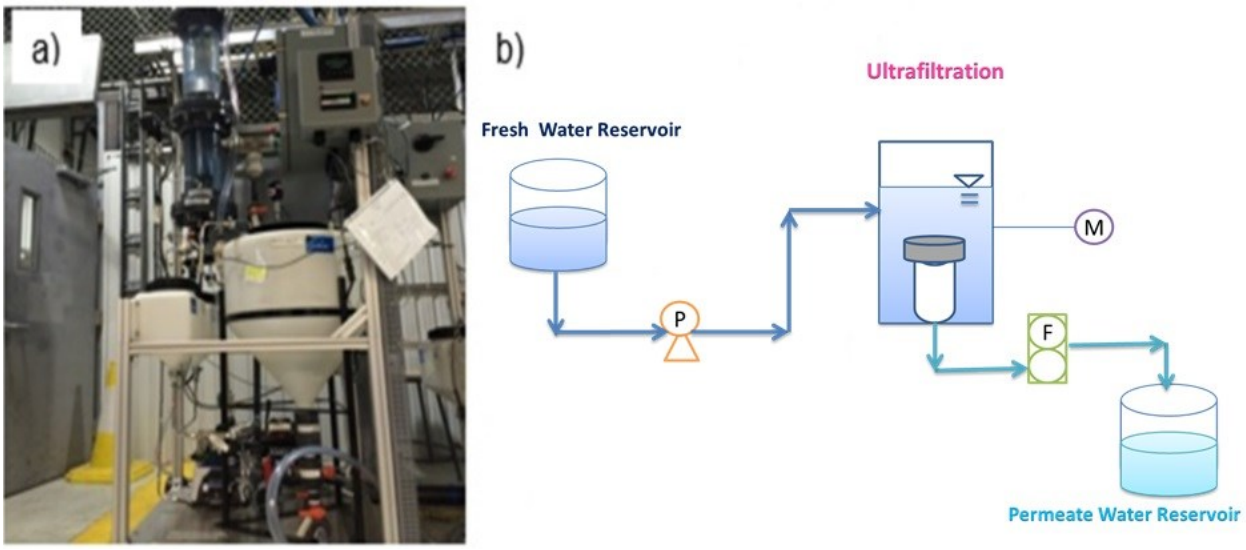


**Figure 3-6: a) Ultrafiltration setup at Hydro-Québec and b) schematic of ultrafiltration bench system.**

**Table 3-4: Materials and equipment in the ultrafiltration bench system (Hydro-Québec, 2013).**

| Material | Quantity | Supplier | Code | Capacity |
|---|---|---|---|---|
| **Pumps** | | | | |
| Feed Pump | 1 | Cole Parmer | 72012-00 | 2 L/min -2 bar (200 kPa) |
| Backwashing Pump | 1 | Cole Parmer | 07528-10 | 60-3600 rpm |
| **Reservoirs** | | | | |
| Reservoir of Permeate water | 1 | Ace | AC-INFD1519 | 50 L |
| Reservoir of Detergents | 2 | Ace | AC-SP002.5RT | 5 L |
| **Sensors** | | | | |
| Manometer | 1 | Swagelok | PGI-63B-PG30-LAQX | 0-30 psi (0-206.84 kPa) |
| Temperature Probe | 1 | Omega | PR-24-3-100-A-1/4-1/4-6 | RTD |
| Flow meter for Liquid | 1 | Omega | FTB331 | 0.03-0.3 LPM |
| Flow meter for Air | 1 | Omega | FTB604B-T | 0-30 LPM |
| **Membrane ZeeWeed** | | | | |
| Cartridge ZeeWeed ZW-1 | 1 | GE/Degrémont | 3080171 | - |

#### 3.3.2.2 Cross Flow Ultrafiltration

Four cross flow hollow fiber ultrafiltration membranes with different MWCOs (100, 300, and 500 kDa) were used in order to compare the performance of the dead-end ultrafiltration and crossflow ultrafiltration for the removal of turbidity, hardness and TOC from water. As the MWCO of the dead-end ultrafiltration was 400 kDa, the average of the obtained results from two crossflow ultrafiltration membranes with MWCOs of 500 and 300 kDa was considered as acquired results from a crossflow ultrafiltration with MWCO of 400 kDa in order to compare both dead-end and crossflow ultrafiltration systems.

### 3.3.3 Microfiltration

Figure 3-7 indicates the experimental setup for microfiltration at LTE Hydro-Québec. Materials and equipment that were used in the microfiltration bench system are demonstrated in Table 3-5. The used membrane was a double open end glass fiber filter cartridge with pore size of 3 microns and filtration area of 0.4 $m^2$. As Figure 3-7 b shows,

water was pumped from the fresh water reservoir to the microfiltration cartridge and permeate water was collected in the permeate reservoir after passing fresh water through the microfiltration membrane. The permeate was used for the fouling tests.

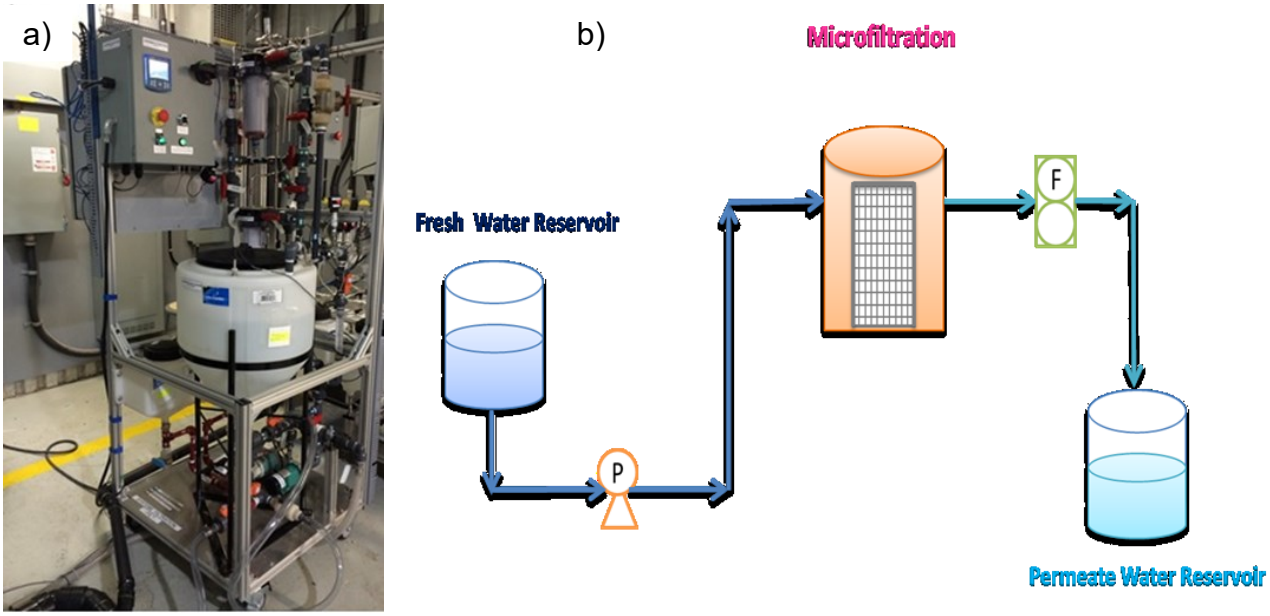


**Figure 3-7: a) Microfiltration setup at Hydro-Québec and b) schematic of microfiltration bench system.**

**Table 3-5: Materials and equipment in microfiltration bench system (Hydro-Québec, 2013).**

| Material | Quantity | Supplier | Code | Capacity |
|---|---|---|---|---|
| **Pumps** | | | | |
| Feed Pump | 1 | Cole Parmer | 72012-00 | 2 L/min -2 bar (200 kPa) |
| Detergent Pump | 1 | Atlantis Pompe Ste-Foy | 147002 Mega/EBARA | 21 L/min - 2 bar (200 kPa) |
| **Reservoirs** | | | | |
| Reservoir of Permeate Water | 1 | Ace | AC-INFD1519 | 50 L |
| Reservoir of Detergents | 2 | Ace | AC-SP002.5RT | 5 L |
| **Sensors** | | | | |
| Manometer | 1 | Swagelok | PGI-63B-PG30-LAQX | 0-30 psi (0-206.84 kPa) |
| Temperature Probe | 1 | Omega | PR-24-3-100-A-1/4-1/4-6 | RTD |
| Flow meter for Liquid | 1 | Omega | FMG3001-PP | 0-3,33 L/min |
| **Filter Cartridge** | | | | |
| 3 micron Filter Cartridge | 1 | Cole Parmer | S-06479-24 | 2.5 in X 10 in (0.0635 m X 0.254 m) |

### 3.3.4 PRO Unit

The used PRO membrane was a thin-film composite (TFC) membrane with hydrophilic support layer provided by Porifera Inc. (Porifera Inc., 2014). In PRO and FO membranes, the pore sizes are usually smaller than the salt molecules to allow only water molecules and not salt to pass through the membrane surface (Lee *et al.*, 2015). The % of salt rejection is generally used to compare these membranes. In this research, the salt rejection % of the used membrane was 99.6% (Porifera Inc., 2014). The active surface area of the membrane was 0.00875 $m^2$. Table 3-6 indicates some specific parameters of the used TFC membrane. The membrane was soaked in deionized water for 15-20 minutes before each PRO experiment (Porifera Inc., 2014). Then the wet membrane was rinsed with deionized water and was placed in the osmotic cell. The skin was faced toward the salt side (Thelin *et al.*, 2013). In the last step, the osmotic cell was connected to the bench system while it was housed in a water bath at constant temperature. Two spacers, one on the fresh side and the other one on the salt side, were placed in the osmotic cell for all PRO tests. The spacers were provided by Filmtec Company. The spacers had a diamond-type mesh with a thickness of 0.9 mm (filament spacing 3 mm).

**Table 3-6: PRO membrane parameters (Porifera Inc., 2014).**

| Parameter | Unit | Value |
|---|---|---|
| Water Permeation (PRO mode) | LMH | 58± 3 |
| Reverse Salt Flux (RSF) | g/L | 0.25± 0.1 |
| Salt Rejection | % | 99.6 ± 0.15 |
| Membrane Structural Parameter | Microns | 215± 30 |
| Maximum Operating Temperature | ℃ | 70 |
| Maximum Transmembrane Pressure | kPa | 1241 |
| pH Operating Range | - | 2-11 |
| Maximum Chlorine | ppm | < 0.1 |

Figure 3-8 demonstrates the PRO membrane setup at Hydro-Québec and Table 3-7 shows the materials and equipment that were used on PRO membrane bench system. As Figure 3-8 part b indicates salt and fresh water were pumped from salt and fresh water reservoirs to the osmotic cell which was placed in a water bath including a temperature probe, then the permeate water was passed through the PRO membrane from the fresh water side to the salt water side.

**Table 3-7: Materials and equipment in the PRO membrane bench system (Hydro-Québec, 2013).**

| Material | Quantity | Supplier | Code | Capacity |
|---|---|---|---|---|
| **Pumps** | | | | |
| Salt and Fresh Water Pumps | 2 | Cole Parmer | EW-07128-10 | 31 mL/min |
| Detergents Pump | 1 | Cole Parmer | EW-07128-25 | 390 mL/min |
| **Reservoirs** | | | | |
| Reservoirs | 2 | Ace | AC-SP0003RT | 10 L |
| **Sensors** | | | | |
| Manometer | 1 | Swagelok | PGI-63B-PG30-LAQX | 0-30 psi (0-206.84 kPa) |
| Pressure Gauge | 1 | Cole Parmer | 68403-00 | 0-30 psi (0-206.84 kPa) |
| Flow meter | 3 | Bronkhorst | Liqui-flow #L23-ABG-22-K | 0-10 mL/min |
| Temperature Probe | 1 | Omega | PR-24-3-100-A-1/4-1/4-6 | RTD |
| **Osmotic Cell** | | | | |
| Osmotic Cell | 1 | Local Fabrication | - | 87.5 $cm^2$ of surface active |
| Water Bath | 1 | Cole Parmer | PD07R-20 | -20 to 150 °C<br>± 0,005 °C<br>reservoir of 7 litres |

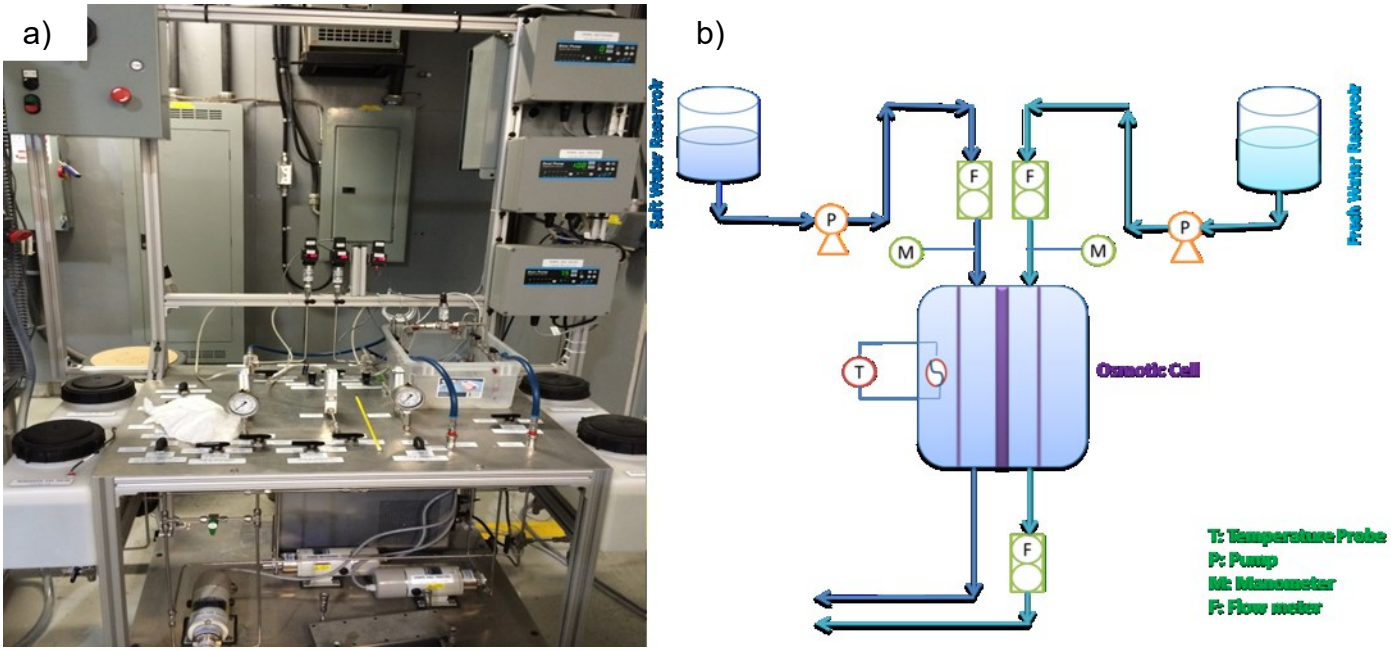


**Figure 3-8: a) PRO membrane setup at Hydro-Québec Research Institute, b) schematic of PRO membrane setup.**

The osmotic cell dimensions are indicated in Figure 3-9. The input and output flow rates of the feed water on the fresh side were measured continuously using two Bronkhorst flow meters (Table 3-7) connected to a computer with a logging interval of one minute or 60 seconds during the PRO experiments in the lab. The difference between these input and output flow rates was measured as the permeate flow rate. Permeate flux was calculated using Equation 3-2. All experiments were performed at Hydro-Québec LTE. Cross flow velocities of 5 cm/s and 4.84 cm/s were applied on the salt and fresh sides, respectively. In recent PRO research, hydraulic pressure was applied on the salt side in a range of 0.48 to 15.4 bar (48 to 1540 kPa) (Achilli *et al.*, 2009; Kim *et al.*, 2012; Saito *et al.*, 2012; She *et al.*, 2012; Chou *et al.*, 2013; Han *et al.*, 2013; Hoover *et al.*, 2013; Kim and Elimelech, 2013; Kim *et al.*, 2013; She *et al.*, 2013; Bui and McCutcheon, 2014; Li and Chung, 2014). In this research the applied hydraulic pressure on the salt side was 3

bar (300 kPa) due to the device limitation. The initial conditions such as pressure, temperature, synthetic salt concentration, and sea water salt concentration were constant for all fouling experiments and were 300 kPa (3 bars), 25℃, 30 g/L respectively.

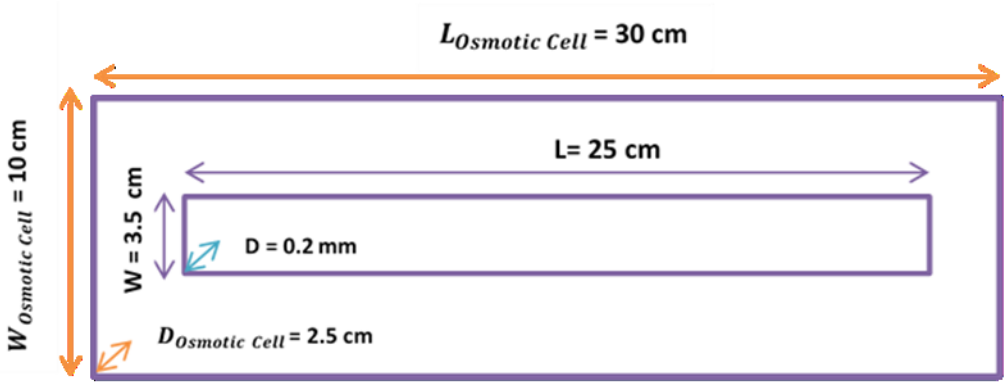


**Figure 3-9: Osmotic cell dimensions.**

Figure 3-10 indicates the procedure for performing the tests. After collecting the river water, water from the reservoir passes through the sand filter and the ultrafiltration system. The river water before and after filtration was collected to do the analyses. The permeate and filtered waters were used as feed waters in PRO system and the outlets of the PRO system were discharged into a waste disposal system in the lab at Hydro-Quebec.

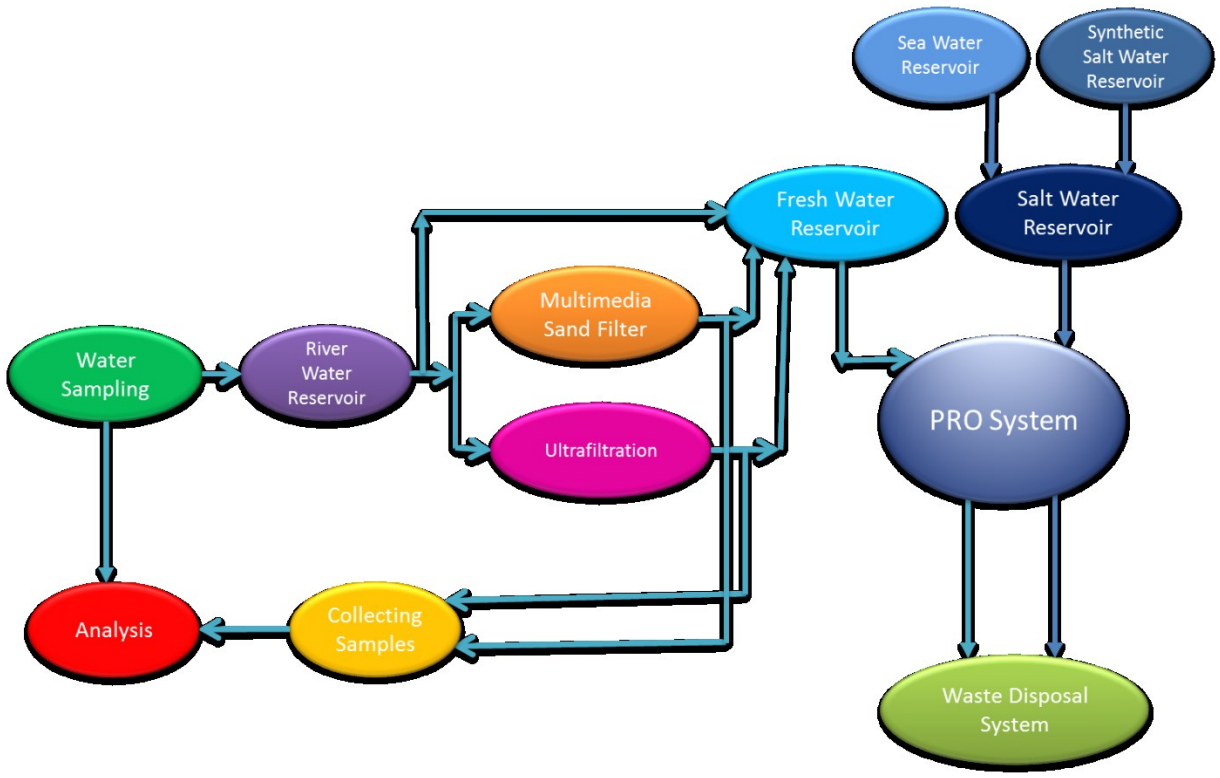


**Figure 3-10: Procedure for performing the experiments.**

### 3.3.5 Overall Efficiency of Osmotic Power Plant

Figure 3-11 indicates the main parts of a PRO power plant including pretreatment, membrane module, pressure exchanger that pressurizes the input sea water, and turbine. The output power from an osmotic power plant depends on the amount of loads and losses in different parts of the plant such as pretreatment, pressure exchanger, pickup heads on the feed and draw sides, and turbine and generator.

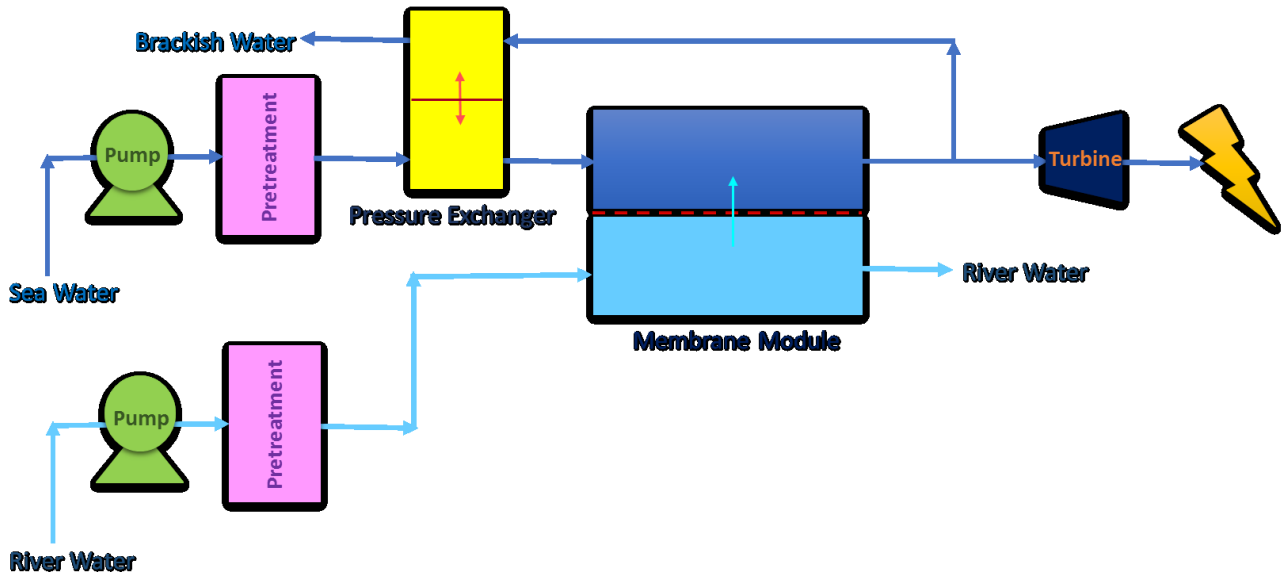


**Figure 3-11: PRO power plant diagram**

The overall efficiency of the osmotic power plant was calculated using Equation 3-4.

$$\eta = \frac{W_{net}^{e}}{W_{max}} \times 100 \qquad \textbf{Equation 3-4}$$

Where $\eta$ (%) is the overall efficiency, $W_{net}^{e}$ (W/$m^2$) is the net electrical power that can be harvested from the osmotic power plant, and $W_{max}$ (W/$m^2$) is the maximum power that can be extracted from the osmotic power plant under ideal conditions (neglecting the losses in the system). The maximum power can be exploited, when the applied pressure is equal to half of the difference in osmotic pressure between two sides of a membrane and is calculated using Equation 3-5 (Ramon *et al.*, 2011).

$$W_{max} = A_w . (\Delta\pi/_2)^2 \qquad \textbf{Equation 3-5}$$

$$\pi = 100\ (A_\pi C_s + B_\pi C_s^{3/2} + C_\pi C_s^2) \qquad \textbf{Equation 3-6}$$

$$A_\pi = 0.70249 + 2.3938 \times 10^{-3}T - 3.7170 \times 10^{-6}T^2$$ **Equation 3-7**

$$B_\pi = -2.1601 \times 10^{-2} + 4.8460 \times 10^{-6}T - 1.0492 \times 10^{-6}T^2$$ **Equation 3-8**

$$C_\pi = 2.7984 \times 10^{-3} + 1.5520 \times 10^{-5}T - 2.7048 \times 10^{-8}T^2$$ **Equation 3-9**

Where $A_w$ ($\frac{m^3}{Pa.s.m^2}$) is the water permeability and was equal to $11.7 \times 10^{-12}$ according to the reported results by Maisonneuve (2015) and $\Delta\pi$ (Pa) is the difference of osmotic pressure between two sides of the membrane which was calculated using equations (3-6 to 3-9) where T was temperature (℃) and $C_s$ was salt concentration ($^{kg}/_{m^3}$) . Equation 3-6 is valid for temperatures between 10-40 ℃ and a salt concentration in the range of 0-40 $^{kg}/_{m^3}$ (Millero and Wing, 1976). In order to calculate $W_{net}^e$ the following equations (3-10 to 3-16) were used (Maisonneuve, 2015).

$$W_{net}^e = W_{gross}^e - \sum W_{pumps}^e$$ **Equation 3-10**

$$W_{gross}^e = W_{gross}^{PRO} . \eta_{turbine} . \eta_{generator}$$ **Equation 3-11**

$$W_{gross}^{PRO} = J_w . \Delta P$$ **Equation 3-12**

$$\sum W_{pumps}^e = W_{F,pump}^e + W_{D,pump}^e + W_{PX,pump}^e$$ **Equation 3-13**

$$W_{F,pump}^e = \frac{\left(P_{F,drop} + P_{F,pretreatment} + P_{F,pickup}\right) \times J_F}{\eta_{pump} . \eta_{motor}}$$ **Equation 3-14**

$$W_{D,pump}^e = \frac{\left(P_{D,pretreatment} + P_{D,pickup}\right) \times J_D}{\eta_{pump} . \eta_{motor}}$$ **Equation 3-15**

$$W_{PX,pump}^e = \frac{\left[\left(P_{D,drop} + \Delta P . (1 - \eta_{px})\right)\right] \times J_D}{\eta_{pump} . \eta_{motor}}$$ **Equation 3-16**

Where $W^{e}_{gross}$ (W/$m^2$) is the gross electric power, $W^{e}_{pumps}$(W/$m^2$) is the power that is consumed by the electric pumps on the feed side, draw side, and pressure exchanger, $W^{PRO}_{gross}$ (W/$m^2$) is the available power at the inlet to the turbine, $W^{e}_{F,pump}$, $W^{e}_{D,pump}$, and $W^{e}_{PX,pump}$ (W/$m^2$) are losses on the feed side, draw side and pressure exchanger respectively. $P_{F,pretreatment}$ and $P_{D,pretreatment}$(Pa) are the pressure loads in pretreatment on feed and draw sides. $P_{F,pickup}$ and $P_{D,pickup}$ (Pa) are pick up heads on feed and draw sides. $P_{F,drop}$ and $P_{D,drop}$ (Pa) are losses on the feed and draw sides of the membrane. $\eta_{pump}.\eta_{motor}$ are the pump and motor efficiencies. $\eta_{turbine}.\eta_{generator}$ are turbine and generator efficiencies. $J_F$ and $J_D$ ($\frac{m^3}{s.m^2}$) are the water fluxes on the feed and draw sides.

Table 3-8 shows the assumptions that were made for the overall efficiency calculations. Also, the pick-up heads on the feed and draw sides and losses for pretreatment on the draw side were considered as zero.

**Table 3-8: Assumptions for calculating the overall efficiency of the osmotic power plant (Maisonneuve, 2015).**

| Parameters | Values |
|---|---|
| Turbine and Generator Efficiencies | 0.85 |
| Pump and Motor Efficiencies | 0.77 |
| Pressure Exchanger Efficiency | 0.97 |

### 3.3.6 Operating Conditions

Operating conditions such as temperature, pressure, and salt concentration have a critical influence on the performance of the PRO membranes. Therefore, the effect of these

operating conditions on the permeate flux should be evaluated. To understand the effect of temperature on permeate flux, various ranges of temperature (5, 10, 15, 20, 25, and 30℃) were used for both FO and PRO modes when pressure and salt concentration were fixed at 300 kPa in PRO mode and 30 g/L respectively. To investigate the effect of pressure on permeate flux, different pressures such as 0, 300, 600, and 900 kPa were applied while the salt concentration (30 g/L) and temperature (25℃) were constant. In order to study the effect of salt concentration on permeate flux, various ranges of salt concentrations (10, 20, 30, 40, 50, 60 g/L) were studied at constant pressure (300 kPa) and temperature (25℃).

It is important to determine the maximum power that can be harvested from the available PRO membrane. Therefore, different pressures (0, 300, 600, and 900 kPa) were applied to observe the effect of these different pressures on the permeate flux. The power density is the generated power divided by the surface area of the membrane and power is a function of flow rate and pressure. Power density was calculated using Equation 3-17 (Achilli and Childress, 2010; She *et al.*, 2012; Li and Chung, 2014; Altaee and Sharif, 2015) which is as follows:

$$\boldsymbol{W = J_w . \Delta P} \qquad \textbf{Equation 3-17}$$

Where:

W: Power density (W/$m^2$)

$J_w$: PRO membrane permeate flux ($\frac{m^3}{m^2 . s}$)

$\Delta P$: Differential hydraulic pressure across the membrane (Pa)

### 3.3.7 Membrane Fouling

In terms of studying fouling phenomena in the PRO membrane, four different feed waters including untreated water (river water), permeate water from ultrafiltration system, filtered water from multimedia sand filter, and permeate water from microfiltration system were used to perform the fouling tests at fixed pressure, temperature and salt concentration (synthetic salt water, sea water) of 300 kPa, 25℃, and 30 g/L respectively. In this research, for simplification, these four feed waters were mentioned as untreated water, ultrafiltration, multimedia sand filter, and microfiltration waters, respectively. In order to study the fouling of the PRO membrane, different draw solutions such as synthetic salt water and sea water were used. The initial conditions such as pressure, and temperature (300 kPa, and 25℃) were the same for both draw solutions. The baseline test was also done to show the decrease of the permeate flux without foulants (flux of the unfouled membrane). In the baseline test, the feed water was deionized water and draw solution was synthetic salt water.

### 3.3.8 Fouling Mechanisms

It is important to investigate and identify the fouling mechanisms to identify a better cleaning method and also reduce the frequency of the fouling. Hermans and Bredée (1935) proposed four fouling models (cake fouling (CFM), standard blocking (SBM), complete blocking (CBM) and intermediate blocking (IBM)) for investigation of the membrane fouling mechanisms (Hermia, 1982; Bolton *et al.*, 2006; Londono, 2011; Rezaei *et al.*, 2011). These well-known and extensively used models were utilized in order to investigate the fouling behavior of the membrane in PRO mode. In all fouling tests, the

decline in permeate flux over time at constant pressure (3 bars or 300 kPa) was studied. The equations for permeate flow rate at constant pressure are summarized in Table 3-9. As using linearized forms are more suitable for data analysis and model identification (Reis and Zydney, 2007; Rezaei *et al.*, 2011), the linearized forms of these models were used in this research.

**Table 3-9: Four constant pressure fouling models (Rezaei *et al.*, 2011).**

| Fouling Mechanisms | Flux Equations | Linearized Forms |
|---|---|---|
| Complete Blocking (CBM) | $\frac{Q}{Q_0} = \exp(-\beta t)$ | $Ln\ Q = at + b$ |
| Intermediate Blocking (IBM) | $\frac{Q}{Q_0} = (1+\beta t)^{-1}$ | $\frac{1}{Q} = at + b$ |
| Standard Blocking (SBM) | $\frac{Q}{Q_0} = (1+\beta t)^{-2}$ | $\frac{t}{V} = at + b$ |
| Cake Filtration (CFM) | $\frac{Q}{Q_0} = (1+\beta t)^{-0.5}$ | $\frac{t}{V} = aV + b$ |

The difference of squared regression ($R^2$) was used as an index to investigate the agreement of the experimental data with the used model. This means that when the $R^2$ is equal to one, the experimental data is completely in agreement with the used model. The equations for permeate flow rate in two forms (linearized and non-linearized) are presented in Table 3-9. It should be noted that a, b and β parameters mentioned in Table 3-9 are constant.

### 3.3.9 Foulant Identification

To remove, control and clean the PRO membrane, it is necessary to determine the type of foulants that cause the fouling. The inorganic characterization of foulants was done by using scanning electron microscope (SEM) and energy dispersive spectroscopy (EDS)

(Hitachi 4300) of the membrane samples before and after fouling. Membrane samples were totally dried at room temperature (23 ℃) before using SEM-EDS for the accuracy of the analyses. Attenuated Total Reflection Fourier Transform Infrared (ATR-FTIR) spectroscopy was used to determine the type of organic foulants on the surface of the membrane samples that were collected after complete fouling using the four different feed waters (Table 3-2) and the two various draw solutions. Each spectrum demonstrated is the result of 1024 scans. Background was collected for each sample separately. The membrane samples were dried prior to analysis. ATR-FTIR spectra were recorded inside the range of 4000–650 $cm^{-1}$. For organic characterization, Attenuated Total Reflectance-Fourier Transform Infrared Spectroscopy (ATR-FTIR) (Nicolet 6700) was used at the Loyola Campus, Concordia University.

### 3.3.10 Membrane Cleaning Procedure

In both physical and chemical cleaning methods, the used draw solution was sea water and the used fresh water was prepared from an ultrafiltration system. The water flux recovery was calculated using Equation 3-18.

$$Water\ Flux\ Recovery\ (\%) = \left(\frac{J_w - J_{fw}}{J_{iw} - J_{fw}}\right) \times 100 \qquad \textbf{Equation 3-18}$$

Where $J_w$ is the water flux after cleaning, $J_{fw}$ is the water flux after fouling, and $J_{iw}$ is the water flux before fouling (Wei *et al.*, 2010).

#### 3.3.10.1 Physical Cleaning:

In this method, demineralized water was used to rinse the membrane once a week. The duration of each flushing was 40-45 minutes. Both sides of the membrane were flushed

during the process. The surface velocities on both sides were the same and the inlet flow rates on both sides were 60 mL/min.

#### 3.3.10.2 Chemical Cleaning:

For chemical cleaning of the membrane, a combination of acidic and basic cleaners was used due to the type of foulants. The acidic and basic cleaners were AM-11 (Trade Secret) and Lavasol (potassium hydroxide) that were provided by Applied Membranes Inc. and Professional Water Technologies Inc. respectively. Both sides of the membrane (fresh and salt sides) were cleaned during the process. The temperature was fixed at 35 ℃ using a water bath (Table 3-7) and the surface velocities on both sides were the same. The inlet flow rates on both fresh and salt sides were 60 mL/min. The cleaning process was performed once a week from when the experiment was started. Both cleaners were designed to remove foulants from thin film composite membranes (TFC). The basic and acidic solutions were prepared according to the instructions provided by the companies (Professional Water Technologies Inc, 2011; Applied Membranes Inc, 2015). The used water for preparing the solutions was demineralized water. First, the basic solution was circulated through the system for two hours and then the system was rinsed with demineralized water for 30 minutes. In the next step, a prepared acidic solution was circulated through the system for two hours. Finally, the system was flushed with demineralized water until the pH was almost the same as the pH of the demineralized water.

# 4 Results and Discussion

## 4.1 Introduction

This chapter includes the results regarding the physiochemical characteristics of the raw water, pretreatment of fresh water including ultrafiltration and sand filter, the efficiency of the PRO power plant in terms of using different pretreatment methods, membrane fouling experiments in continuous mode, fouling mechanisms, identification of the types of foulants, and membrane cleaning methods.

## 4.2 Physicochemical Characteristic of Raw Water

The quality of the raw water before and after filtration was examined in order to determine the amount of parameters such as turbidity, hardness, and total organic carbon (TOC) for each batch of raw water that was brought to LTE Hydro-Québec during winter and spring in 2014. These parameters are important in membrane fouling. The used raw water in all experiments was from the Saint-Maurice River. The results for the rest of the parameters are presented in the appendix.

### 4.2.1 Silt Density Index (SDI)

SDI is an empirical parameter that indicates the fouling potential of a feed water stream (Alhadidi *et al.*, 2011). Figure 4-1 demonstrates the results for $SDI_{15}(500\ mL)$ during the spring and winter in 2014. As Figure 4-1 shows the average amount of $SDI_{15}(500\ mL)$ in spring was higher than in winter. This occurs due to the increase in runoff in spring

compared to winter. The maximum and minimum amounts of $SDI_{15}(500\,mL)$ were 19.2 and 10.3 during these two seasons respectively.

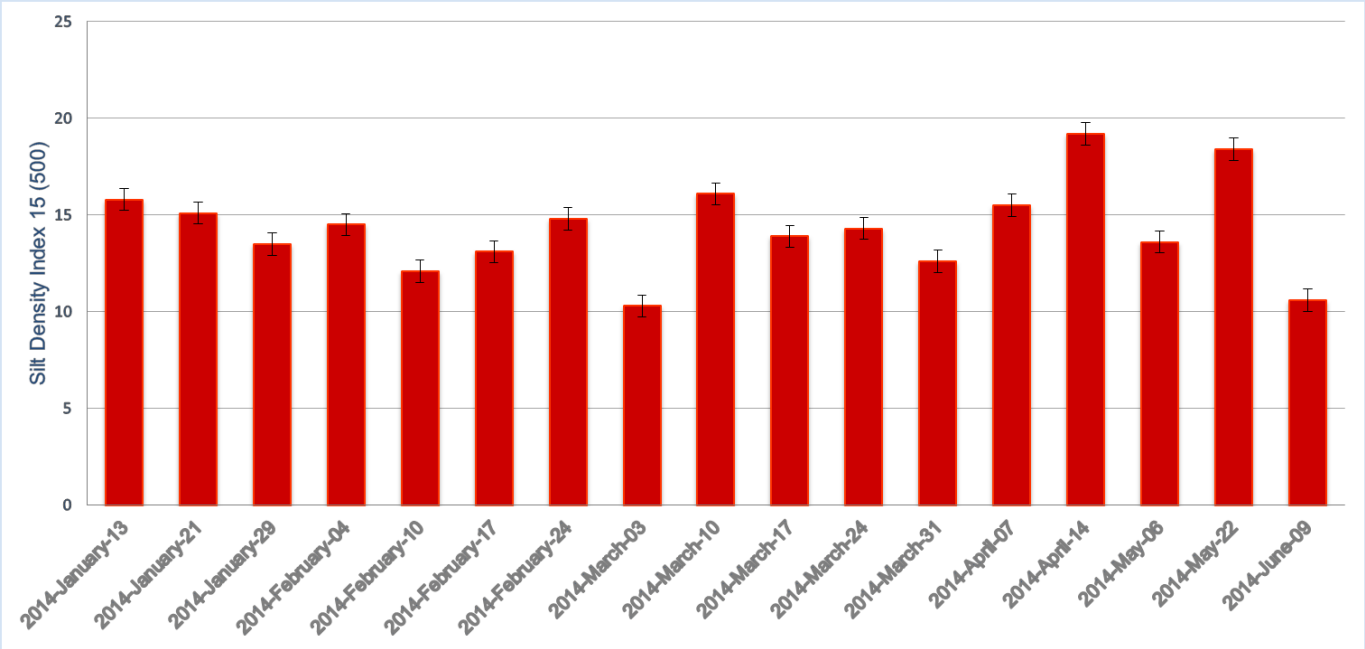


**Figure 4-1: Changes in SDI in winter and spring (Saint-Maurice River).**

Practically, the SDI for osmosis membranes must be lower than 3 to avoid fouling and if it becomes more than 4 or 5 then pretreatment is required (Alhadidi *et al.*, 2011). However, as the results in Figure 4-1 indicate, the amount of SDI at its lowest amount was 10.3, which is much higher than 5. This means that the potential of this water for membrane fouling is significantly high and pretreatment should be used for reducing and controlling the membrane fouling.

### 4.2.2 Total Organic Carbon (TOC)

The results for TOC were monitored during the winter and spring of 2014. Figure 4-2 shows the changes of TOC throughout these two seasons. As Figure 4-2 demonstrates,

the TOC concentration in the spring is more than that in the winter. TOC ranged from 4.4 to 6.4 mg/L in winter and varied from 4.77 to 10.44 mg/L in the spring. The reason can be related to the amount of runoff in the spring which is higher than winter. The surface runoff picks up and transports natural organic matter from the ground or earth's surface into the rivers, lakes. etc.

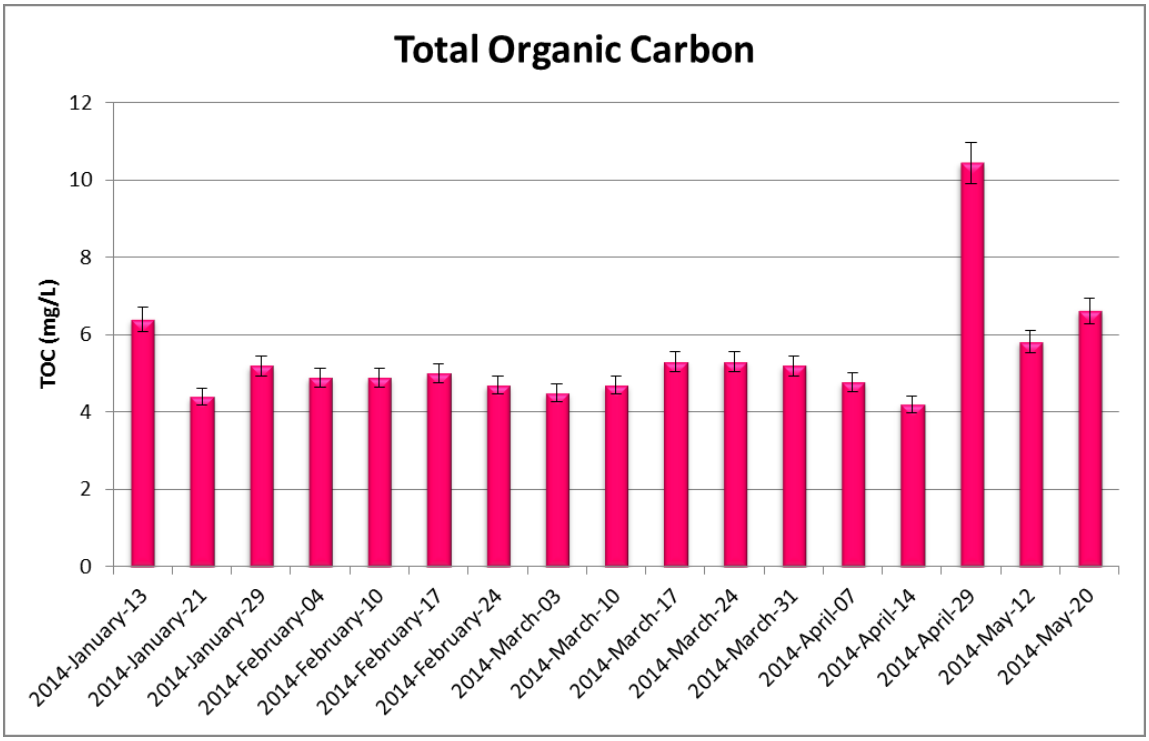


**Figure 4-2: Changes in TOC in winter and spring (Saint-Maurice River).**

However, surface waters such as rivers and lakes are surrounded by snow and ice and this prevents the increase of the NOMs in rivers and lakes in the winter.

### 4.2.3 Turbidity

Turbidity of the raw water (Saint Maurice River) was measured during the winter and spring. As Figure 4-3 indicates, the average amount of turbidity in the spring is higher

than in the winter. It changed from 0.55 to 3.2 NTU in the winter and fluctuated between 0.74 and 3.72 NTU in the spring. The reason is similar to what it was explained for TOC in the previous section.

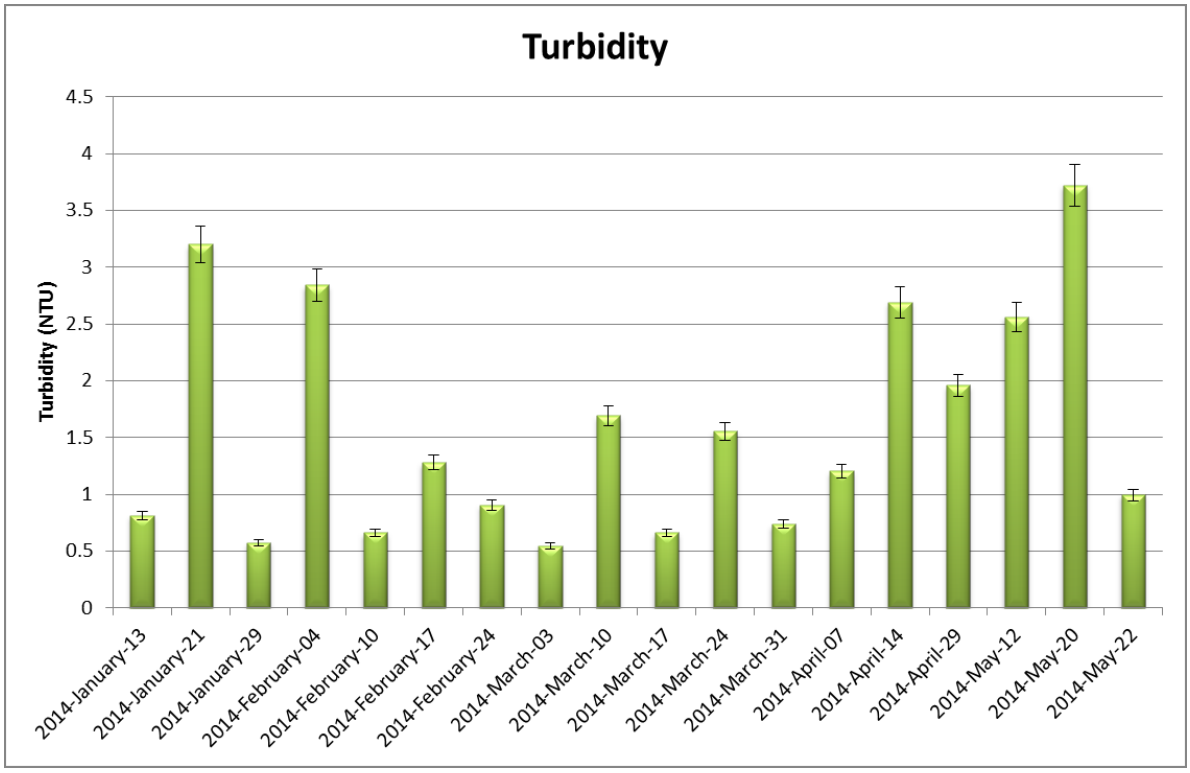


**Figure 4-3: Changes of turbidity in winter and spring (Saint-Maurice River).**

Based on the demonstrated results in Figure 4-3, the turbidity of the raw water in some batches of water samples is more and this indicates that an increased number of particles exist in the water that can increase the membrane fouling potential.

### 4.2.4 Hardness

The other parameter that plays an important role in the fouling and scaling of the membrane is hardness. This parameter was monitored during winter and spring 2014. As Figure 4-4 shows, the amount of hardness in the winter was higher compared to its

amount in spring. It ranged from 8 to 12 mg/L as $CaCO_3$ in winter and changed from 4 to 10 mg/L as $CaCO_3$ in spring. The hardness decrease in the spring is the result of surface runoff that occurs during this season and is diluted in the river waters. This reduces the concentration of multivalent cations such as calcium and magnesium ions in the water.

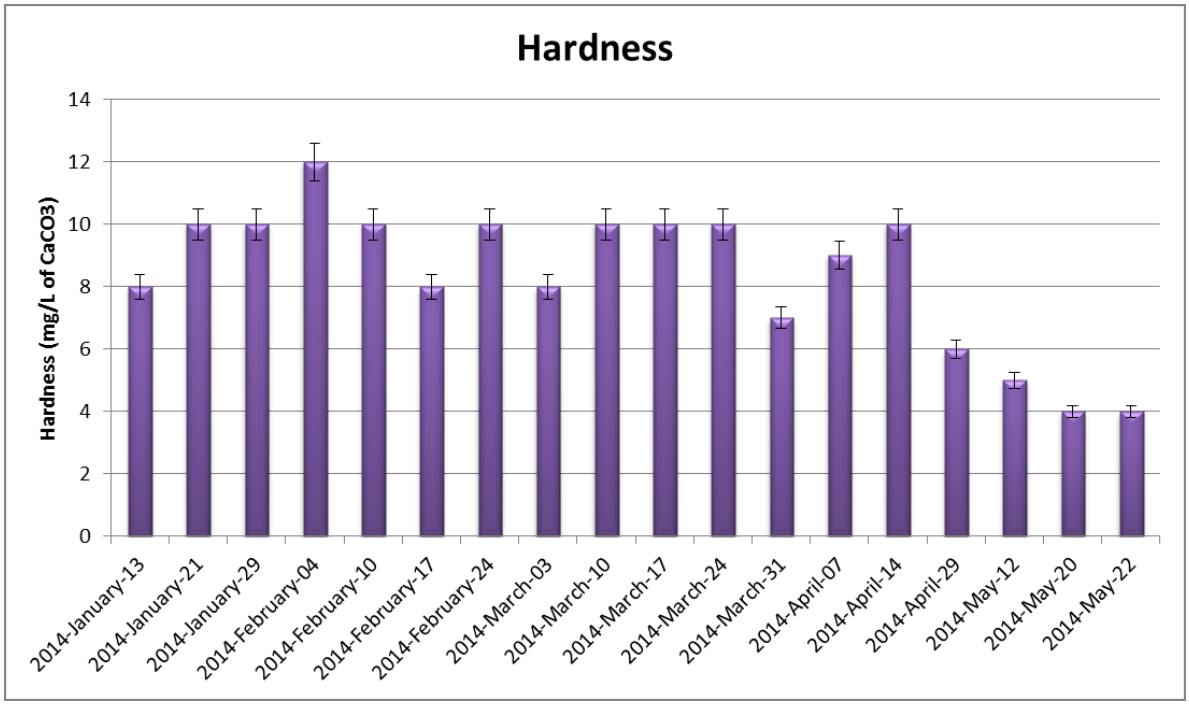


**Figure 4-4: Changes of hardness in winter and spring (Saint-Maurice River).**

Based on the U.S. Environmental Protection Agency (USEPA), when the amount of hardness in surface water is between 0 and 75 mg/L as $CaCO_3$ it is considered as a soft water (without hardness) (EPA, 1986). As the results indicate, the concentration of the hardness for water samples for both seasons was significantly lower than its regulated concentration. This means that the membrane fouling and scaling potential due to the hardness is not very high.

## 4.3 Pretreatment

As it was mentioned in the previous section, pretreatment plays an important role in the quality of the feed water that enters the PRO membrane and helps control membrane fouling and as a result reduces the amount of required energy in the PRO membrane system. In the pretreatment study, two different pretreatment methods including ultrafiltration and multimedia sand filter were investigated. The quality of the raw water before and after filtration was examined in order to determine the amount of parameters such as turbidity, hardness, and total organic carbon (TOC) for each batch of raw water that was brought to LTE Hydro-Québec during winter and spring in 2014. These parameters are important in membrane fouling. The used raw water in all experiments was from the Saint-Maurice River.

### 4.3.1 Efficiency of Ultrafiltration and Multimedia Sand Filter in Removal of TOC

As total organic carbon (TOC) has a significant effect in causing the membrane fouling, its amounts before and after using ultrafiltration and multimedia sand filter were measured in order to compare the performance of these two pretreatment methods in removal of this parameter. This experiment was done at pH of 6-8 and room temperature at 23± 0.5 ℃. Four different batches of river water with different initial concentrations of TOC (4.77, 5.3, 5.83, and 6.62 mg/L) were used. These initial concentrations were the average (mean) of the three measurements and their standard deviations were 0.08, 0.11, 0.07, and 0.08 for the initial concentrations of 4.77, 5.3, 5.83, and 6.62 mg/L, respectively.

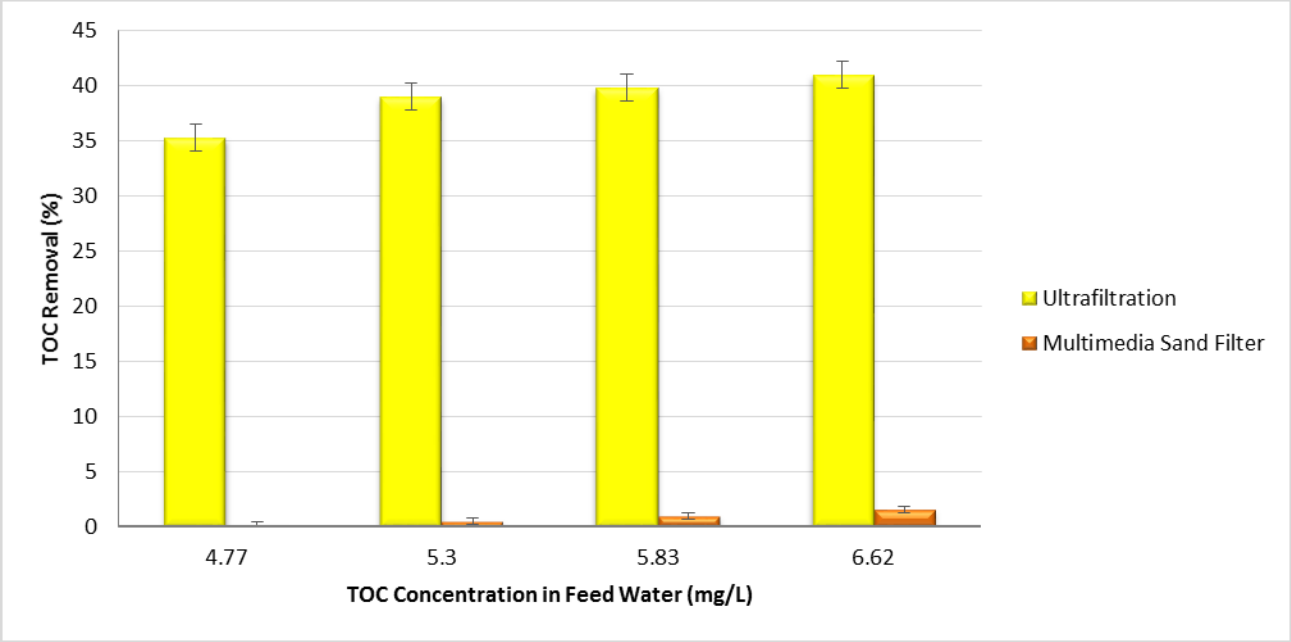


**Figure 4-5: TOC removal in ultrafiltration and multimedia sand filter**

Figure 4-5 demonstrates a comparison between ultrafiltration and multimedia sand filter for removal of TOC. It is clear that the removal efficiency of TOC in ultrafiltration is much higher than that in the multimedia sand filter. This means the amount of TOC in permeate water was much less than its amount in the feed water in ultrafiltration compared to the multimedia sand filter. Maximum TOC removal efficiency occurred at 6.62 mg/L of TOC and it was 41% in ultrafiltration which was higher than the TOC removal efficiency (27%) reported by Wan and Chung in 2015 (Wan and Chung, 2015). They used a dead-end flat sheet ultrafiltration system as a pretreatment for osmotic power generation while a dead-end hollow fiber ultrafiltration system was used in this study. The maximum TOC removal efficiency was 1.5% at the 6.62 mg/L of TOC in multimedia sand filter.

### 4.3.2 Efficiency of Ultrafiltration and Multimedia Sand Filter in Removal of Turbidity

In this experiment, the performance of ultrafiltration and multimedia sand filter for the removal of turbidity was investigated. The initial conditions including temperature and pH were the same as previous experiments (studying the TOC) for both methods. Five different batches of river water with different initial amounts of turbidity (0.74, 0.91, 1.55, 2.56, and 3.72 NTU) were used. According to the demonstrated results in Figure 4-6, the ability of the ultrafiltration method for removal of turbidity was significantly higher in comparison with the multimedia sand filter. Maximum removal efficiency of turbidity occurred at 3.72 NTU of turbidity and it was 100% and 68.6% for ultrafiltration and the multimedia sand filter, respectively.

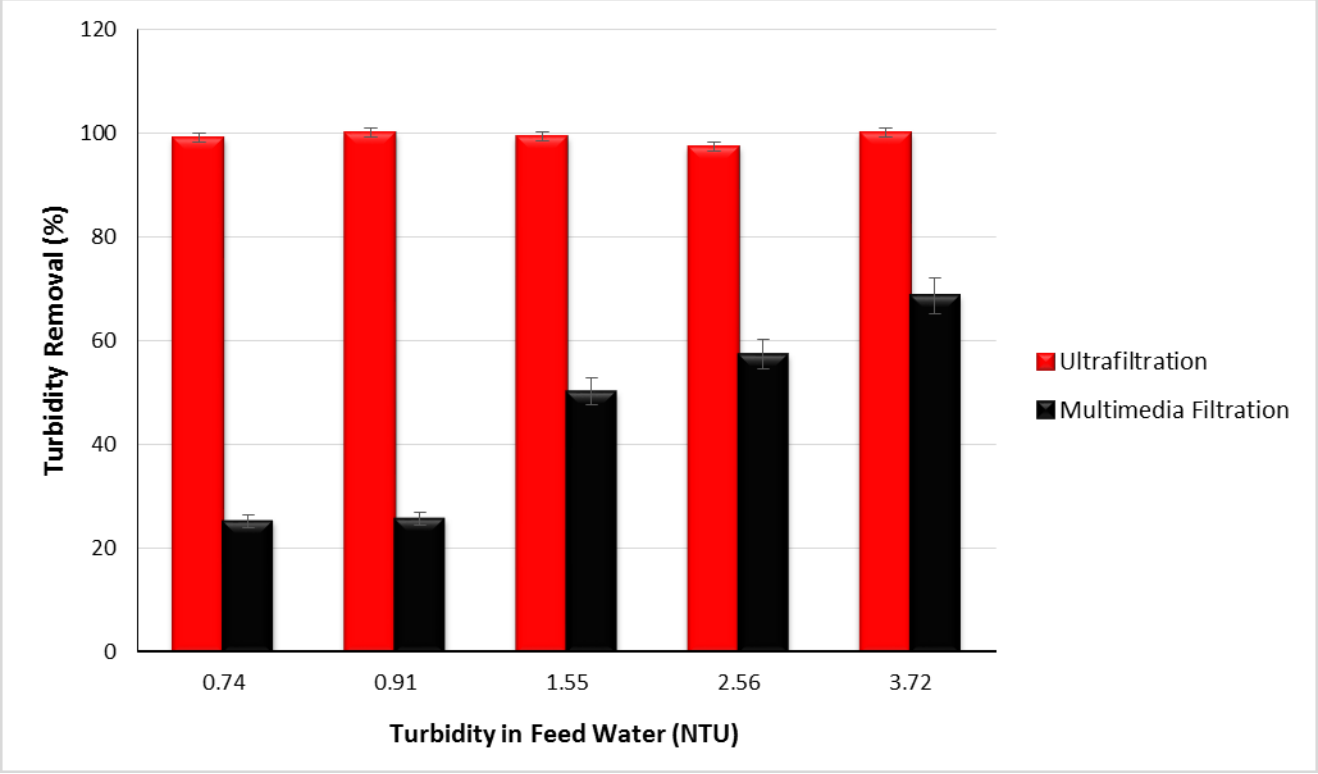


**Figure 4-6: Turbidity removal in ultrafiltration and multimedia sand filter**

As Figure 4-6 shows, the removal efficiency in the multimedia sand filter increases with turbidity in the feed water while the removal efficiency of turbidity in ultrafiltration is almost 100% for all amounts of turbidity in the feed water.

### 4.3.3 Efficiency of Ultrafiltration and Multimedia Sand Filter in Removal of Hardness

As it is known, hardness is generally removed by chemical addition. In this experiment, the aim was to examine and compare the role of ultrafiltration and multimedia sand filter in removal of hardness. The initial conditions such as pH, temperature and pressure were the same for both methods during the experiment. Four different batches of river water with different initial concentrations of hardness (4, 6, 8, and 10 mg/L as $CaCO_3$) were used. As Figure 4-7 shows, by increasing the amount of hardness, its removal increases in multimedia sand filter while a different behaviour was observed for removal of hardness in ultrafiltration.

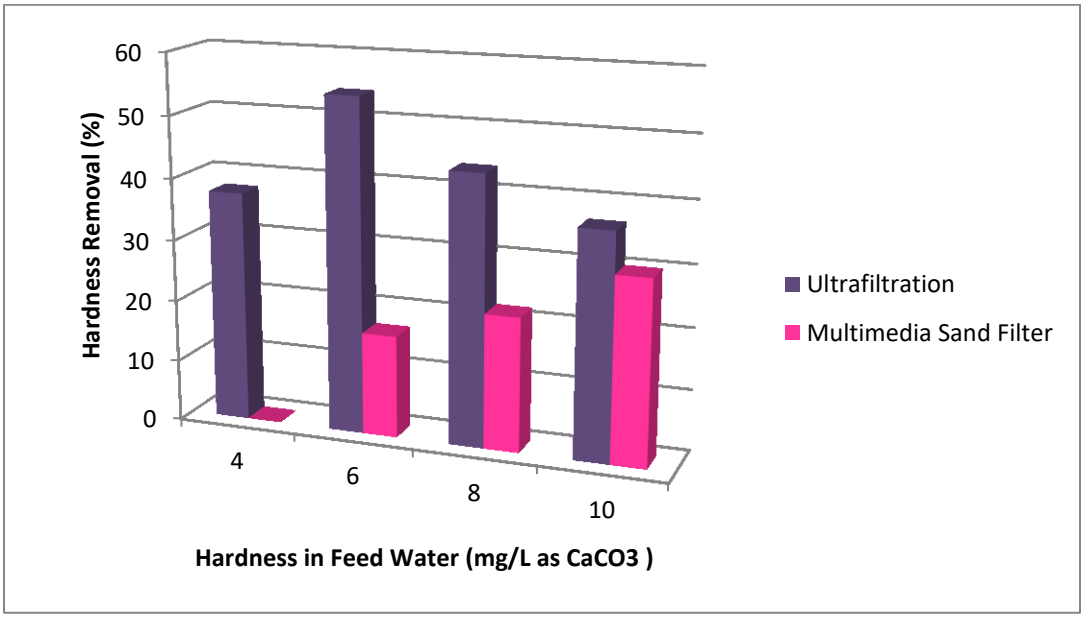


**Figure 4-7: Hardness removal in ultrafiltration and the multimedia sand filter**

Removal of hardness reaches its maximum amount at 6 mg/L as $CaCO_3$ which was 54.2% and then it decreases to 36.7% at 10 mg/L as $CaCO_3$. However, the minimum removal of hardness in ultrafiltration (36.7%) is still higher than its maximum amount obtained by the multimedia sand filter (30%). Since the removal of hardness as calcium carbonate is difficult to achieve by using the filtration methods, this result raises some doubts about the removal of hardness by using ultrafiltration and the multimedia sand filter. This behavior related to hardness might be linked to the amount of iron in the raw water which was 0.75 mg/L. Iron exists in the water as $Fe^{2+}$ and when it interacts with the atmospheric oxygen at the water surface, ferrous iron ($Fe^{2+}$) is oxidized to ferric iron ($Fe^{3+}$) and as a result, ferric hydroxide is produced and precipitated in the water (Nazarenko and Zarubina, 2013). As seen in the following reactions (Elazher *et al.*, 2008), oxidization of the iron was stopped due to its precipitation and its removal as the hardness by ultrafiltration and multimedia sand filter.

$$\mathbf{4\,Fe^{2+} + O_2 + 4H_3O^{+} \rightarrow 4\,Fe^{3+} + 6\,H_2O} \qquad \textbf{Equation 4-1}$$

$$\mathbf{4Fe^{3+} + 12\,OH^{-} \rightarrow 4\,Fe(OH)_{3_s}} \qquad \textbf{Equation 4-2}$$

### 4.3.4 Effect of Pressure on Permeate and Filter Fluxes

In this experiment, the influence of transmembrane pressure (TMP) and water pressure on permeate and filter fluxes were investigated in ultrafiltration and multimedia sand filter respectively. Temperature and pH were room temperature 23 ±0.5℃ and 6-8 during this experiment. At the beginning, TMP and water pressure were 17.7 and 20.7 kPa respectively. The selection of these values was based on some limitations for working

with the two systems. Both, TMP and water pressure were measured by Swagelok manometers. The experiment was run for 15 hours for both pretreatment methods.

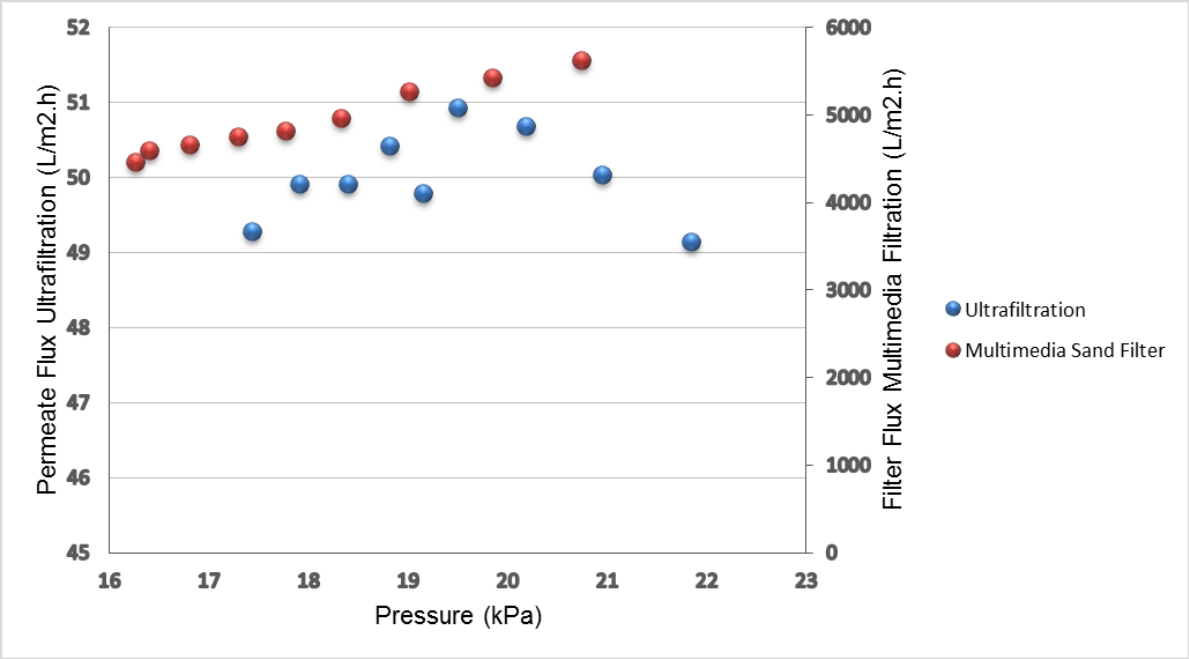


**Figure 4-8: Effect of pressure on permeate flux and filter fluxes in ultrafiltration and multimedia sand filter.**

As Figure 4-8 indicates, there is a positive correlation between pressure and filter flux in the multimedia sand filter. In other words, when the pressure of water above the media decreases, the filter flux decreases as well. Also Figure 4-8 shows that over time in ultrafiltration, when the pressure increases, the permeate flux increases too and reaches its maximum amount at 19.5 kPa, but after this point, by increasing the pressure, the permeate flux decreases and this means the fouling was about to occur. In other words, by increasing the pressure in ultrafiltration systems, permeate flux increases correspondingly (Wijmans *et al.*, 1985; Arthanareeswaran *et al.*, 2007; Abbasi-Garravand and Mulligan, 2014). However, fouling causes a resistance against passing water through the membrane and consequently the permeate flux decreases regardless of the increase

of pressure. The lowest fluxes occurred at pressures of 21.8 kPa and 16.2 kPa and the highest fluxes occurred at pressures of 19.5 kPa and 20.7 kPa in ultrafiltration and multimedia sand filter, respectively.

### 4.3.5 Required Specific Energy for Ultrafiltration and Multimedia Sand Filter

The aim of this experiment was to study and compare the specific energy that is needed for operation of the ultrafiltration and multimedia sand filter. Both systems were operated at room temperature which was 23 ±0.5℃. To calculate the required specific energy, flowrate and pressure in ultrafiltration system were measured every 30 minutes by using flowmeters and manometers that were mentioned in the previous experiments (section 3.3.2). The required energy was calculated using Equation 3-3.

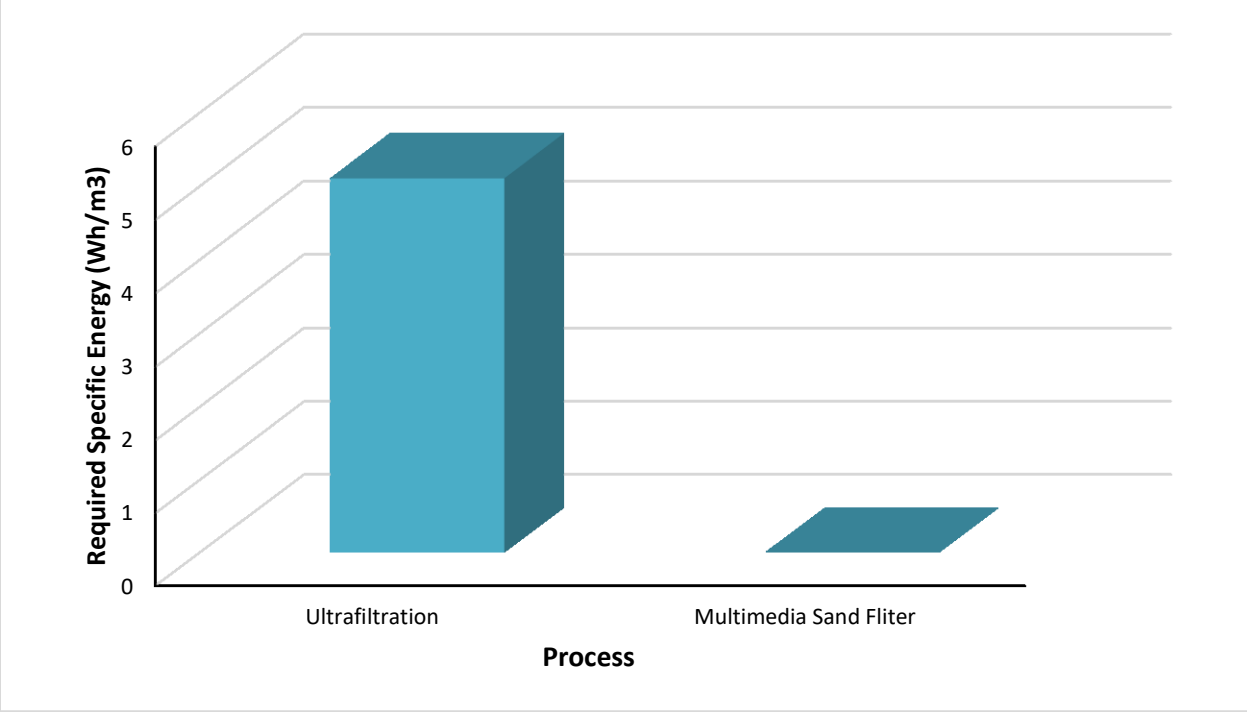


**Figure 4-9: Required power for ultrafiltration and multimedia sand filter.**

As the multimedia sand filter is a gravimetric filter, its required external pressure (e.g. from pumps) was zero. As Figure 4-9 indicates, the required specific energy for multimedia sand filter was zero and it occurred due to the nature of multimedia sand filter which was a gravimetric and non-pressurized filter. This means when the pressure is zero, no power and energy is required and subsequently, the cost decreases as well. In addition, Figure 4-9 demonstrates the average amount of required specific energy for ultrafiltration which was 5.1 $^{Wh}/_{m^3}$ of the permeate water at a range of pressure from 16.7 kPa to 19.2 kPa. Since the osmotic power generation process must be cost effective when it can provide the required electrical energy for the pretreatment section by itself, it seems that the multimedia sand filter is a better option from an investment point of view compared to ultrafiltration for the pretreatment due to its lower cost. However, it has much less purification performance compared to ultrafiltration and this can decrease the power density and PRO membrane efficiency and consequently decreases the overall efficiency of the PRO power plant.

### 4.3.6 Effect of Fouling on Permeate and Filter Fluxes

It is required to determine the time that ultrafiltration and multimedia sand filter should be cleaned and backwashed to avoid clogging the filters. When the flux is reduced 15% as compared to its initial amount, it is time to clean and backwash the filters (Chesters and Armstrong, 2013). In this experiment, permeate and filter fluxes were measured using flow meters for 15 hours at constant pressure (2 psi or 13.8 kPa) and room temperature. The initial conditions were identical for both pretreatment methods during this trial.

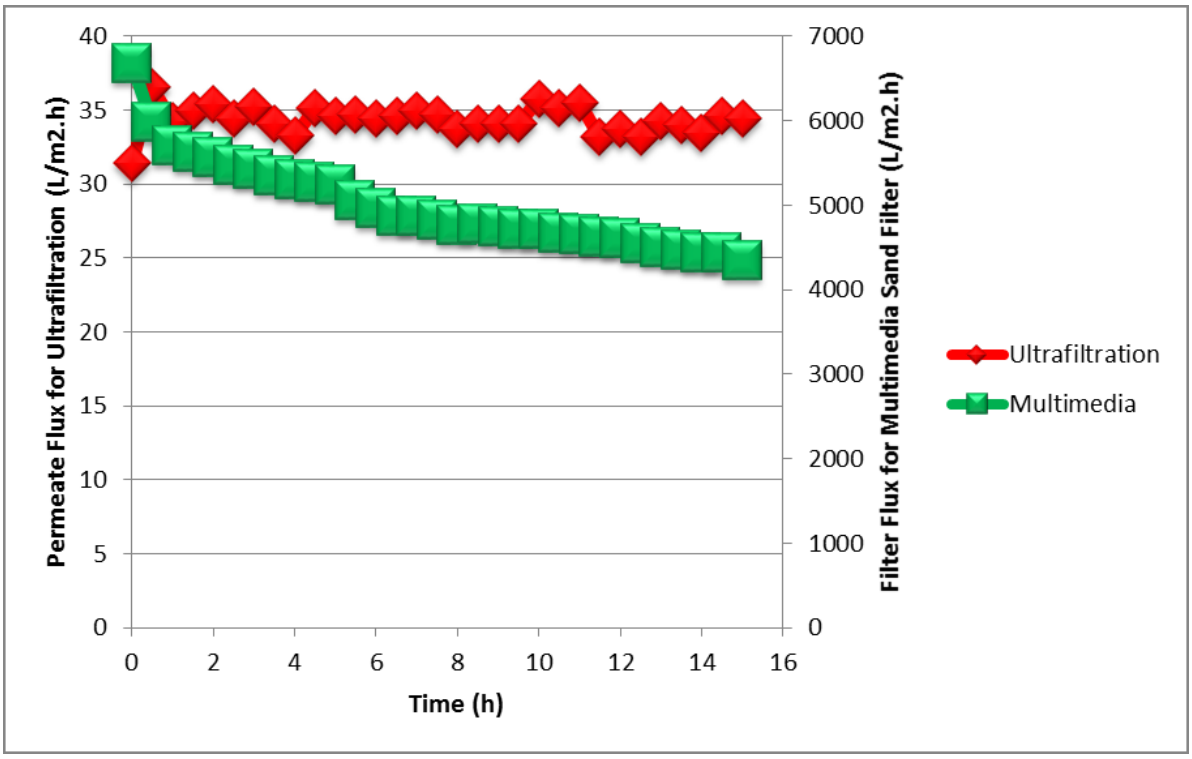


**Figure 4-10: Effect of time on permeate and filter fluxes for ultrafiltration and multimedia sand filter.**

As Figure 4-10 demonstrates, the decrease of permeate flux in the ultrafiltration is not very significant compared to the filter flux decline in the multimedia sand filter over time. Permeate and filter fluxes decreased by 1.7% and 34.9% in ultrafiltration and the multimedia sand filter respectively. According to the results indicated in Figure 4-10, fouling occurs faster in the multimedia sand filter in comparison with ultrafiltration. Subsequently, the multimedia sand filter should be cleaned earlier and more frequently compared to ultrafiltration. Consequently, based on the results from this research, it has been observed that the ultrafiltration method has an extremely good efficiency for removal of TOC, turbidity and hardness from water compared to the multimedia sand filter. Therefore, using the ultrafiltration as pretreatment can decrease PRO membrane fouling and consequently increase the overall efficiency of the PRO power plant.

### 4.3.7 Effect of Various Ultrafiltration Systems on TOC, Turbidity and Hardness Removal

In this experiment different crossflow ultrafiltration membranes with different MWCOs were used in order to compare the removal efficiency of the crossflow ultrafiltration with dead-end ultrafiltration in removal of TOC, turbidity, and hardness. The experiments were triplicated. The initial conditions such as temperature, and pH (23$\pm$ 0.5℃, 6-8) were the same in all experiments.

Figure 4-11 shows the effect of different ultrafiltration systems on removal of TOC from river water. As Figure 4-11 indicates, the TOC removal increased by reducing the MWCO in crossflow ultrafiltration which was expected. The lower MWCO means that only small particles can pass through the membrane (the pore sizes on the ultrafiltration membrane are smaller) and as a result the amount of particles that can pass through the ultrafiltration membrane decreases. However, it should be mentioned that by decreasing the MWCO of the ultrafiltration membranes, the amount of transmembrane pressure (TMP), that should be applied, increases as well and this raises the cost. Although the TOC removal in crossflow ultrafiltration-100 kDa was relatively higher than the two other ultrafiltration systems, it would not be cost effective because of the required TMP. According to the results demonstrated in Figure 4-11, the TOC removal using crossflow ultrafiltration (54.6%) was higher compared to the dead-end ultrafiltration (41%) when their MWCOs were the same.

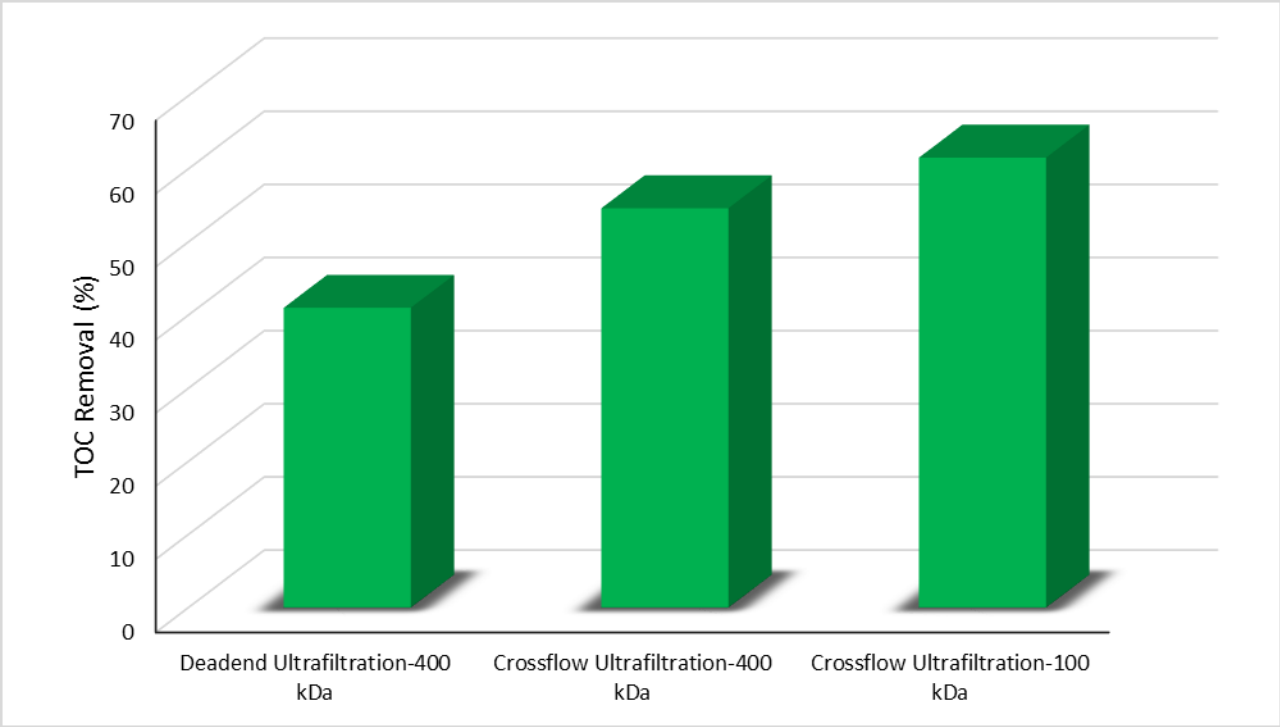


**Figure 4-11: Effect of dead-end ultrafiltration and crossflow ultrafiltration on TOC removal.**

However, the required TMP for crossflow ultrafiltration was 1.5 times higher than that of dead-end ultrafiltration. Therefore, it seems that the dead-end ultrafiltration will be a better choice for the removal of TOC compared to crossflow ultrafiltration. This statement will be verified in section 4.4.1.

As Figure 4-12 demonstrates, the turbidity removal was almost 100% regardless of the type of ultrafiltration membranes (dead-end and crossflow). As using crossflow ultrafiltration is more expensive due to the required TMP, it seems that the dead-end ultrafiltration is a better option for removal of turbidity.

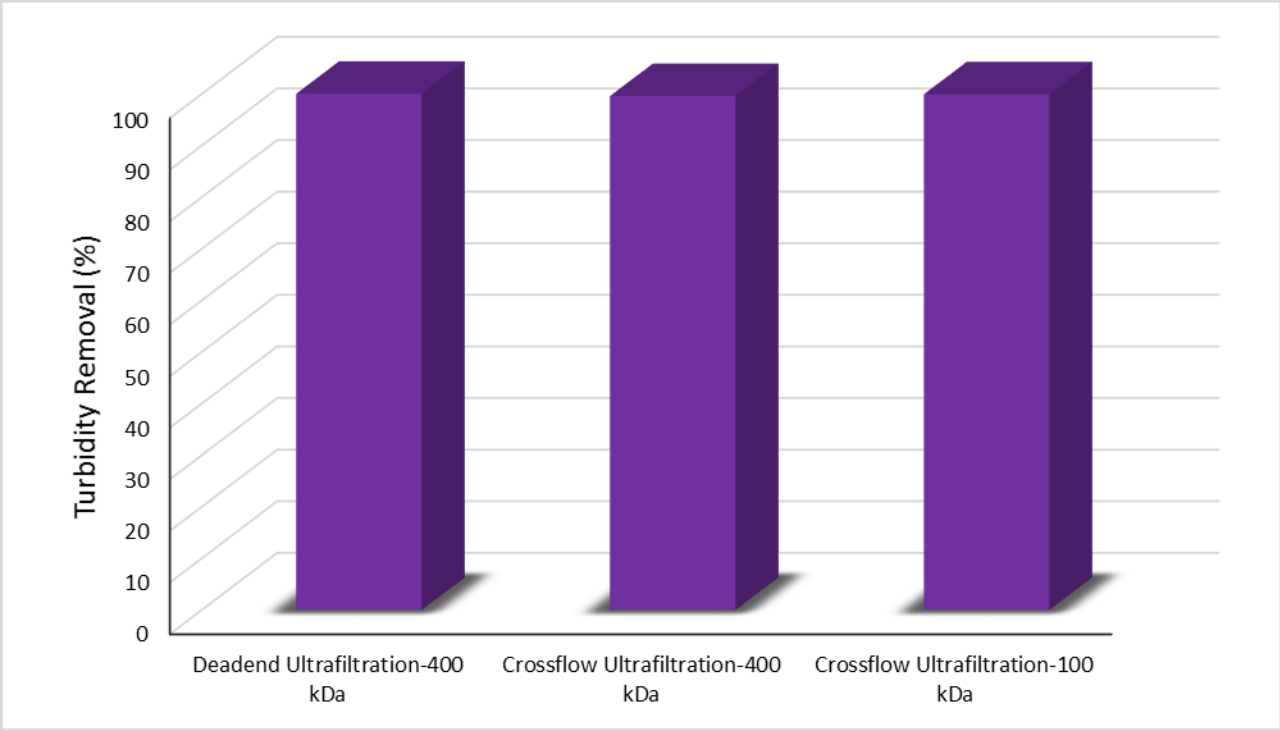


**Figure 4-12: Effect of different ultrafiltration membranes on turbidity removal.**

As Figure 4-13 shows, the type of ultrafiltration did not have a significant effect on hardness removal. This result was expected because as it is mentioned in section 4.3.3, the removal of hardness as calcium carbonate is difficult to achieve by using the filtration methods. Therefore, it seems that the dead-end ultrafiltration is a better choice for hardness removal in comparison with crossflow ultrafiltration in terms of energy consumption.

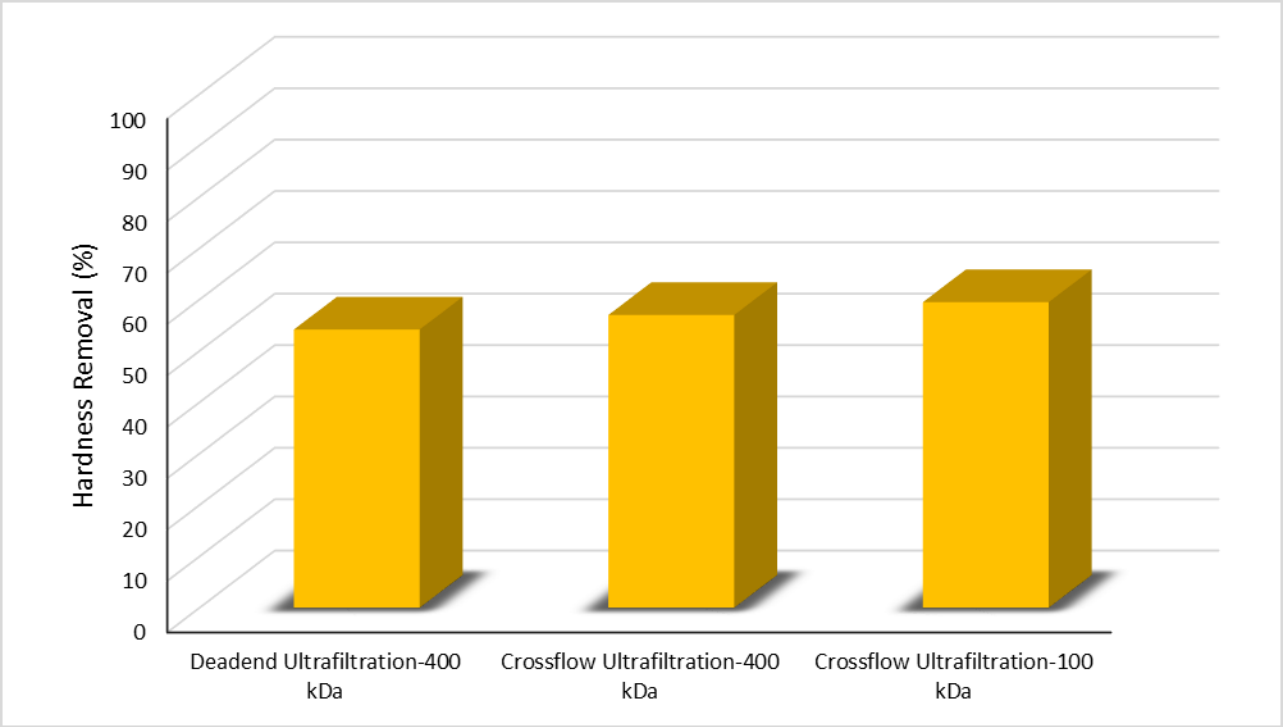


**Figure 4-13: Effect of various ultrafiltration membranes on hardness removal.**

## 4.4 Pressure Retarded Osmosis (PRO)

### 4.4.1 Osmotic Power Plant Efficiency using Different Pretreatment Methods

In this section the efficiency of the osmotic power plant was studied using various pretreatment methods such as multimedia sand filter, dead-end ultrafiltration, and crossflow ultrafiltration with different MWCOs. The temperature, pressure, salt concentration, and feed and draw side flow rates were 25 ℃, 3 bars (300 kPa), 30 g/L, and 10 mL/min respectively. As it was not possible to have access to a membrane module, the coupon membranes were used instead of the membrane module for overall efficiency calculations in this research.

As it is known, the pressure drop is proportional with flow rate (Schock and Miquel, 1987; Farkova, 1991). Therefore, the pressure drop on feed and draw sides of the membrane were assumed as zero because the flow rates on both sides were not very high. The required pressures for pretreatment on the feed side were 9.1, 13.8, 20.7, and 34.5 kPa for the multimedia sand filter, dead-end ultrafiltration, crossflow ultrafiltration, and crossflow ultrafiltration-100 kDa respectively.

**Table 4-1: Efficiency of osmotic power plant using different feed waters.**

| Feed Water | $W_{gross}^{PRO}$ $(W/m^2)$ | $W_{gross}^{e}$ $(W/m^2)$ | $W_{net}^{e}$ $(W/m^2)$ | Overall Efficiency (%) |
|---|---|---|---|---|
| Multimedia Sand Filter | 0.84 | 0.72 | 0.27 | 1.88 |
| Dead-end Ultrafiltration-400 kDa | 1.06 | 0.90 | 0.34 | 2.37 |
| Crossflow Ultrafiltration-400 kDa | 1.08 | 0.92 | 0.19 | 1.32 |
| Crossflow Ultrafiltration-100 kDa | 1.12 | 0.95 | - 0.13 | - 0.89 |

As mentioned before, the gross PRO power is the product of permeate flux and applied pressure on the draw solution (Equation 3-13) and net electrical power is the power that can be harvested from the osmotic power plant after considering parasitic loads. According to the results demonstrated in Table 4-1, the gross power increased by increasing the quality of the feed water and reach to 1.12 $W/m^2$ when the used feed water was prepared from crossflow ultrafiltration with MWCO of 100 kDa. The same trend was also observed for the electric gross power. Although the maximum power that could be exploited from this membrane was 14.2 $W/m^2$, the maximum obtained net electric power after considering the losses and required pressure for pretreatment was decreased to 0.34 $W/m^2$ using the dead-end ultrafiltration as the pretreatment method. In addition, according to the obtained results in Table 4-1, the maximum produced PRO gross power was 1.12 $W/m^2$ using the crossflow ultrafiltration-100 kDa while the overall efficiency of

the osmotic power plant for using the same pretreatment method was negative (– 0.89%). However, the maximum overall efficiency of the osmotic power plant was 2.37% when the dead-end ultrafiltration was used. This means that although the generated PRO gross power using crossflow ultrafiltration-100 kDa is higher than that of using dead-end ultrafiltration, its produced net electric power was much lower compared to that using dead-end ultrafiltration. The reason was associated with the amount of required pressure in crossflow ultrafiltration-100 kDa as the pretreatment in the osmotic power plant which is significantly higher than that in the dead-end ultrafiltration system. Therefore, dead-end ultrafiltration seems to be a good pretreatment method for generating osmotic power in this research.

### 4.4.2 Operating Conditions

#### 4.4.2.1 Effect of Temperature on Permeate Flux

In this experiment, the effect of temperature on permeate flux was studied over a range of 5 ℃ to 30℃ in both PRO and FO modes. The used feed and draw waters were demineralized water and synthetic salt water. Temperature was controlled using a water bath (Table 3-7).

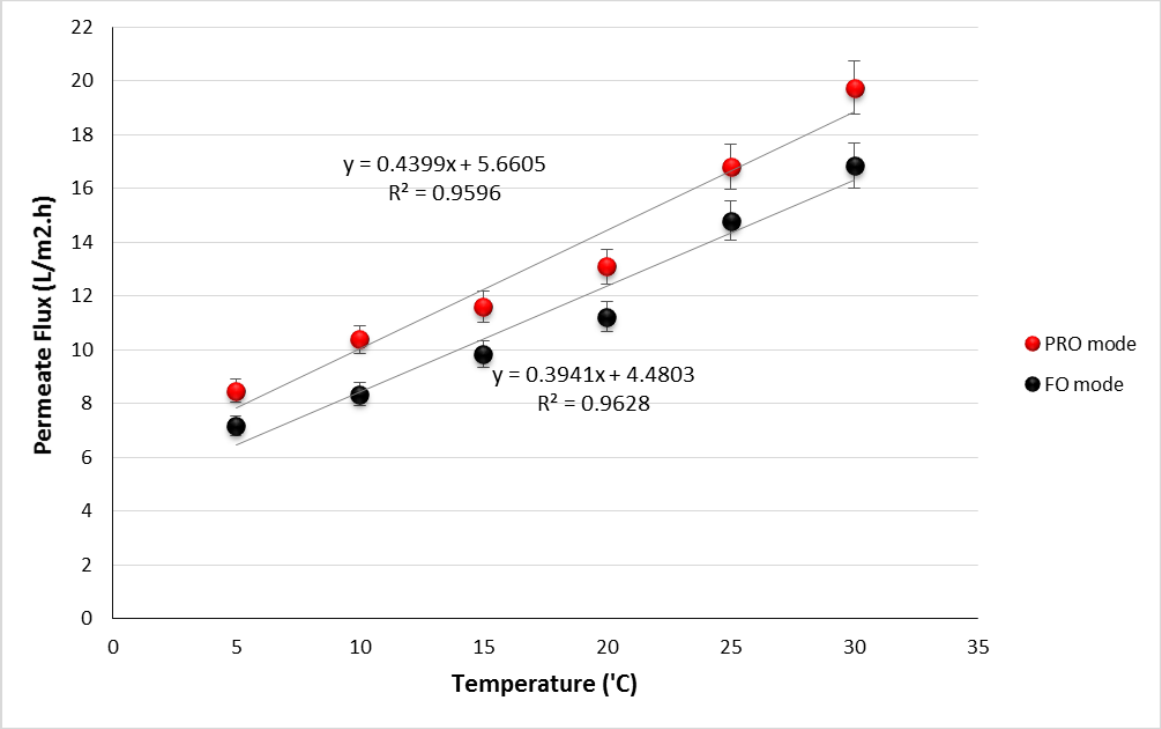


**Figure 4-14: Effect of temperature on permeate flux in PRO and FO modes.**

The initial conditions such as salt concentration (30 g/L) and feed and draw flow rates (10 mL/min) were the same for both modes. The applied pressure on the draw side in PRO mode was 300 kPa (3 bars). In FO mode, no pressure was applied on the draw solution. As Figure 4-14 shows by increasing the temperature, the permeate flux in both PRO and FO modes increases as well. By increasing the temperature, the viscosity of the feed water decreases and this causes the flux to increase.

#### 4.4.2.2 Effect of Salt Concentration on Permeate Flux

In this trial, the influence of the salt concentration on permeate flux was investigated over a range of 10 g/L to 60 g/L in both PRO and FO modes. The initial conditions including temperature (25 ℃) and feed and draw sides flowrates (10 mL/min) were the same for both modes. The applied pressure on the draw side was 3 bars (300 kPa).

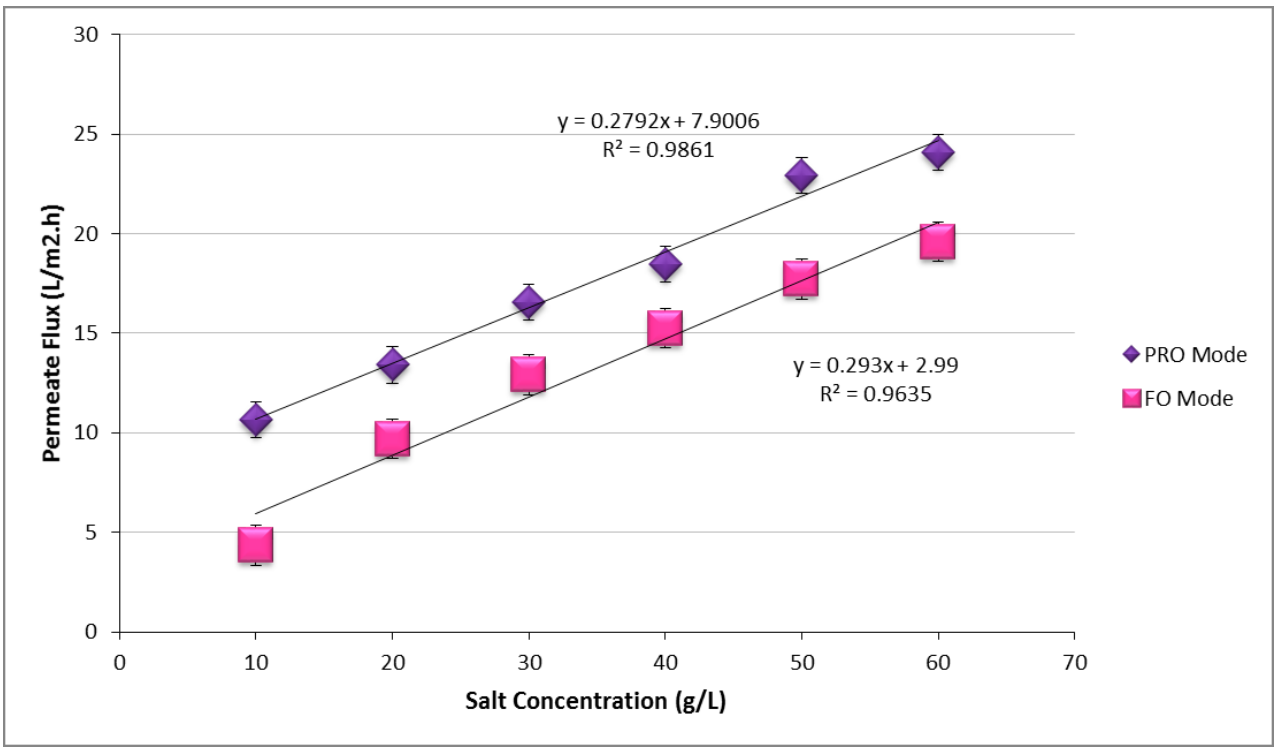


**Figure 4-15: Effect of salt concentration on permeate flux in PRO and FO modes.**

As Figure 4-15 demonstrates, there is a positive correlation between the salt concentration on the draw side and the permeate flux for both PRO and FO modes. This means that when the salt concentration of the draw solution increases the permeate flux also increases. The reason is associated with the osmotic driving force. The increase in salt concentration raises the osmotic driving force and as a results the permeate flux enhances as well. This trend was also observed by Duong *et al.* (2013) for both PRO and FO modes.

#### 4.4.2.3 Effect of Pressure on Permeate Flux and Power Density

In this experiment, the effect of different pressures (0, 300, 600, and 900 kPa) was studied. The other conditions such as temperature (25 ℃), salt concentration (30 g/L) and feed and draw side flow rates (10 mL/min) were constant during the experiment.

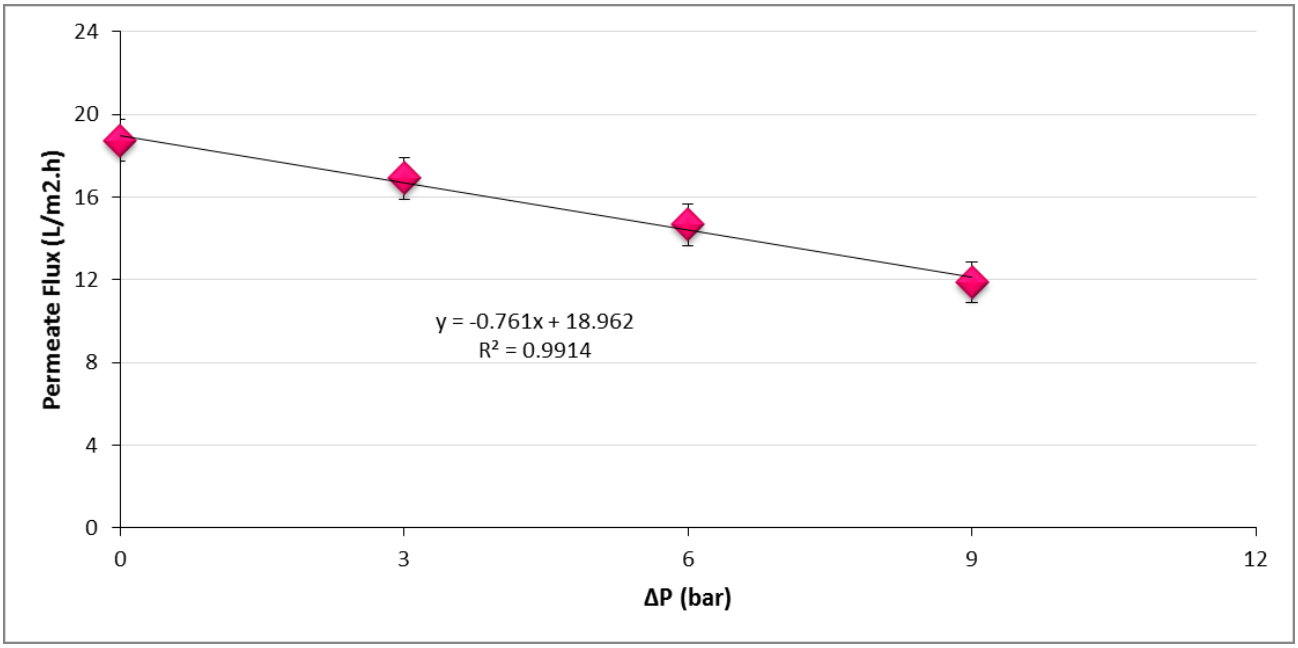


**Figure 4-16: Effect of pressure on permeate flux in PRO mode.**

According to the results demonstrated in Figure 4-16, by increasing the applied pressure on draw side, the permeate flux decreased. This means that by increasing the pressure, the amount of water that can pass through the membrane decreases and consequently the permeate flux declines (Chen *et al.*, 2016). These results are in agreement with the results obtained by Chou *et al.* (2012), She *et al.* (2013), and She *et al.* (2012).

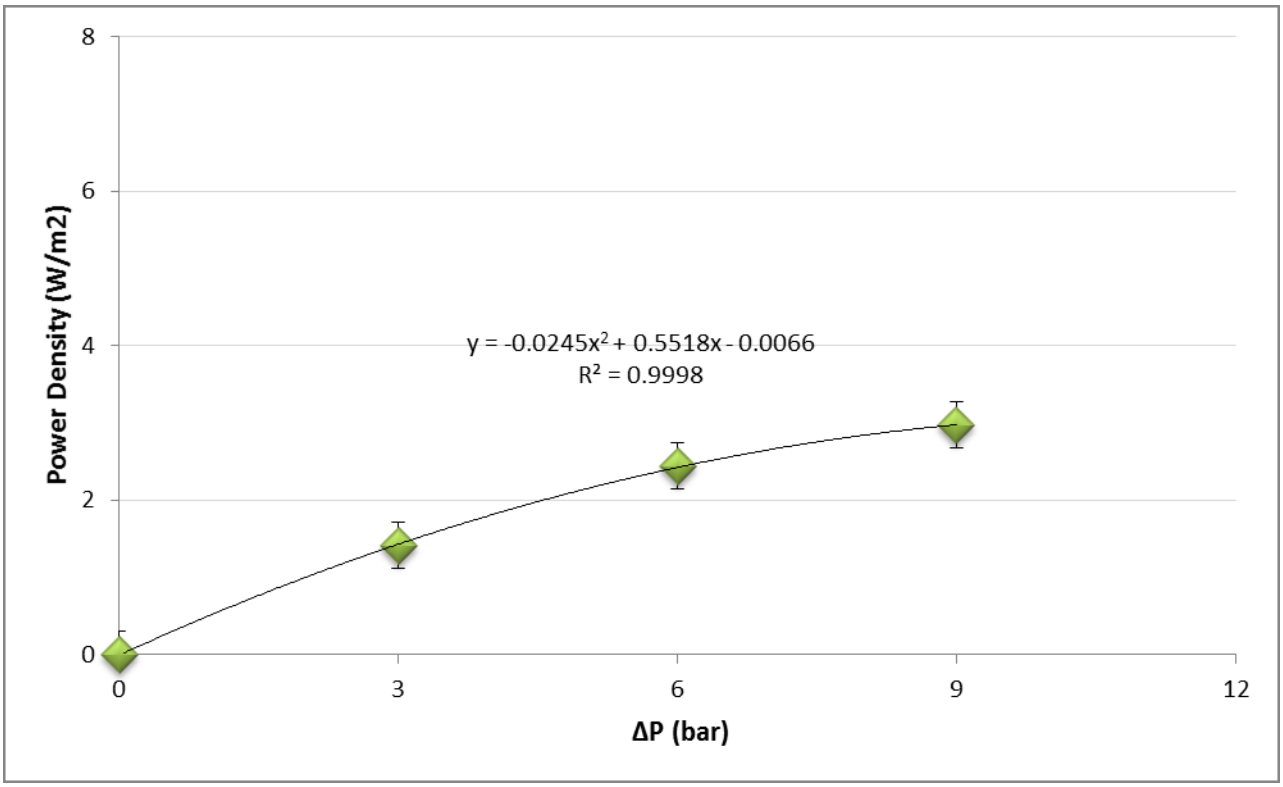


**Figure 4-17: Effect of pressure on power density in PRO mode.**

As Figure 4-17 demonstrates, by increasing the applied pressure, the power density increases as well and it reaches to 3 $W/m^2$ at 900 kPa (9 bars). As it is known that the PRO membrane needs to have a power density above 3-5 W/$m^2$ for PRO power generation to be economic (Achilli and Childress, 2010; Patel, 2010; Zhao *et al.*, 2012; Han *et al.*, 2013; Sivertsen *et al.*, 2013). The maximum achieved power densities reported in this study was 3 W/$m^2$ when the flow rate and pressure were 10 mL/min and 900 kPa (9 bar) respectively. It should be mentioned that a higher power density from this membrane (more than 3 W/$m^2$) will be exploited at higher flow rates (more than 10 mL/min). The used flow rates in this study were selected due to some device limitations for working with the system at higher flow rates.

### 4.4.3 PRO Membrane Fouling

#### 4.4.3.1 Effect of Different Feed Solutions on PRO Membrane Fouling Using Synthetic Salt Water

As it was mentioned in section 3.3.4, all fouling tests were done at constant temperature, salinity and pressure. All fouling tests were continued until complete fouling was reached (permeate flux was negligible). The used draw solution was synthetic salt water for all four feed waters (untreated river water, ultrafiltration, microfiltration, multimedia sand filter effluents). The flow rates on both feed and draw sides were 10 mL/min for all the experiments. All experiments were done in duplicate. The PRO experimental setup was an open system which means the draw solution was not recirculated in the system and was continuously discharged into a waste disposal system that was in the Hydro-Québec lab, so the draw solution could not be diluted and as a result, the salt concentration remained constant during the experiments. Therefore dilution did not have any effect on the fouling and the flux drop in the experiments.

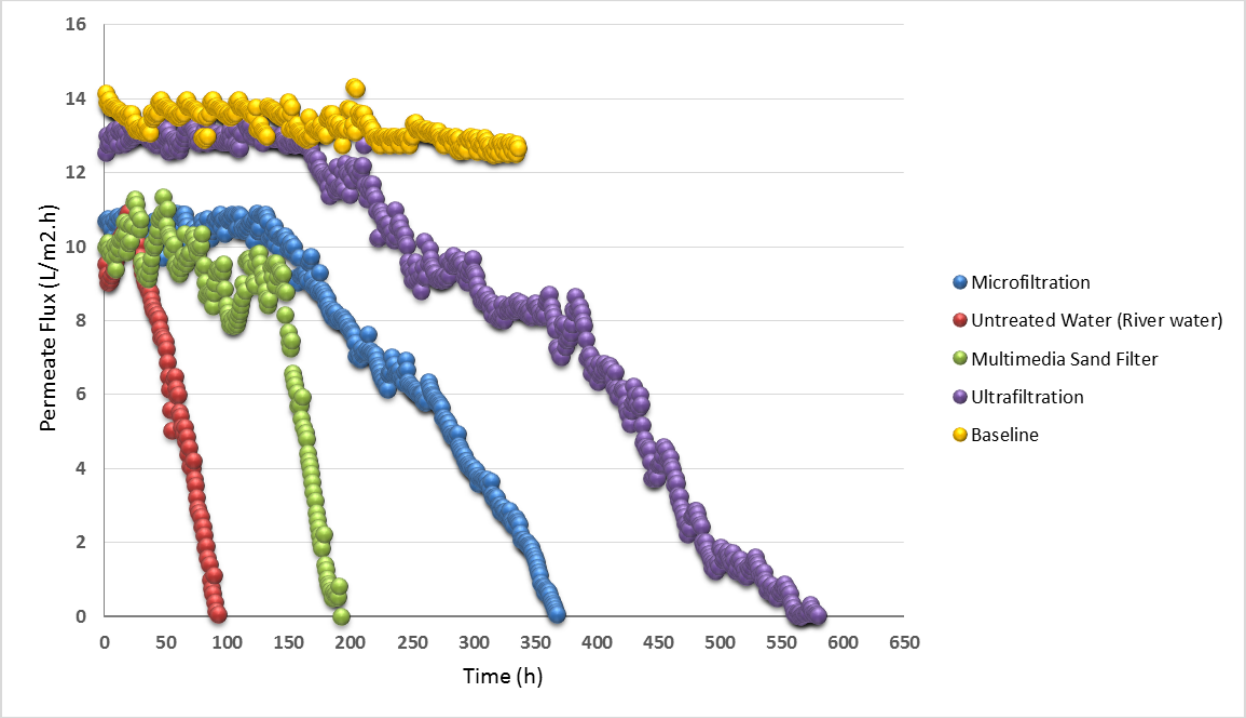


**Figure 4-18: Effect of fouling on permeate flux using different feed waters.**

According to the indicated results in Table 3-2, ultrafiltration had a better quality compared to microfiltration, multimedia sand filter and untreated water. The order based on their qualities was as follows: ultrafiltration > microfiltration > multimedia sand filter > untreated water (river water). As Figure 4-18 shows, complete fouling occurred faster when the used feed water was river water which is in the agreement with the results in Table 3-2. Complete fouling occurred in ultrafiltration, microfiltration, multimedia sand filter effluents and untreated river water after passing 580, 368, 192, and 92 hours respectively. Based on the results in Figure 4-18, permeate flux in the fouling tests reduced very smoothly at the beginning (it was almost constant). However, after passing a certain time, it started to decline dramatically with a higher rate until it reached zero. Lee *et al.* (2010) also observed the same behavior regarding the changes of the permeate flux over time (permeate flux was nearly constant).

The smoothness of the permeate flux at the beginning might have occurred due to two reasons. The first reason can be related to the type of driving force in the PRO membrane processes which is the difference in osmotic pressure between the feed and draw solutions. This means no hydraulic pressure is applied on the feed side and as a result, it does not even accelerate the fouling but assists in delaying it. The second one is related to the quality of the feed water. The better the quality of the water, the lower the amount of particles and colloids in the water. Therefore, the aggregation of particles will be time consuming and consequently, the fouling occurs gradually. As Figure 4-18 demonstrates, the results are in agreement with the second reason. Wherever the quality of the feed water was better, it took more time to reach the point when the fouling rate increased.

The power density of PRO membrane was calculated for four feed waters by multiplying the permeate flux in applied hydraulic pressure (Equation 3-17) to compare the effect of these four feed waters on power density. As the graph of power density versus time had the same pattern as the graph of permeate flux versus time (Figure 4-18) (due to the pressure that was constant and the same for both feed waters), this figure has not been shown in this research to avoid repetition. According to the results, power density decreased from 1.06 to 1.05 $^{W}/_{m^2}$ (over one week) using ultrafiltration as the feed water while it declined from 0.89 to 0.7 $^{W}/_{m^2}$ (over one week), 0.84 to 0.32 $^{W}/_{m^2}$ (over one week), and 0.75 to 0.01 $^{W}/_{m^2}$ (over 3 days) using microfiltration, multimedia sand filter and river water, respectively. The results from this experiment indicate that using ultrafiltration as a pretreatment method can reduce the fouling effect in PRO membrane and produces a more stable and sustainable power density compared to multimedia sand

filter, microfiltration and river water and consequently it can improve the efficiency of the PRO membrane and will improve the salinity gradient energy generation.

#### 4.4.3.2 Effect of Different Feed Solutions on PRO Membrane Fouling Using Sea Water

This experiment was performed at constant pressure and temperature (300 kPa and 25℃).

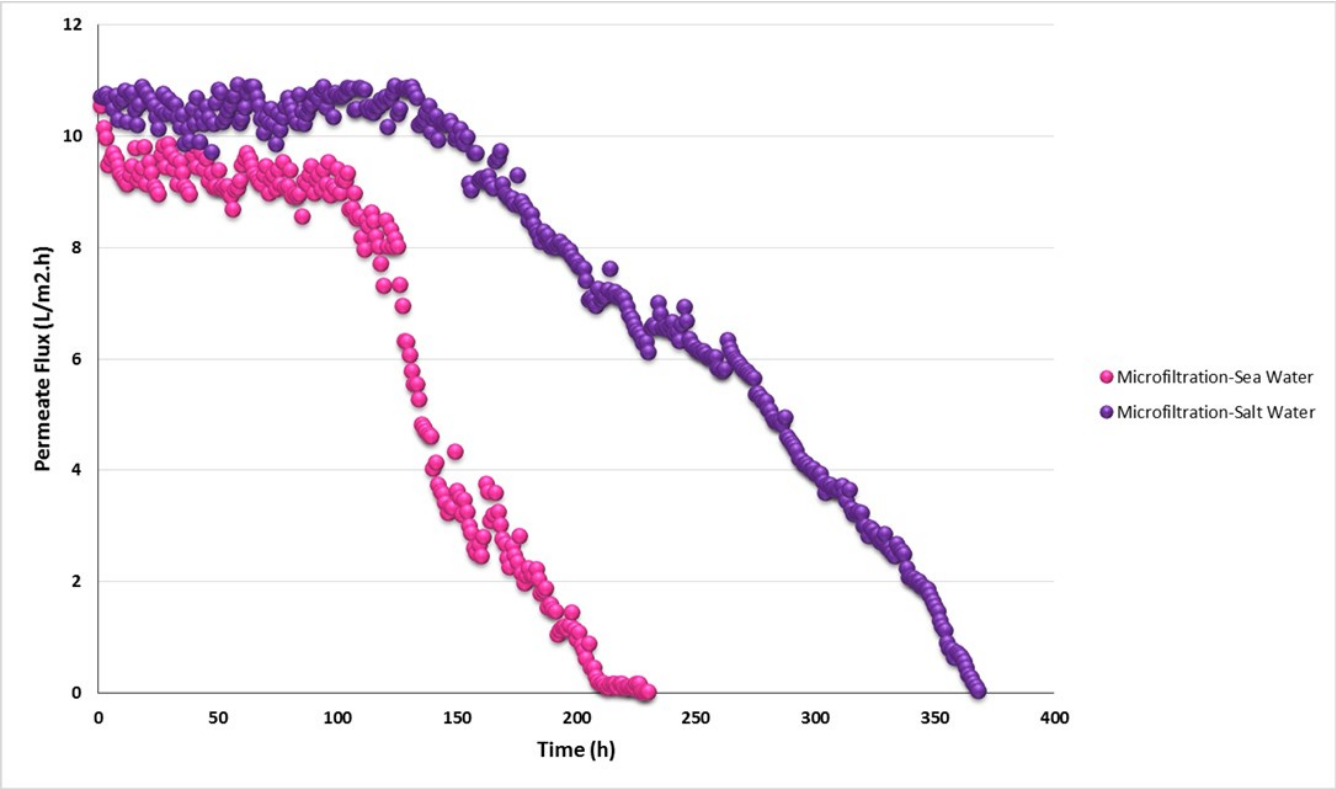


**Figure 4-19: Effect of fouling on permeate flux using microfiltration as the feed water and sea water and synthetic salt water as the draw water.**

Based on the results in the previous section, ultrafiltration and microfiltration treatments indicated better results compared to no treatment and multimedia sand filter treatment. Therefore, these two feed waters were selected to perform the fouling tests with the sea water. According to the results demonstrated in Figures 4-19 and 4-20, the fouling occurred faster and earlier when the draw solution was sea water. Complete fouling

occurred in ultrafiltration and microfiltration effluents after passing 405, and 230 hours respectively. This indicates that the fouling using ultrafiltration and microfiltration effluents with sea water occurred 30.2% and 37.5% faster compared to the results for synthetic salt water.

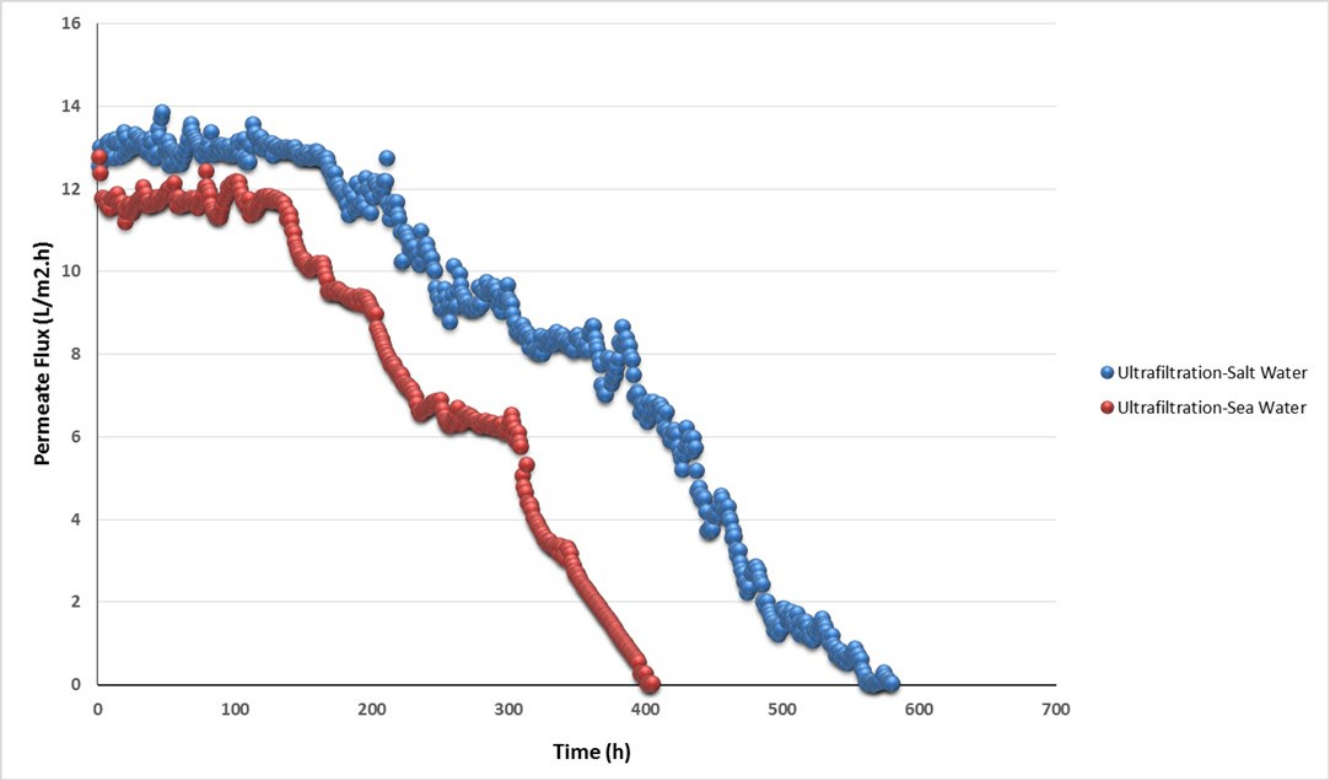


**Figure 4-20: Effect of fouling on permeate flux using ultrafiltration as the feed water and sea water and synthetic salt water as the draw water.**

In addition, when the used draw solution was sea water and feed water was from microfiltration, the permeate flux decreased about 71.3% after one week (168 hours). However, the decline in the permeate flux for the synthetic salt water, when the used feed water was from microfiltration, was 9.2% at the same time. For ultrafiltration effluent as the feed water, the decreases in the permeate fluxes were 25.4% and 3.1% simultaneously (168 hours) for both sea water and synthetic salt water respectively. The

reason can be related to the quality of sea water. As the qualities of ultrafiltration and microfiltration effluents were the same for both sea water and synthetic salt water, it seems that the quality of sea water played an important role on the membrane fouling in the PRO process. Because the synthetic salt water contained only sodium chloride, calcium chloride and demineralized water while the other components including higher concentrations of divalent cations ($Ca^{+2}$ and $Mg^{+2}$) were observed in the sea water (Table 3-1) that can influence the fouling rate.

### 4.4.4 Fouling Mechanisms

#### 4.4.4.1 Complete Blocking Model (CBM)

In CBM, particles block the pores and prevent flow (Katsoufidou *et al.*, 2005; Bolton *et al.*, 2006; Bolton *et al.*, 2006; Rezaei *et al.*, 2011). As all fouling experiments were done at constant pressure (3 bars or 300 kPa), four classic fouling models at constant pressure were used (Table 3-9) (Hermans and Bredée, 1935; Hermia, 1982; Bolton *et al.*, 2006; Rezaei *et al.*, 2011). In order to simplify data processing, the linearized forms of these models were used for analyzing the experimental data (Rezaei *et al.*, 2011). The difference of squared regression ($R^2$) was used as an index to investigate the agreement of the experimental data with the used model. The equations for permeate flow rate in two forms (linearized and non-linearized) are presented in Table 3-9. It should be noted that a, b and β parameters mentioned in Table 3-9 are constant.

The CBM (Table 3-9) was applied to the obtained experimental data in section 4.4.3 in order to determine if the CBM was in agreement with the experimental data. As it was mentioned in section 4.4.3, the permeate fluxes were almost constant at the beginning,

so the experimental data were selected from where the fouling started to occur until the flux was reduced by 95%. Figures 4-21 and 4-22 show the natural logarithm of permeate flow rate versus the time for both synthetic salt and sea waters. According to the results, it can be observed that the experimental data were in high agreement with the CBM. The maximum and minimum values of R-squared were 0.91 and 0.80 for river water-synthetic salt water and ultrafiltration-synthetic salt water, respectively.

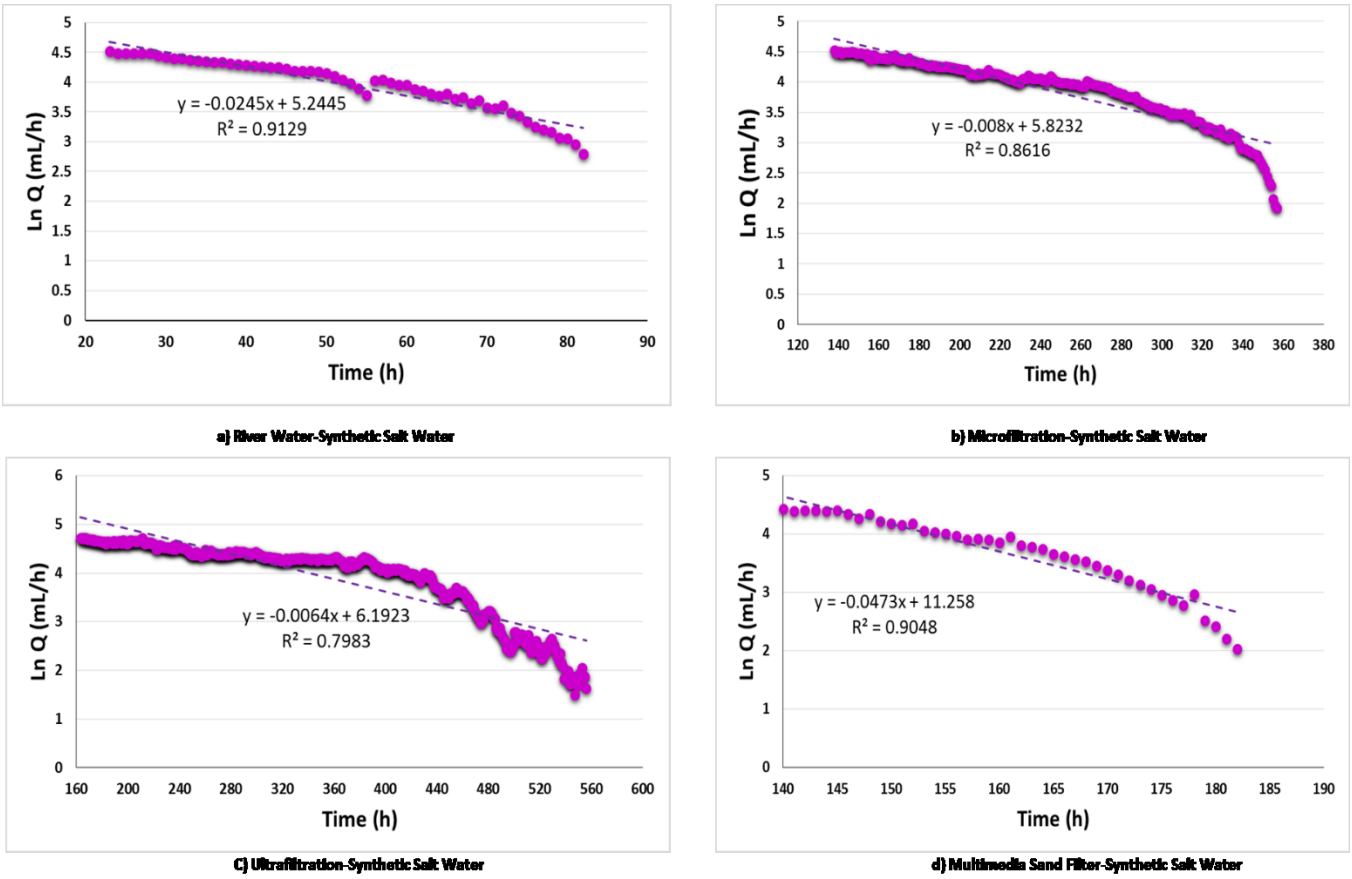


**Figure 4-21: CBM using synthetic salt water for a) river water, b) microfiltration, c) ultrafiltration, and d) multimedia sand filter.**

According to the results, it seems that the CBM was the main fouling mechanism for all different feed waters. The value of R-squared followed the order of: river water > multimedia sand filter > microfiltration-sea water > microfiltration-synthetic salt water >

ultrafiltration-sea water > ultrafiltration-synthetic salt water. These results are in accordance with the demonstrated results in section 4.4.3. As there were more suspended and colloidal particles in the river water, fouling due to the pore blocking occurred more quickly compared to the rest of the feed waters ($R^2$= 0.91). Therefore, the rapid reduction of permeate fluxes shown in Figures 4-18 to 4-20 were likely because of the pore blocking.

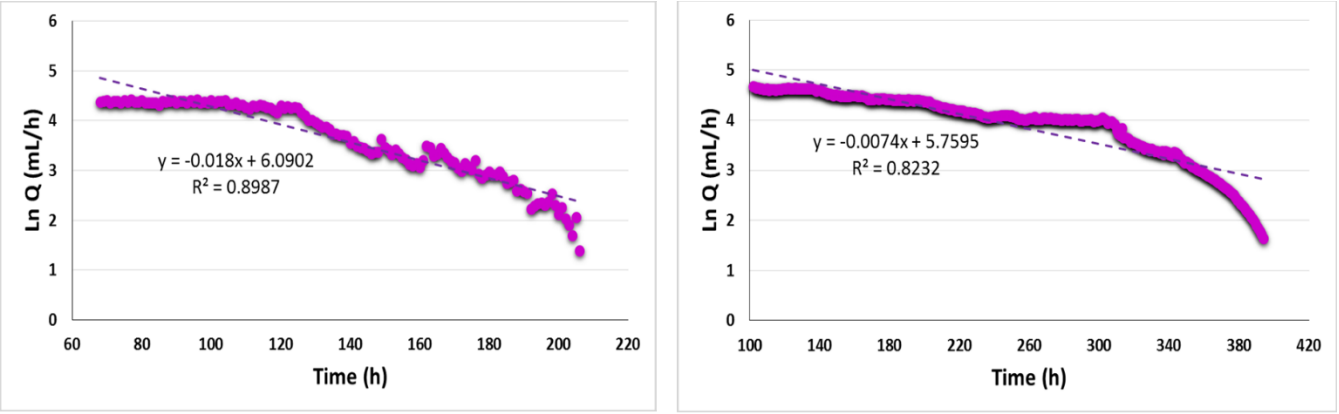


a) Microfiltration-Sea Water

b) Ultrafiltration-Sea Water

**Figure 4-22: CBM using sea water for a) microfiltration, and b) ultrafiltration.**

#### 4.4.4.2 Cake Filtration Model (CFM)

In CFM as the most frequently used model, it is assumed that the particles settle on the membrane surface as a porous layer. The thickness of this layer increases over time and subsequently it decreases the permeate flux (Katsoufidou *et al.*, 2005; Bolton *et al.*, 2006; Bolton *et al.*, 2006; Rezaei *et al.*, 2011). The linearized equation that was used to study the CF model is shown in Table 3-9. According to the results demonstrated in Figure 4-23, the experimental data are relatively in accordance with CFM. As it was mentioned in the previous section, the rapid decrease in the permeate fluxes was because of the pore

blocking (CBM). Over time, particles accumulated and were deposited on the membrane surface and created an incompressible cake layer (as no hydraulic pressure was applied) which reduced the permeate flux due to the hydraulic resistance. Pore blocking is a fast process in comparison with cake formation (Song, 1998). The highest and lowest amounts of R-squared were 0.83 and 0.68 for river water and ultrafiltration-synthetic salt water.

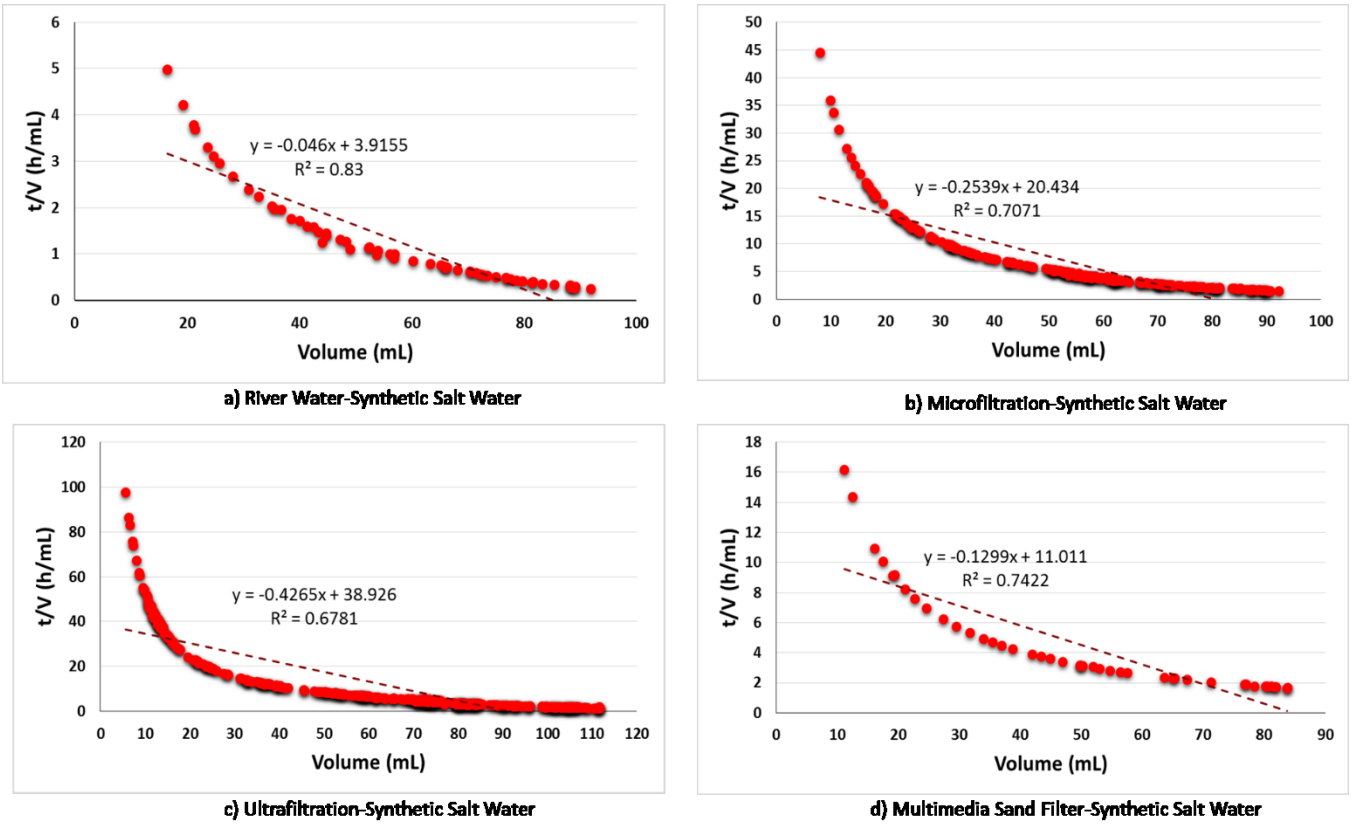


**Figure 4-23: CFM using synthetic salt water for a) river water, b) microfiltration, c) ultrafiltration, and d) multimedia sand filter.**

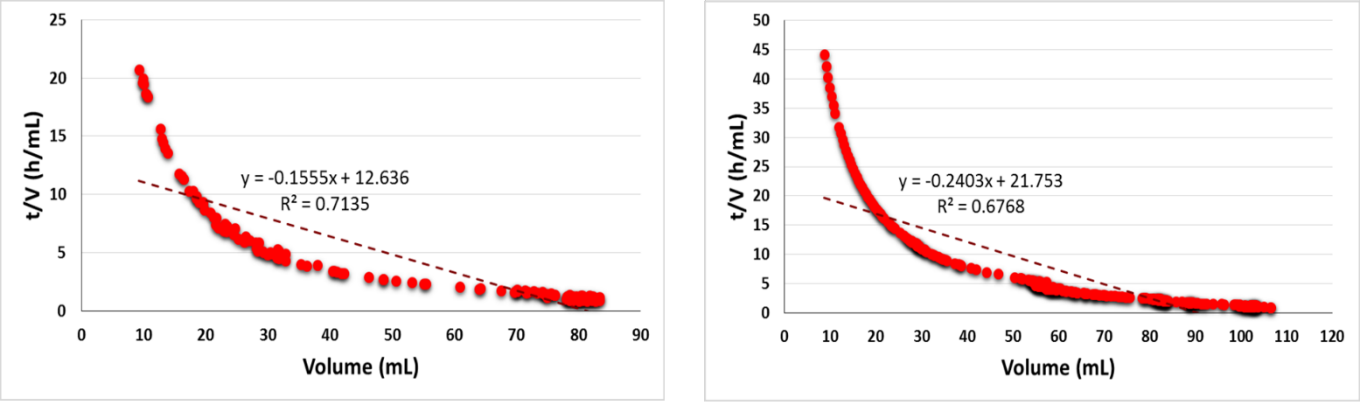


**Figure 4-24: CFM using sea water for a) microfiltration, and b) ultrafiltration.**

It was interesting that the $R^2$ values for ultrafiltration using both draw solutions were almost the same. The same results were observed for microfiltration using sea and synthetic salt waters. According to the results in section 4.4.3, fouling occurred faster for ultrafiltration and microfiltration when sea water was used as the draw solution. Therefore, it can be concluded that this classic mechanism was not completely able to elaborate and explain this different behavior for osmotically driven membranes when different draw solutions were used. The reason for this phenomenon will be discussed in section 4.4.4.4.

#### 4.4.4.3 Intermediate and Standard Blocking Models (IBM and SBM)

In IBM, it is assumed that part of the particles block the pores and the remainder are gathered on top of other deposited particles (Katsoufidou *et al.*, 2005; Bolton *et al.*, 2006; Bolton *et al.*, 2006). SBM is based on the accumulation of the particles within the membrane pores on the wall of cylindrical pores. When the deposition of the particles starts, the pores become narrower and consequently, the permeability of the membrane is decreased (Bolton *et al.*, 2006; Bolton *et al.*, 2006; Rezaei *et al.*, 2011).

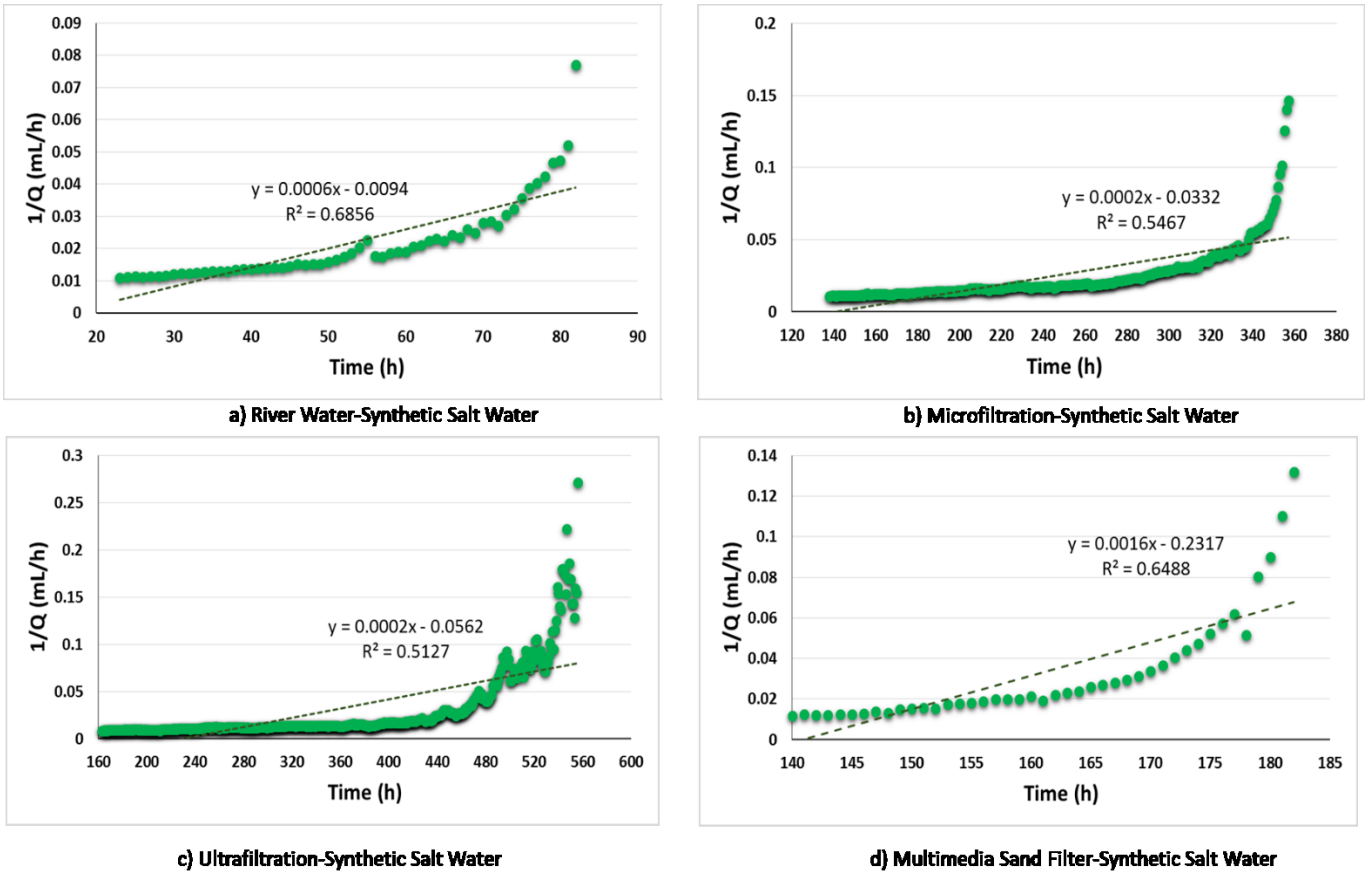


**Figure 4-25: IBM using synthetic salt water for a) river water, b) microfiltration, c) ultrafiltration, and d) multimedia sand filter.**

The IBM (Table 3-9) was applied to the obtained experimental data in section 4.4.3 in order to determine if the IBM was in agreement with the experimental data. According to the results shown in Figures 4-25 and 4-26, the experimental data from ultrafiltration, microfiltration, multimedia sand filter and river water using synthetic salt and sea waters are not in agreement with IBM. The maximum and minimum R-squared values were 0.69 and 0.51 for river water-synthetic salt water and ultrafiltration-synthetic salt water, respectively. These values are much lower than the R-squared values in CBM. It should be mentioned that the R-squared values for ultrafiltration- synthetic salt water and ultrafiltration-sea water were close to each other. The same trend was observed for

microfiltration using sea water and synthetic salt water as well. The results in Figures 4-25 and 4-26 indicate that the feasibility of this mechanism is not very high.

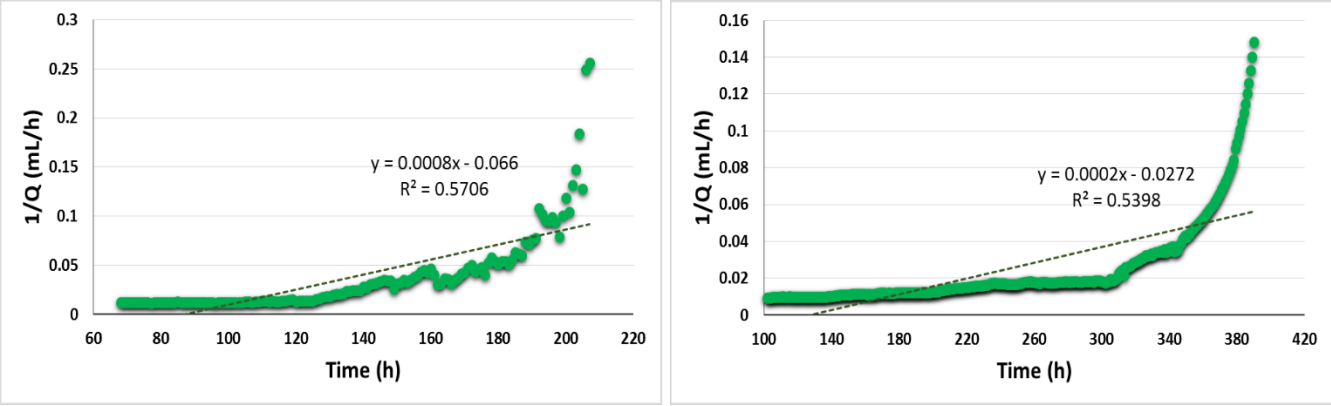


a) Microfiltration-Sea Water

b) Ultrafiltration-Sea Water

**Figure 4-26: IBM using sea water for a) microfiltration, and b) ultrafiltration.**

As Figures 4-27 and 4-28 demonstrate, the experimental data were not in the agreement with the SBM as well. The maximum and minimum R-squared values were 0.67 and 0.53 for river water-synthetic salt water and ultrafiltration-synthetic salt water respectively.

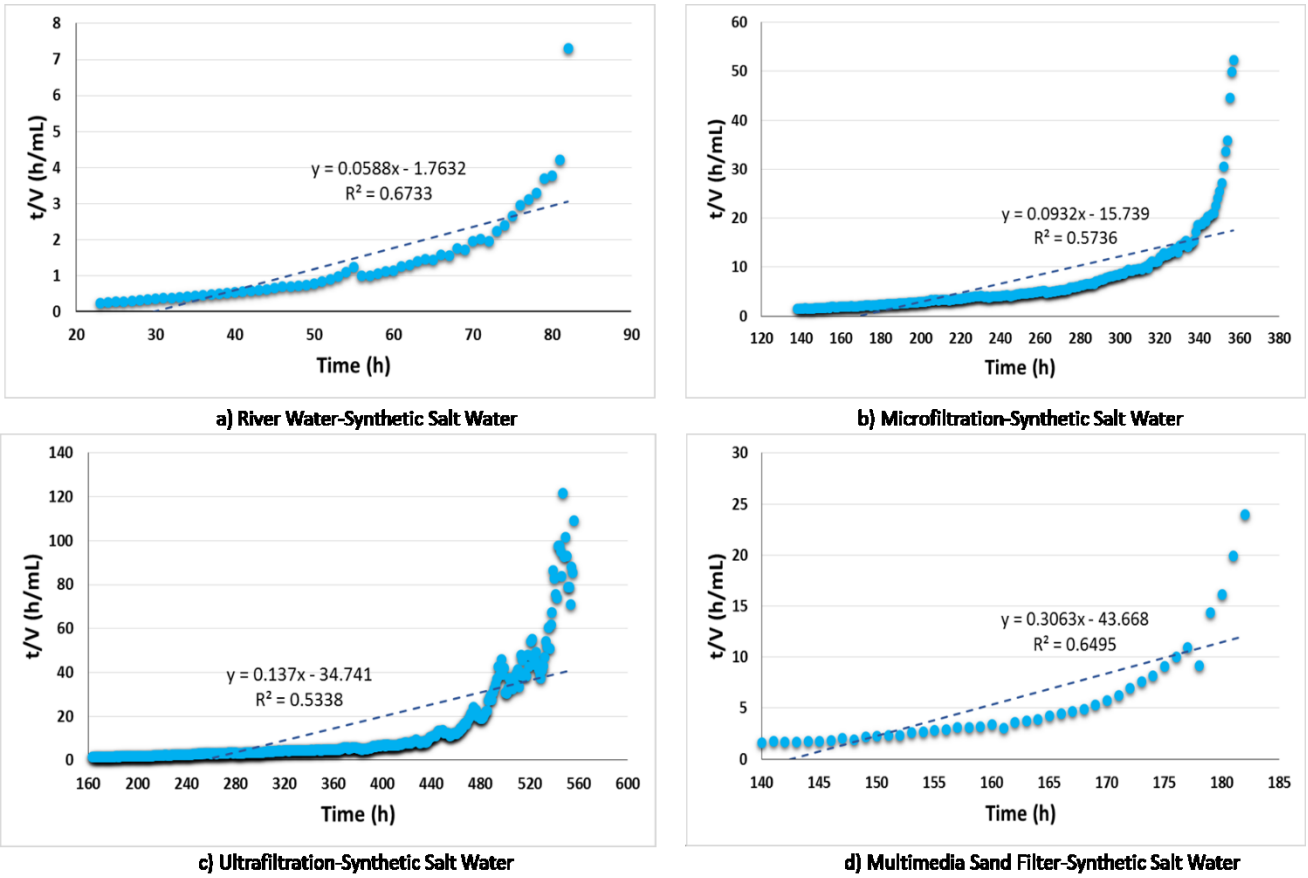


**Figure 4-27: SBM using synthetic salt water for a) river water, b) microfiltration, c) ultrafiltration, and d) multimedia sand filter.**

It should be mentioned that the R-squared values in SBM were lower than the CBM. Therefore, based on the indicated results in Figures 4-27 and 4-28, SBM cannot be considered as one of the main fouling mechanisms to explain the decrease of permeate flux in this research.

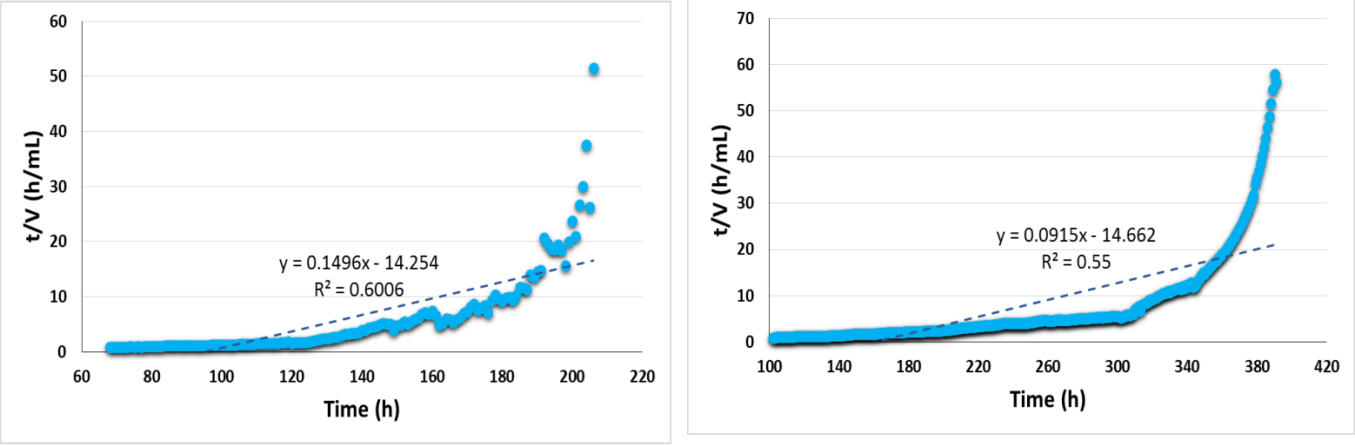


**Figure 4-28: SBM using sea water for a) microfiltration, and b) ultrafiltration.**

As Table 4-2 shows, the $R^2$ values of the four different feed waters were higher for using complete blocking model compared to the other models. It seems that the experimental data were in high agreement with the CBM and the rapid reduction of permeate fluxes shown in Figure 4-18 were likely because of the pore blocking. Therefore, complete blocking (CBM) was the main fouling mechanism for all different feed waters.

**Table 4-2: Comparison between $R^2$ values for each model.**

| Type of Feed Water | $R^2$ Value | | | |
|---|---|---|---|---|
| | CBM | CFM | SBM | IBM |
| River Water-Synthetic Salt Water | 0.9129 | 0.8300 | 0.6733 | 0.6856 |
| Multimedia Sand Filter-Synthetic Salt Water | 0.9048 | 0.7422 | 0.6495 | 0.6488 |
| Microfiltration-Synthetic Salt Water | 0.8616 | 0.7071 | 0.5736 | 0.5467 |
| Ultrafiltration-Synthetic Salt Water | 0.7983 | 0.6781 | 0.5338 | 0.5127 |

#### 4.4.4.4 Cake Enhanced Osmotic Pressure Mechanism (CEOPM)

As it was mentioned in section 4.4.4.2, the cake filtration fouling model (CFM) was not able to explain why the R-squared values were the same for ultrafiltration-synthetic salt water and ultrafiltration-sea water while the results in section 4.4.3 showed that the fouling

rate was not the same and occurred faster for ultrafiltration-sea water compared to ultrafiltration-synthetic salt water. The same trend was also observed for microfiltration-synthetic salt water and microfiltration-sea water. A mechanism for salt rejecting membranes has been introduced which is called cake enhanced osmotic pressure (CEOP) (Hoek *et al.*, 2002; Hoek and Elimelech, 2003; Lee *et al.*, 2004; Herzberg and Elimelech, 2007). In this mechanism, the back diffusion of salt is prevented by a cake layer and as a result, the osmotic pressure increases close to the membrane surface. In osmotically driven membranes such as FO and PRO, solutes can penetrate through the membrane from the high concentration draw solution to the feed solution. This causes a considerable decline in the permeate flux and driving force in these membranes (FO and PRO) (Hancock and Cath, 2009; Phillip *et al.*, 2010; Tang *et al.*, 2010; She *et al.*, 2012). In this experiment, the cation concentrations of sodium, calcium, magnesium and potassium were measured in sea water and synthetic salt water in order to investigate the effect of these cations on the membrane fouling in PRO mode.

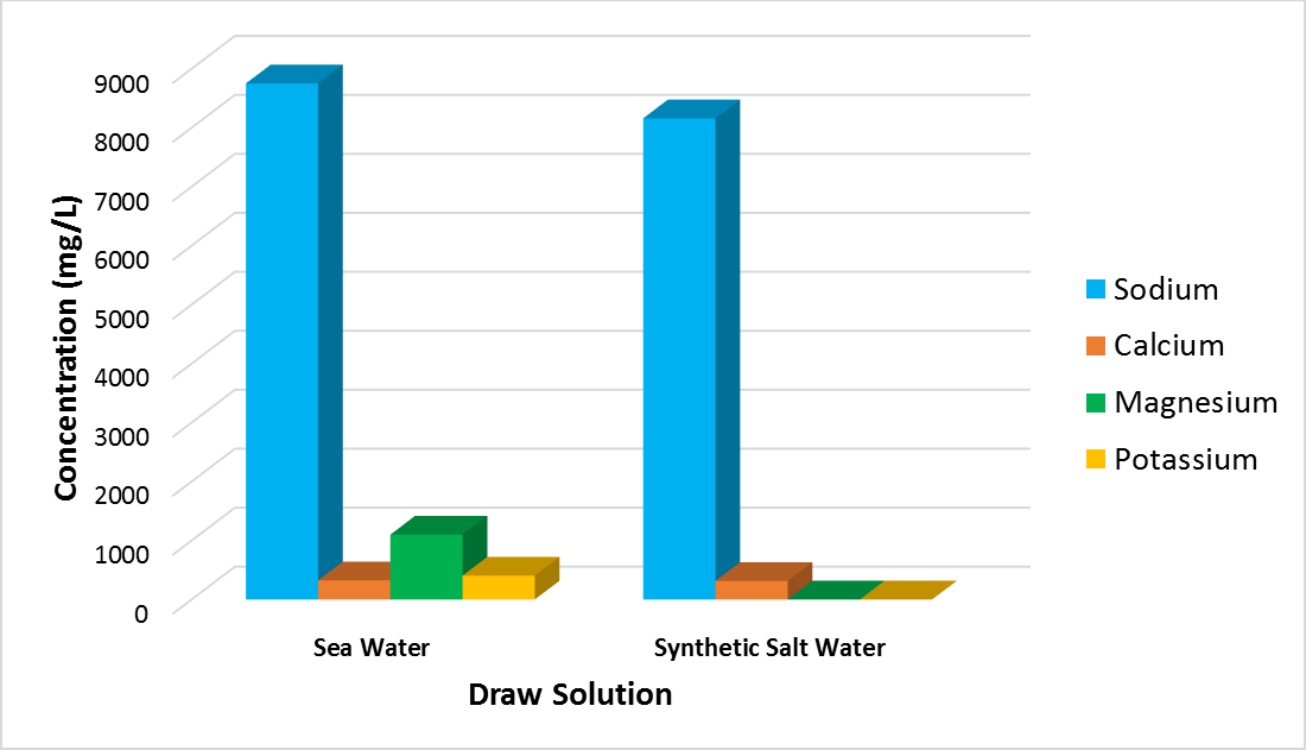


**Figure 4-29: Comparison between the concentration of monovalent and divalent cations in sea water and synthetic salt water.**

As Figure 4-29 indicates, the concentrations of sodium and calcium in synthetic salt water were lower than in sea water. In addition, there are magnesium and potassium ions in sea water which were not present in synthetic salt water. She *et al.* (2012) observed that sodium had the largest reverse solute diffusion rate compared to calcium and magnesium. However, it had a lower fouling rate in comparison with calcium and magnesium. In this study, although the concentration of sodium is higher in the sea water (8750 mg/L) compared to synthetic salt water (8158 mg/L), it cannot have a significant effect on the fouling rate when the draw solution was from sea water.

On the other hand, the concentration of calcium in sea water (324 mg/L) is not considerably higher than in synthetic salt water (314 mg/L), so its effect on the fouling rate when sea water was used as the draw solution was not very significant. Therefore,

magnesium and potassium had a meaningful influence in governing the fouling rate and that is why the fouling occurred faster for both ultrafiltration and microfiltration when the used draw solution was sea water compared to when it was synthetic salt water. In order to reach the electro-neutrality of solution, more cations have to penetrate across the membrane (Heo *et al.*, 2015). As the concentrations of magnesium and potassium were higher in sea water, subsequently their concentrations increased in the feed solution to sustain the electro-neutrality. The reverse diffusion of magnesium and potassium could alter the feed solution chemistry and consequently, can enhance the membrane fouling on the feed side.

### 4.4.5 Foulant Identification

As mentioned above, four different feed waters such as ultrafiltration, microfiltration, multimedia sand filter and untreated river water and two various draw solutions such as synthetic salt water and sea water were utilized in this set of experiments.

#### 4.4.5.1 Physicochemical Characterization of Foulants Using SEM-EDS

The inorganic characterization of the foulants was done by using scanning electron microscopy (SEM) and energy dispersive spectroscopy (EDS) on the membrane samples that were prepared before and after complete fouling (permeate flux was negligible). Membrane samples were totally dried at room temperature (23 ℃) before using SEM-EDS for the accuracy of the analyses.

##### 4.4.5.1.1 Using Synthetic Salt Water

Figure 4-30 demonstrates the images of the membrane samples before and after fouling using four different feed waters. The used draw solution was synthetic salt water. The

voltage was 15 kV and the working distance was 10 mm. The images were taken from the top with a magnification of 50x. The top views of the SEM images show the structure of the membrane samples before (pristine) and after fouling. Image (a) in Figure 4-30 indicates the surface of the pristine membrane sample before fouling. The image (b) in Figure 4-30 demonstrates the surface of the membrane sample after fouling when the feed water was untreated river water. As shown in Figure 4-30 (b), the surface of the membrane sample was covered by a deposited layer which was not observed in the clean membrane surface (pristine membrane). Images (c) and (d) in Figure 4-30 show the surface of the membrane samples after fouling when the feed waters were prepared from multimedia sand filter and microfiltration systems, respectively. As the images (c) and (d) show the surface of the deposited layer on the membrane samples surface was less compared to that in the image (b) (untreated river water) and more compared to that in the image (a) (pristine membrane). Image (e) in Figure 4-30 indicates the surface of the membrane sample after fouling when the feed water was from the ultrafiltration system. According to image (e) demonstrated in Figure 4-30, it seems that the surface of the membrane sample is more similar to the membrane surface in the image (a) in comparison with the other images ((b), (c), and (d)). Unlike images (b), (c), and (d), the membrane sample surface in image (e) was not concealed by a continuous layer and instead of that, some scattered spots were observed on the surface of the membrane sample.

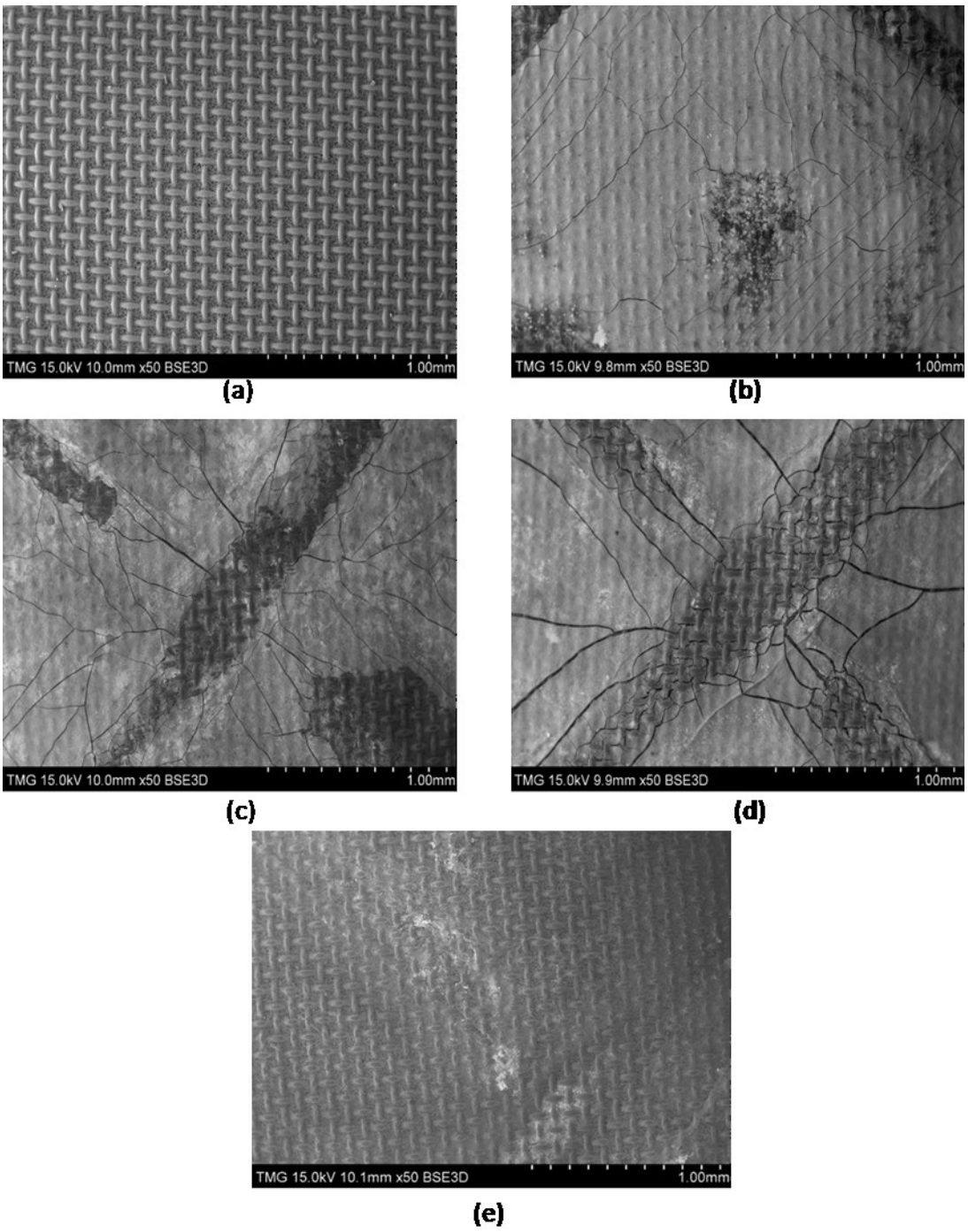


**Figure 4-30: SEM results on the feed side using synthetic salt water. (a) pristine membrane, (b) untreated river water, (c) multimedia sand filter, (d) microfiltration, (e) ultrafiltration.**

All behaviors that were observed in images (b), (c), (d), and (e) are in agreement with the quality of the feed waters that were used (Table 3-2). In other words, by increasing and

improving the quality of the feed waters, the surface of the deposited layer on the membrane samples decreased. Due to some limitations with the SEM device for taking images from the cross section of the membrane samples, the thickness of the deposited layer was not measured.

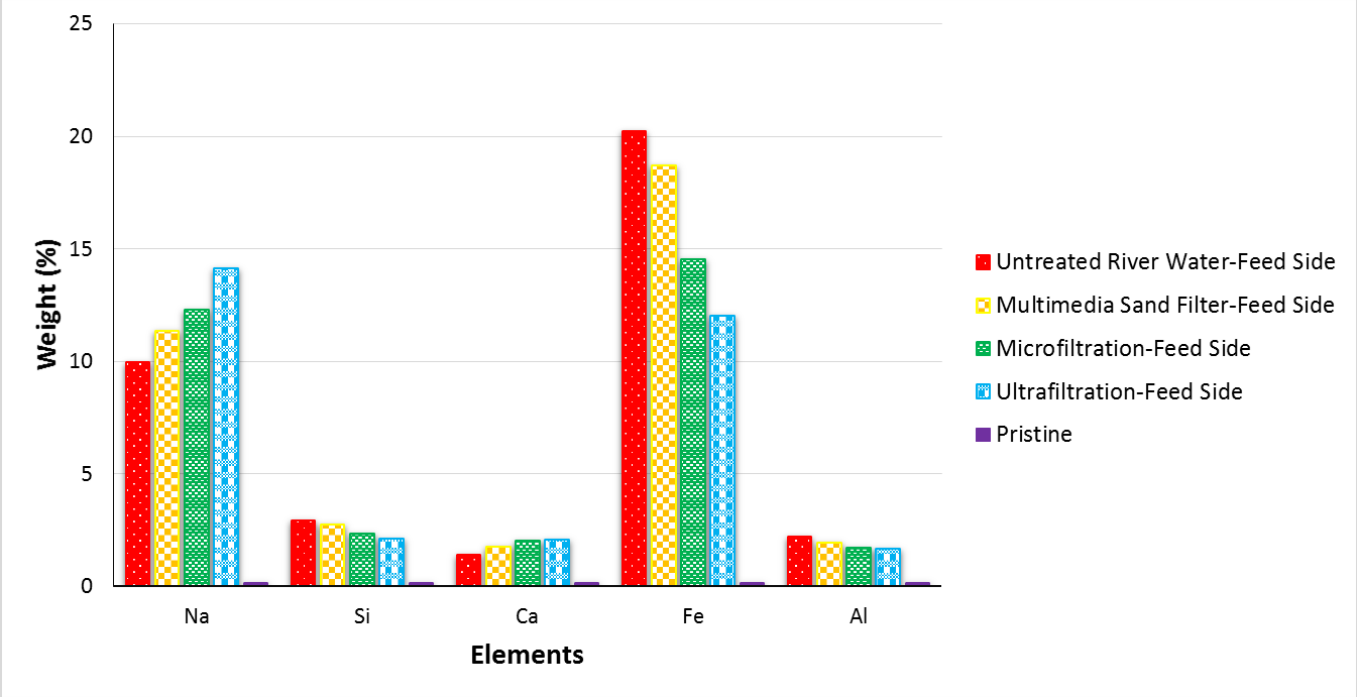


**Figure 4-31: EDS results on feed side using synthetic salt water as draw solution.**

Figure 4-31 shows the EDS results for identification of the main foulants on the feed side when the synthetic salt water was used as a draw solution. According to the results demonstrated in Figure 4-31, silica (Si), aluminum (Al), calcium (Ca), sodium (Na) and iron (Fe) were the main foulants in four membrane samples that were prepared after complete fouling using untreated river water, multimedia sand filter, microfiltration, and ultrafiltration effluents as the feed water (Figure 4-30). The pristine membrane was used as a control in this study. The presence of silica and aluminum shows that they were aluminum silicates that are known as foulants in membrane processes (Fernandez-

Álvarez *et al.*, 2010). The appearance of calcium is due to the calcium that existed in the feed water (Table 3-2) as well as the calcium that was transported from the draw side to the feed side because of the back diffusion of solutes in osmotically driven membranes (Hancock and Cath, 2009; Fernandez-Álvarez *et al.*, 2010; Tang *et al.*, 2010; She *et al.*, 2012). The same trend for sodium was observed for the same reason that was explained for calcium. Iron appeared in high concentrations in the EDS results indicated in Figure 4-31 for all membrane samples using different feed waters. The reason is linked to the iron in the feed water (Table 3-2).

#### 4.4.5.1.2 Using Sea Water

Figure 4-32 indicates the top view of SEM images for three membrane samples (pristine, ultrafiltration, and microfiltration) using sea water as the draw solution. Based on the results in the previous section, ultrafiltration and microfiltration treatments indicated better results compared to no treatment and multimedia sand filter treatment. Therefore, these two feed waters were selected to perform the fouling tests with the sea water. Image (a) in Figure 4-32 indicates the surface of the pristine membrane sample before fouling. Images (b) and (c) show the surface of the membrane samples after fouling when the feed water was from microfiltration and ultrafiltration systems respectively. According to images (b) and (c) demonstrated in Figure 4-32, it seems that the surface of the membrane sample in image (c) (ultrafiltration) was more similar to the membrane surface in the image (a) (pristine membrane) in comparison with the image (b) (microfiltration). The membrane sample shown in Figure 4-32 (b) was covered by a deposited layer that was created after fouling and during the operation time. As mentioned in the previous

section, the reason is associated with the quality of the used feed water which in this case is permeate water from microfiltration system.

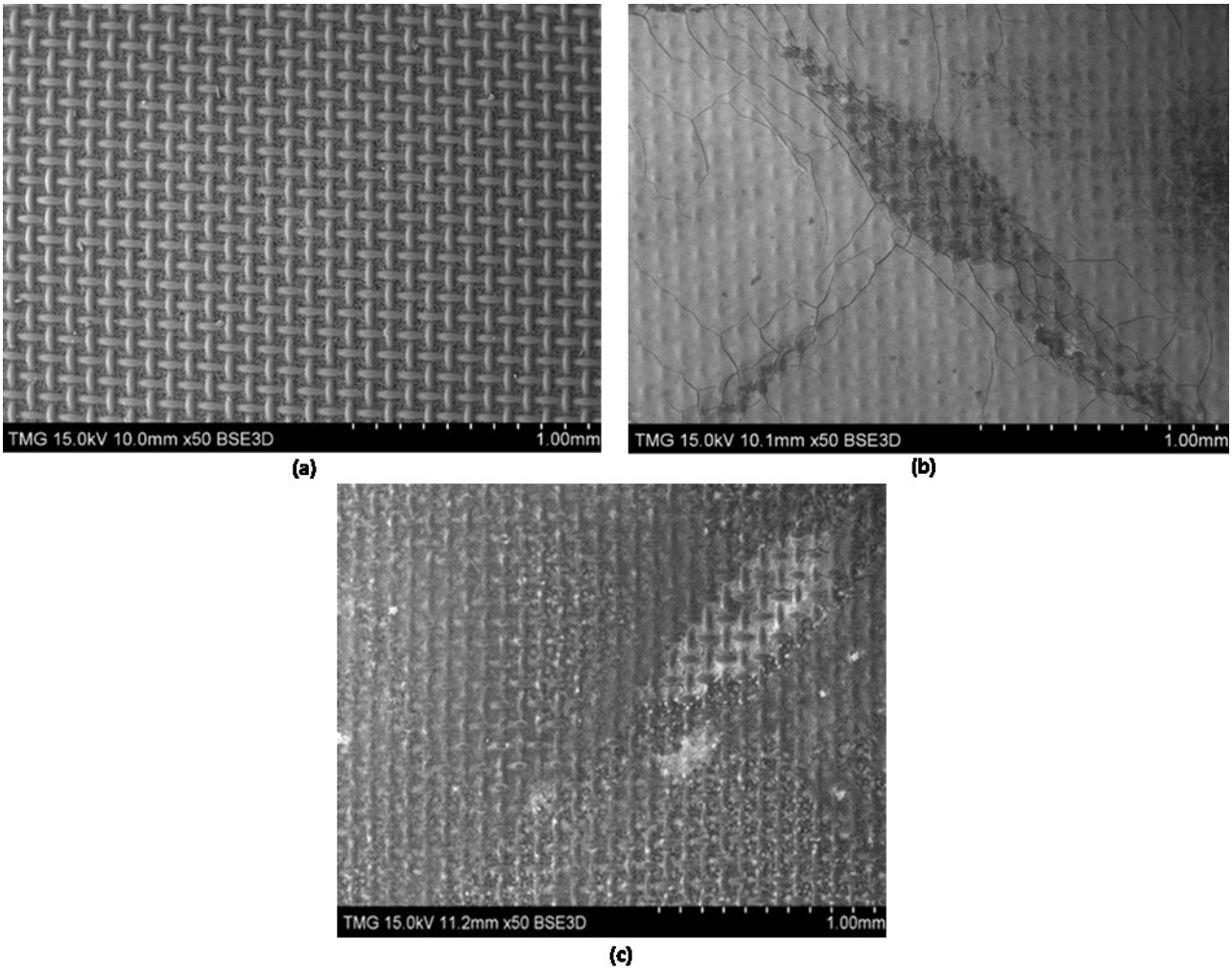


**Figure 4-32: SEM results on feed side using sea water. (a) pristine membrane, (b) microfiltration, (c) ultrafiltration.**

According to the results demonstrated in Table 3-2, the quality of the microfiltration water was lower than that in the ultrafiltration water. On the other hand, the SEM results shown in Figures 4-30 and 4-32 indicate that the quality of the draw solution has a direct effect on the fouling on the feed side of the membrane in PRO mode. Because the synthetic salt water contained only sodium chloride, calcium chloride and demineralized water while

the other components including higher concentrations of divalent cations ($Ca^{+2}$ and $Mg^{+2}$) were observed in the sea water (Table 3-1). By a comparison between the surface of the membrane samples in images (d) and (e) in Figure 4-30 and images (b) and (c) in Figure 4-32, it was noticed that the amount of deposited particles on the surface of the membrane samples using sea water was more than that on the surface of the membrane samples using synthetic salt water. This means that some ions and cations could pass through the membrane from the draw side to the feed side and enhance the membrane fouling on the feed side. This result is in agreement with the new proposed fouling mechanism for osmotically driven membranes which explains how solutes can penetrate through the membrane from the high concentration draw solution to the feed solution and alter the feed solution chemistry and consequently, enhance the membrane fouling on the feed side (Hancock and Cath, 2009; Phillip *et al.*, 2010; Tang *et al.*, 2010; She *et al.*, 2012).

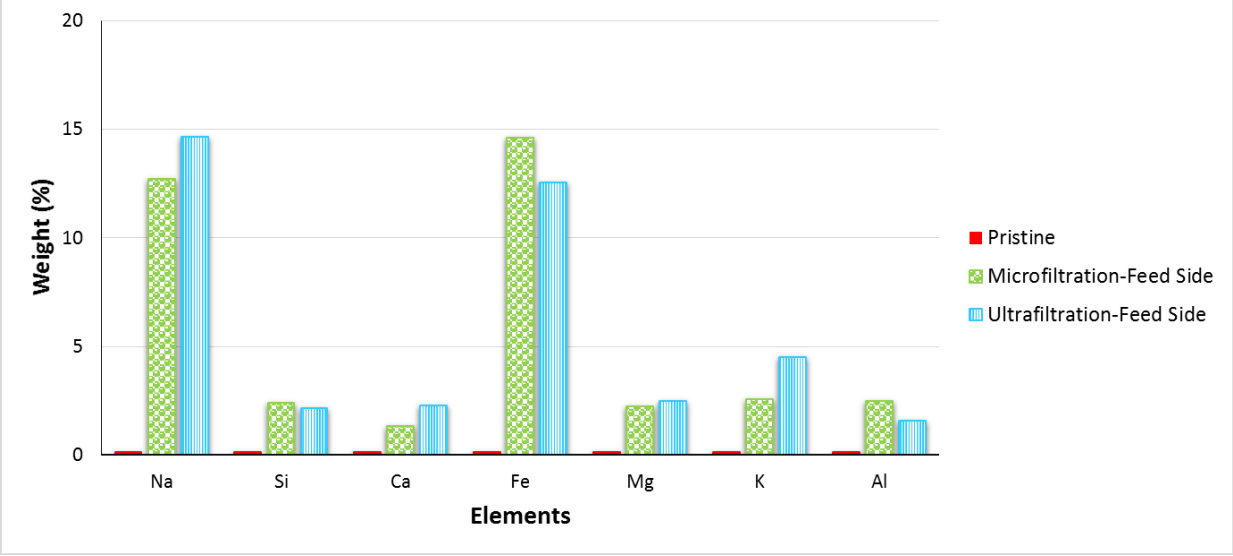


**Figure 4-33: EDS results on the feed side using sea water as draw solution.**

Figure 4-33 shows the results for EDS analysis when sea water was used as the draw solution. Components such as silica (Si), calcium (Ca), iron (Fe), aluminum (Al), sodium (Na), potassium (K) and magnesium (Mg) were observed on the surface of the membrane samples. Some of these components like silica, calcium, iron, aluminum, and sodium were common between the obtained results from EDS analysis for using both synthetic salt water and sea water as the draw solutions. However, some elements such as magnesium and potassium were not found on the surface of membrane samples when the draw solution was synthetic salt water. This means that the components such as magnesium and potassium that existed in the sea water could pass through the membrane to the feed side and, subsequently, enhance the fouling on the surface of the membrane on the feed side according to the back diffusion phenomena that was explained above.

#### 4.4.5.2 Physicochemical Characterization of Foulants Using ATR-FTIR

Attenuated Total Reflection Fourier Transform Infrared (ATR-FTIR) spectroscopy was used to determine the type of organic foulant on the surface of the membrane samples that were collected after complete fouling using four different feed waters (Table 3-2) and two various draw solutions. Each spectrum demonstrated is the result of 1024 scans. Background was collected for each sample separately. The membrane samples were dried before analysis. ATR-FTIR spectra were recorded inside the range of 4000–650 $cm^{-1}$.

##### 4.4.5.2.1 Using Synthetic Salt Water

Figure 4-34 shows the ATR-FTIR results for fouled membrane samples using four various feed waters (untreated river water, multimedia sand filter, microfiltration, and

ultrafiltration) and synthetic salt water as draw solution. The pristine membrane was used as a control to identify the type of organic foulant which can be humic substances, polysaccharides and proteins (Jarusutthirak, 2002; Zularisam *et al.*, 2006) on the membrane samples. In other words, the organic foulants were determined by comparing the ATR-FTIR profiles of pristine membranes and fouled membranes.

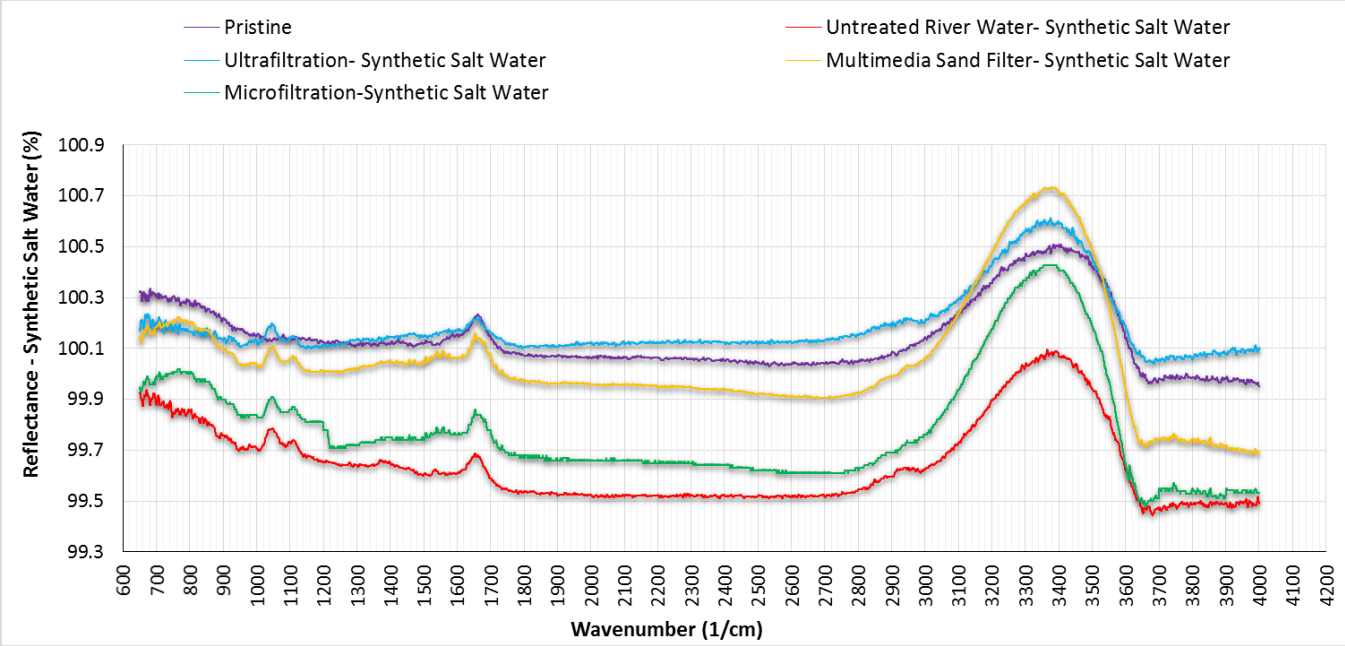


**Figure 4-34: ATR-FTIR results using synthetic salt water as draw solution and untreated river water, multimedia sand filter, microfiltration and ultrafiltration as feed waters.**

Table 4-3 indicates common IR spectra for humic substances, polysaccharides and proteins. According to the results shown in Figure 4-34, some spectra were observed in the ranges of 3600-3100 $cm^{-1}$, and 1700-1600 $cm^{-1}$ that were common between pristine membrane and fouled membrane samples. These ranges were associated with the functional group of membrane materials. As Figure 4-34 indicates, the ATR-FTIR profiles were similar for the fouled membrane samples. For untreated river water, multimedia

sand filter, microfiltration and ultrafiltration IR bands indicative of humic substances were detected in the ranges of 2940-2900 $cm^{-1}$, 1400-1390 $cm^{-1}$, and 1170-950 $cm^{-1}$.

**Table 4-3: Common IR spectra for humic substances, polysaccharides and proteins (Jarusutthirak, 2002; Zularisam *et al.*, 2006) .**

| *Organic matter* | *Band ($cm^{-1}$)* | *Functional Group* |
|---|---|---|
| *Humic Substances* | 3400-3300 | O-H stretching and N-H stretching |
| | 2940-2900 | Aliphatic C-H stretching |
| | 1725-1720 | Carboxylic acids |
| | 1660-1630 | C=O stretching of amide group |
| | 1620-1600 | Aromatic C=C |
| | 1590-1517 | COO–, N-H deformation |
| | 1460-1450 | Aliphatic C-H |
| | 1400-1390 | OH deformation, C–O stretching of phenolic OH |
| | 1280-1200 | C-O stretching, OH deformation of COOH |
| | 1170-950 | C-O stretching of polysaccharide |
| *Polysaccharide Group* | 3400 | Alcohol (1,2,3, Ar) |
| | 2940 | Alkane |
| | 1480 | Alkane |
| | 1370 | 1370 (starch) |
| | 1170 | Tertiary alcohol |
| | 1120 | Secondary alcohol |
| | 1040 | Aliphatic ether |
| | 1000 | Primary alcohol |
| | 775 | Ethyl |
| *Protein Group* | 3300 | Alcohol |
| | 1640 | Alkene in aromatic |
| | 1540 | Mono substituted amide |
| | 1100 | Ether |

Based on the common IR spectra shown in Table 4-3, these ranges were attributed to aliphatic C-H stretching, OH deformation and C-O stretching of phenolic OH and C-O stretching of polysaccharide functional groups respectively. Characteristic signals of polysaccharides group were observed in the wavenumbers of 2940, 1370, 1120, and 1040 $cm^{-1}$ on the fouled membrane samples. These peaks were ascribed to alkane,

starch, secondary alcohol, and aliphatic ether functional groups, respectively. Moreover, several peaks were observed in the wavenumbers of 1540, and 1100 $cm^{-1}$ in the fouled membrane samples which represented protein groups in Table 4-3. These wavenumbers correspond to mono substituted amide and ether functional groups respectively. Thus, these results (Figure 4-34) indicate the accumulation of humic substances, polysaccharides and proteins as organic matter on the surface of fouled membrane samples.

#### 4.4.5.2.2 Using Sea Water

Figure 4-35 indicates the ATR-FTIR results using microfiltration and ultrafiltration as feed waters and sea water as draw solution. As mentioned above, microfiltration and ultrafiltration were selected as the feed water due to their higher qualities (Table 3-2) compared to multimedia and untreated river water. The ATR-FTIR profiles were very similar for both fouled membrane samples demonstrated in Figure 4-35. According to the results demonstrated in Figure 4-35, IR bands associated with humic substances were detected in a range of 2940-2900 $cm^{-1}$, 1660-1630 $cm^{-1}$ , 1460-1450 $cm^{-1}$, 1400-1390 $cm^{-1}$, 1280-1200 $cm^{-1}$, and 1170-950 $cm^{-1}$. These IR bands correspond to C=O stretching of amide group, aliphatic C-H, OH deformation and C–O stretching of phenolic OH, C-O stretching and OH deformation of COOH, and C-O stretching of polysaccharide respectively. Observed IR bands corresponding to the polysaccharides group were 2940 $cm^{-1}$, 1480 $cm^{-1}$, 1370 $cm^{-1}$, 1120 $cm^{-1}$, 1040 $cm^{-1}$ and 775 $cm^{-1}$ which were attributed to alkane, alkane, starch, secondary alcohol, aliphatic ether, and ethyl respectively while the peaks at 1540 $cm^{-1}$, and 1100 $cm^{-1}$ were associated with proteins. These two peaks were assigned to mono substituted amide, and ether respectively.

Therefore, the organic matter including humic substances, polysaccharides and proteins accumulated as foulants on the surface of the fouled membrane samples indicated in Figure 4-35.

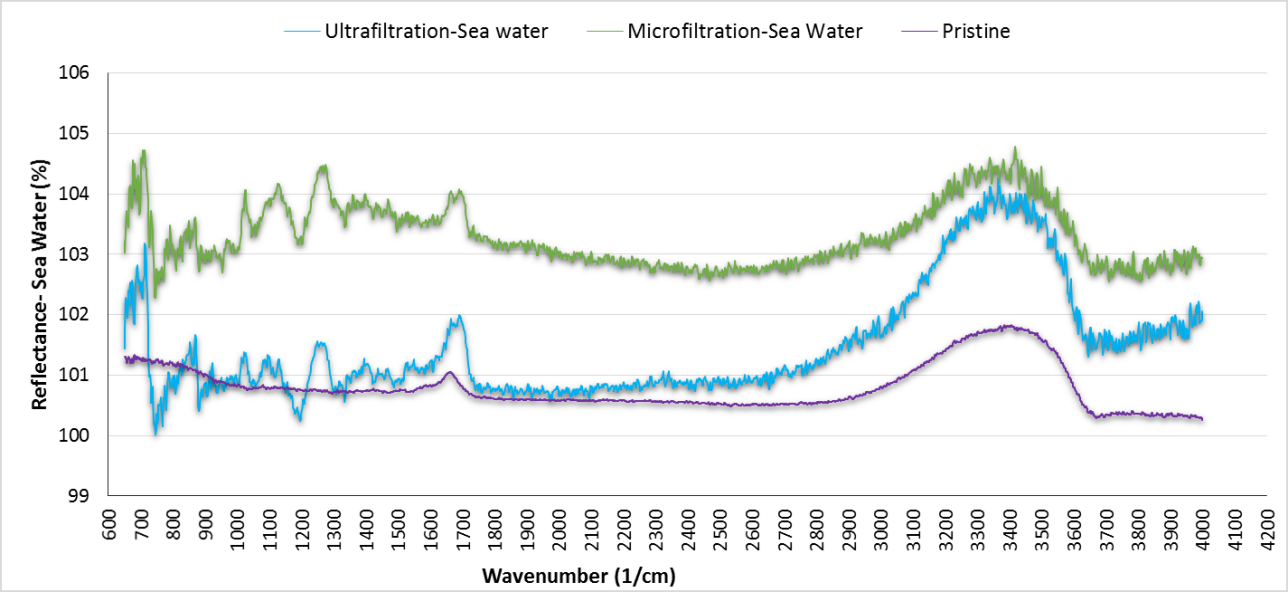


**Figure 4-35: ATR-FTIR results using sea water as the draw solution and microfiltration and ultrafiltration as the feed waters.**

Higher levels of intensities were observed in the ATR-FTIR results for the fouled membrane samples from ultrafiltration and microfiltration using sea water, compared to the ATR-FTIR results for the fouled membrane samples from ultrafiltration and microfiltration using synthetic salt water (Figure 4-34). In addition, more peaks and IR bands corresponding to humic substances and polysaccharides were detected on the surface of the fouled membrane samples when sea water was used as the draw solution compared to when synthetic salt water was used as the draw solution.

These changes might be related to the back diffusion of divalent cations from sea water side (Table 3-1) to the feed water side that could increase the organic matter

accumulation on the membrane surface through the formation of calcium-organic matter and magnesium-organic matter complexes. The back diffusion of calcium could enhance deposition and formation of the organic matter-calcium-iron complexes on the surface of the membrane samples (Yiantsios and Karabelas, 2002; Ma *et al.*, 2014; Xin *et al.*, 2016) on feed side and as a result increases the membrane fouling in PRO processes. However, the concentration of calcium in sea water (324 mg/L) was not significantly higher than that in synthetic salt water (313.77 mg/L), so its effect on the deposition of the organic matter-calcium-iron complexes on the membrane surface would not be very significant compared to when synthetic salt water was used a draw solution. Therefore, it seems that magnesium had a meaningful influence in governing the organic matter formation and accumulation on the membrane surface and that is why more peaks and IR bands corresponding to humic substances and polysaccharides were detected on the surface of the fouled membrane samples for both ultrafiltration and microfiltration when sea water was used as draw solution compared to when synthetic salt water was used. On the other hand, the co-presence of silica and organic matter in feed water might end up with the formation and deposition of the silica-organic matter compounds on the membrane surface as well (Kimura *et al.*, 2016). Further investigations are required to completely understand the interactions between silica, calcium, magnesium, iron and organic matter in the feed water and their roles in PRO membrane fouling.

### 4.4.6 PRO Membrane Cleaning

#### 4.4.6.1 Effect of Physical Cleaning on PRO Membrane Performance

In this experiment, surface flushing was used as a physical cleaning method due to the good results reported by many researchers for cleaning the osmotically driven membranes (Baoxia and Elimelech, 2010; Mi and Elimelech, 2010; Arkhangelsky *et al.*, 2012; Liu and Mi, 2012; Boo *et al.*, 2013; Mi and Elimelech, 2013; Valladares Linares *et al.*, 2013; Choi *et al.*, 2014; Lee *et al.*, 2014; Liu and Mi, 2014; Chun *et al.*, 2015). The osmotic backwashing is also another type of physical cleaning method. In this method, a high concentration saline water is used on the feed water side, while a water with lower salinity is used on the draw side in order to produce a negative water flux to clean the membrane surface. This method was not used because of its negative effect on the osmotic driving force (the agglomeration of salt inside foulant layer during cleaning) and its low efficiency for water flux recovery (Arkhangelsky *et al.*, 2012; Valladares Linares *et al.*, 2013; Valladares Linares *et al.*, 2013). In this trial, ultrafiltration and sea water were used as feed water and draw solutions, respectively.

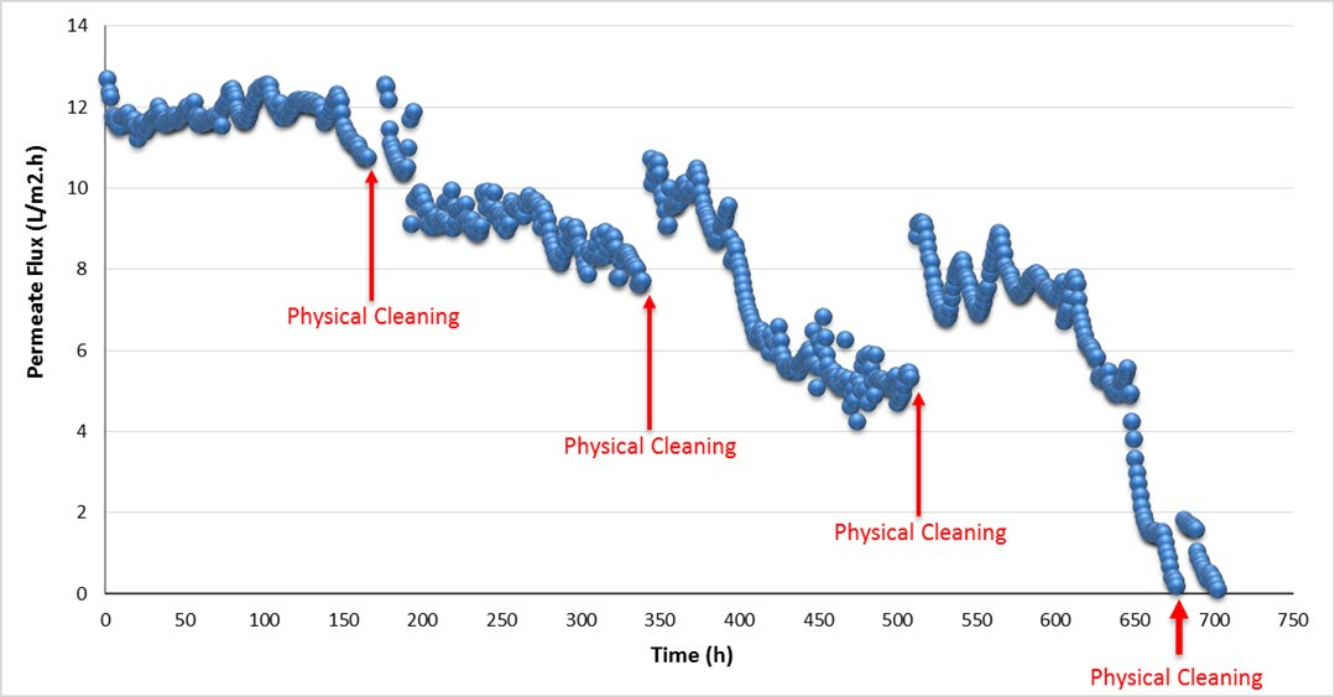


**Figure 4-36: Physical cleaning using ultrafiltration as the feed water and sea water as the draw solution.**

Figure 4-20 shows the effect of fouling on permeate flux over time (ultrafiltration-sea water). According to the results demonstrated in Figure 4-20, complete and irreversible fouling occurred after 405 hours. As the PRO experimental setup was an open system which means the draw solution was not recirculated in the system and was continuously discharged into a waste disposal system that was in the Hydro-Quebec lab, the draw solution could not be diluted and as a result, the salt concentration remained constant during the experiments. Therefore dilution did not have any effect on the fouling and the flux drop in the experiment. The cleaning was started when the permeate flux decreased by 15% as compared to its initial value (Chesters and Armstrong, 2013) and was continued weekly to observe the effect of surface flushing on the membrane cleaning in PRO processes.

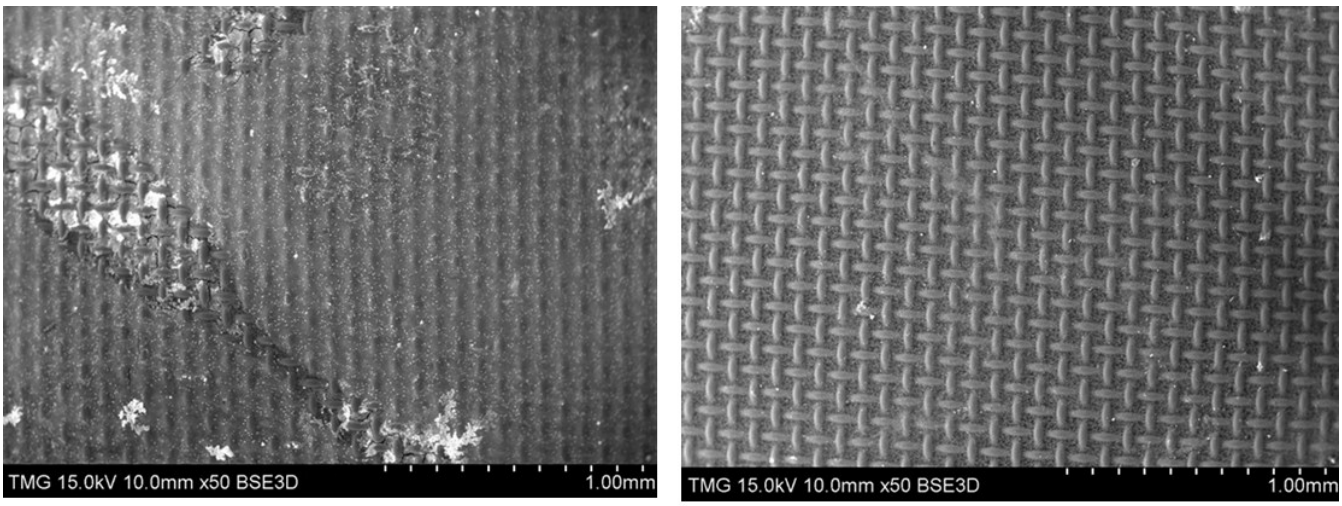


**Figure 4-37: SEM results on the feed side using sea water and ultrafiltration as the draw solution and feed water. (a) membrane surface after physical cleaning, (b) membrane surface after chemical cleaning.**

As Figure 4-36 indicates, the complete fouling occurred after 702 hours using surface flushing. The water flux recovery after first cleaning was 93.2% and then it reduced to 60.4%, 47.3%, 13.2% after second, third, and fourth surface flushings, respectively. The permeate flux was almost negligible (zero) after 22 hours from the last cleaning (the fourth one).

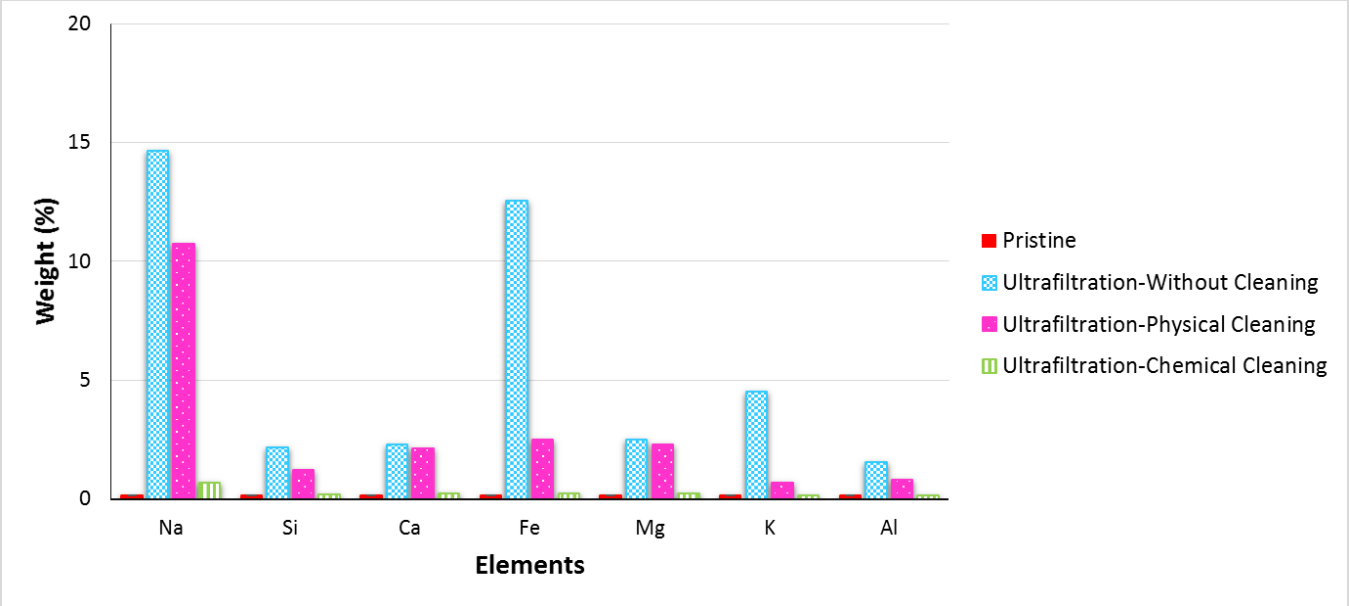


**Figure 4-38: EDS results on the feed side for physical and chemical cleaning using sea water and ultrafiltration as the draw solution and feed water.**

According to the results, the physical cleaning (surface flushing) was not a very effective method for the membrane cleaning in PRO processes. This is in accordance with the SEM results indicated in Figure 4-37 part (a) that shows the surface of the membrane sample after physical cleaning which is similar to the membrane surface in the image (c) in Figure 4-32 (when no cleaning was used). In addition, the EDS results demonstrated in Figure 4-38 shows a lower removal of the inorganic foulants such as calcium, magnesium and silica from the membrane surface after physical cleaning compared to the ultrafiltration without cleaning. However, it seems that the surface flushing was effective for removal of organic matter from the membrane surface based on the ATR-FTIR results indicated in Figure 4-39.

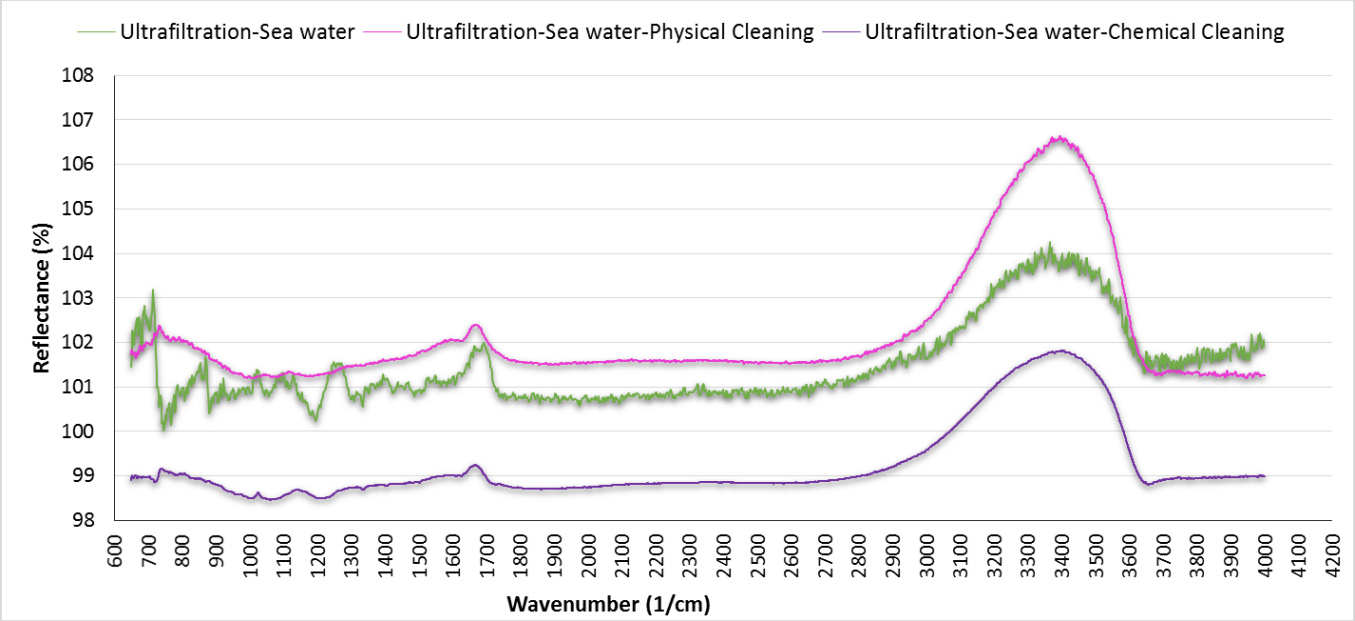


**Figure 4-39: ATR-FTIR results using sea water as the draw solution and ultrafiltration as the feed waters for both physical and chemical cleaning.**

The ATR-FTIR profile after physical cleaning was smoother with very low intensities compared to ATR-FTIR profile of the ultrafiltration without cleaning. Mi and Elimelech (2010) also reported that the surface flushing had a positive influence on the organic matter removal from the membrane surface.

#### 4.4.6.2 Effect of Chemical Cleaning on PRO Membrane Performance

As mentioned in section 4.4.6.1, physical cleaning was not significantly effective for removal of foulants from the membrane surface. In this experiment the effect of cleaning method on membrane fouling was investigated for PRO processes. A combination of basic and acidic agents was used in order to remove both organic and inorganic foulants from the membrane surface. The used feed water and draw solution were ultrafiltration and sea water in this trial to compare this results with physical cleaning results in section 4.4.6.1 For the same reason, cleaning was started when a decrease of 15% in permeate

flux compared to its initial amount was observed and the cleaning was done every week, once a week.

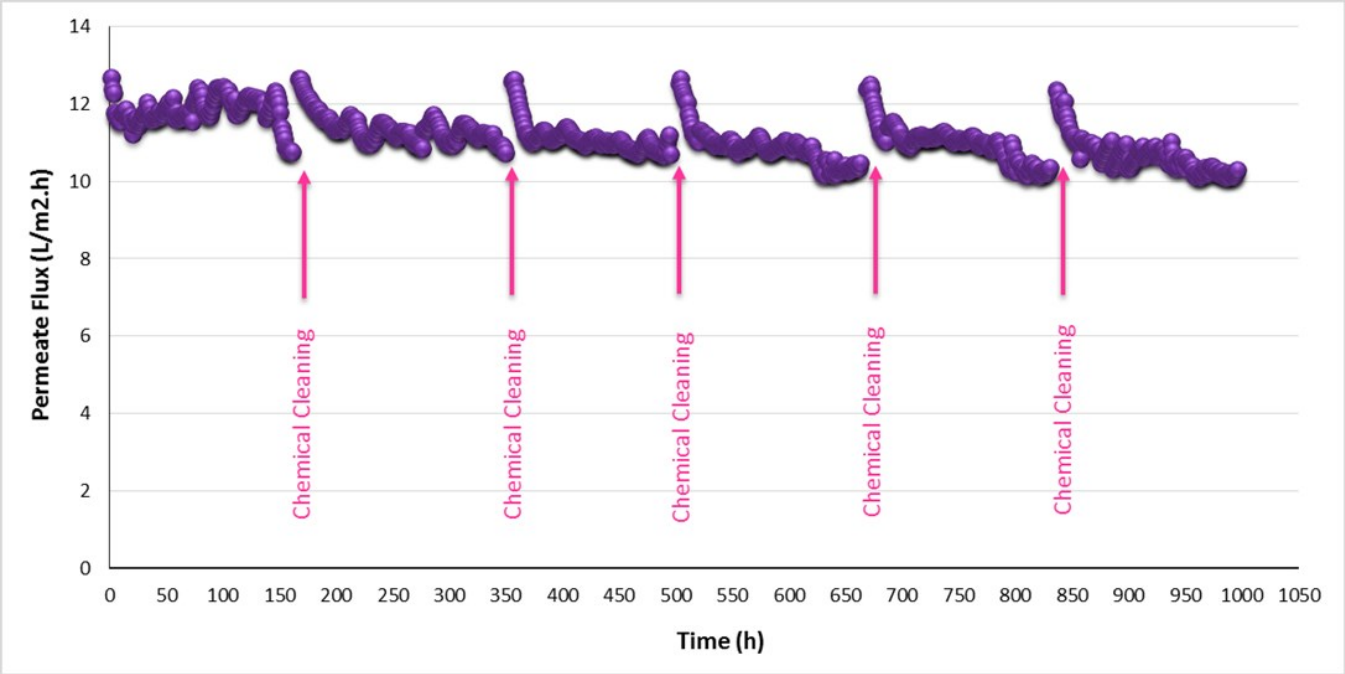


**Figure 4-40: Chemical Cleaning Using Ultrafiltration as the Feed Water and Sea Water as the Draw Solution.**

According to the results indicated in Figure 4-40, the water flux recoveries were 98.4%, 98%, 97.5%, 97.3%, and 97.2% after the first, second, third, fourth and fifth cleanings, respectively. These water flux recoveries using chemical cleaning were much higher than those using physical cleaning. For example, after the fourth cleaning, the water flux recovery was 97.3% for chemical cleaning which was about 7 times higher than that for physical cleaning (13.2%). Moreover, the fouling did not occur even after 996 hours for ultrafiltration using chemical method while the complete fouling occurred after 405, and 702 hours for ultrafiltration without cleaning (Figure 4-20) and ultrafiltration using the physical method (Figure 4-36), respectively. In addition, the obtained results from SEM-EDS and ATR-FTIR demonstrated in Figures 4-37 to 4-39 show the effectiveness of the

proposed chemical cleaning on the membrane fouling in PRO processes which is in accordance with the results indicated in Figure 4-40. Image (b) in Figure 4-37 shows the surface of the membrane sample after chemical cleaning which is significantly similar to the membrane surface in image (a) in Figure 4-32 for the pristine membrane. The EDS results in Figure 4-38 for ultrafiltration-chemical cleaning also indicate that the amounts of inorganics such as silica, calcium, aluminum, magnesium, iron, and potassium on the membrane surface after chemical cleaning were very negligible and very close to the amount of these inorganics on the surface of the pristine membrane. According to the ATR-FTIR results in Figure 4-39, the ultrafiltration-chemical cleaning ATR-FTIR profile was considerably similar to the ATR-FTIR profile of the pristine membrane demonstrated in Figure 4-35 which means the organic foulant removal from the membrane surface was notably achieved by using the proposed chemical cleaning.

Based on what was mentioned in this section, it was clear that the proposed chemical cleaning was remarkably effective for removal of both organic and inorganic foulants from the membrane surface in PRO mode. However, further investigation is needed to understand the environmental effect of these chemical cleaners on the ecosystem over longer period of time in a full scale osmatic power plant.

### 4.4.7 Summary of Fouling Mechanisms and Cleaning Methods

According to the results, the fouling rate when the draw solution was synthetic salt water followed the order of: untreated river water > multimedia sand filter > microfiltration > ultrafiltration effluents. The fouling rate in ultrafiltration and microfiltration effluents using sea water occurred faster compared to the results for untreated synthetic salt water. Using

the cake enhanced osmotic pressure mechanism assisted in understanding the effect of sea water on the membrane fouling in PRO mode when ultrafiltration and microfiltration were used as feed waters. The enhancement of the membrane fouling on the feed side was due to the reverse diffusion of cations such as magnesium and potassium from sea water to the feed waters. It was also observed that complete blocking was the main fouling mechanism that governed the membrane fouling in all cases. The complete blocking might occur due to the interactions between organic and inorganic foulants that form bigger particles in the feed water. SEM-EDS and ATR-FTIR results showed the existence of organic and inorganic compounds as the main foulants on the surface of the membrane. The co-presence of inorganic and organic matter in feed water might lead to the formation and deposition of the inorganic-organic matter compounds on the membrane surface and blocking the membrane completely over time. In order to reduce and control the membrane fouling two cleaning methods (physical and chemical) were used. According to the results, physical cleaning was not a very effective method for the membrane cleaning in PRO processes because it was not very successful for removing the inorganic foulants from the membrane surface, although it was able to reduce the amount of the organic foulants. On the other hand, the obtained results from SEM-EDS and ATR-FTIR showed that the proposed chemical cleaning was remarkably effective because it was able to remove both organic and inorganic foulants from the membrane surface in PRO mode. This research indicates that the chemical cleaning can decrease the membrane fouling in PRO processes and consequently improve the osmotic power generation.

# 5 Conclusions and Recommendations

## 5.1 Summary and Conclusions

In this research, the performance of two pretreatment methods (ultrafiltration and multimedia sand filter) were investigated and compared in terms of removing TOC, turbidity, and hardness. In addition, the effects of parameters such as pressure, required energy and fouling were studied for these two pretreatment methods. Moreover, the fouling behavior and mechanisms of a commercial membrane in PRO mode by using four different feed waters (river water, multimedia sand filter, microfiltration, and ultrafiltration and two different draw solutions (synthetic salt water and sea water) were investigated and compared. Also, the types of foulants on the membrane surface in the PRO processes were identified using SEM-EDS and ATR-FTIR. In addition, the effect of two different cleaning methods (physical and chemical) on reducing and control of membrane fouling in PRO mode were investigated.

Based on the experimental results, the following conclusions were obtained from this work:

- Ultrafiltration indicates better removal efficiency for TOC, hardness and turbidity compared to the multimedia sand filter.

- Fouling occurred faster in the multimedia sand filter compared to ultrafiltration. In other words, reduction of permeate flux in ultrafiltration is less and this makes the ultrafiltration more desirable than the multimedia sand filter.

- Based on the results, the fouling in the PRO membranes was much lower when the used feed water was prepared from ultrafiltration instead of multimedia sand filter.

- According to the results, the maximum overall efficiency of the osmotic power plant was 2.4% while the maximum obtained net electric power after considering the losses and required pressure in pretreatment was decreased to 0.34 $W/m^2$ using the dead-end ultrafiltration as the pretreatment method. The higher performance of the ultrafiltration, although more expensive in energy cost, makes it a better option for producing osmotic power.

- Temperature and salt concentration as the operating factors played important roles in the osmotic power generation. By increasing both, the permeate flux increased. By increasing the applied pressure on the draw solution, the permeate flux decreased and the produced power density increased.

- The fouling rate when the draw solution was synthetic salt water followed the order of: untreated river water > multimedia sand filter> microfiltration > ultrafiltration. The fouling rate in ultrafiltration and microfiltration using sea water occurred faster compared to the results for synthetic salt water.

- Complete blocking (CBM) was the main fouling mechanism for all different feed waters. The further decrease in permeate flux was due to the cake formation (CFM).

- According to the results, cake filtration model was not completely able to predict the observed difference in the behavior of osmotically driven membranes when different draw solutions were used. Using a cake enhanced osmotic pressure mechanism, assisted in understanding the effect of various draw solutions on the membrane fouling in the PRO mode.

- The enhancement of the membrane fouling on the feed side was due to the reverse diffusion of cations such as magnesium and potassium from sea water to the feed waters.

- According to SEM images, a positive correlation was observed between the quality of the feed waters and the deposited layer on the membrane surface using both synthetic salt water and sea water as draw solutions. In other words, by increasing and improving the quality of the feed water, the surface of the deposited layer on the membrane samples decreased.

- The quality of the draw solution had a direct effect on the fouling on feed side of the membrane in PRO mode.

- According to the results from EDS analysis, inorganic foulants were silica (Si), aluminum (Al), calcium (Ca), sodium (Na) and iron (Fe) when the feed waters were untreated river water, multimedia sand filter, microfiltration, and ultrafiltration effluents and synthetic salt water was used as the draw solution. In addition to the identified inorganic foulants using synthetic salt water, other inorganic foulants such as potassium (K) and magnesium (Mg) were also observed on the surface of

the membrane samples when sea water was used as the draw solution and ultrafiltration and microfiltration were used as the feed water.

- The ATR-FTIR results indicated that humic substances, polysaccharides and proteins were the main organic foulants on the surface of the fouled membrane samples using both synthetic salt water and sea water as the draw solution.

- Based on the cleaning results, when the chemical cleaning was used, the fouling in the PRO membranes was reduced considerably compared to when the physical cleaning (surface flushing) was used. Therefore, the proposed chemical cleaning method can improve and control the PRO membrane fouling effect and subsequently, it will improve the production of osmotic power.

## 5.2 Recommendations for Future Studies

- Investigate performance and efficiency of the PRO system at pilot scale (due to limitations at lab scale) using membrane modules (larger membrane units) in four seasons continuously. This pilot plant to be built in Québec would be the first PRO pilot plant in North America.

- Examine the effect of different PRO membranes with various configurations on the permeate flux and power density.

- As these four classic models are able to predict only one mechanism for the whole filtration process, further investigations (considering their combination with the CEOP mechanism) are required for development of these models which will lead

to a better understanding and prediction of the fouling behavior in the osmotically driven membranes.

- Further investigations are required to completely understand the interactions between silica, calcium, magnesium, iron and organic matter in feed water and their roles in PRO membrane fouling.

- Further investigation is needed to understand the environmental effect of the used chemical cleaners on the ecosystem over a long period of time in a full scale osmotic power plant.

## 5.3 Contributions

The technical output of the presented research in this thesis are as follows:

### 5.3.1 Journal Papers

1. Abbasi-Garravand, E., C.M. Mulligan, C.B. Laflamme and G. Clairet, 2016. Role of Two Different Pretreatment Methods in Osmotic Power (Salinity Gradient Energy) Generation, Renewable Energy Journal, 96: p: 98-119.

2. Abbasi-Garravand, E., C.M. Mulligan, C.B. Laflamme and G. Clairet, Investigation of the Fouling Effect on a Commercial Semi-Permeable Membrane in Pressure Retarded Osmosis (PRO) Process, under review.

3. Abbasi-Garravand, E., C.M. Mulligan, C.B. Laflamme and G. Clairet, Identification of the Type of Foulants and Investigation of the Cleaning Methods for PRO Processes in Osmotic Power Application, under review.

4. Abbasi-Garravand, E., C.M. Mulligan, C.B. Laflamme and G. Clairet, Evaluation of the PRO Power Plant Efficiency Using Various Pretreatment Methods and Effect of Operating Conditions on Permeate Flux in PRO and FO modes, in progress.

### 5.3.2 Conference Paper

- Abbasi-Garravand, E., C.M. Mulligan, C.B. Laflamme and G. Clairet, 2015, Using Ultrafiltration and Sand Filters as Two Pretreatment Methods for Improvement of the Osmotic Power (Salinity Gradient Energy) Generation Process, 4th Climate Change Technology Conference, Montreal, Canada. p. 1-12.

### 5.3.3 Innovations and Contributions to Knowledge

- As little research has been done to study the effect of pretreatments on the membrane fouling in PRO processes, it is important to investigate various pretreatment methods in order to understand their role on the decrease of the PRO membrane fouling and the improvement of the osmotic power generation. In this research, various ultrafiltration systems and a multimedia sand filter were used as different pretreatment methods for reducing the amount of TOC, turbidity and hardness from raw water, which are very effective in PRO membrane fouling, and consequently improving the osmotic power generation.

- Although much research has been done on PRO, the membrane fouling and its mechanisms have not been studied very well yet. In the few existing fouling studies on PRO membrane, artificial foulants and synthetic draw and feed solutions were mostly used. In this research, however, river water and sea water were used as the feed and draw waters, respectively, to observe the effect of fouling on a commercial semi permeable membrane in PRO mode in realistic conditions to better understand the PRO membrane fouling in real conditions. An experimental setup was used which avoids recirculation. This way, effects such as dilution and accumulation of draw solutes in the feed are avoided. This is rarely seen in studies like this.

- In the few existing studies on the PRO system efficiency, the role of the pretreatment and its required power on the overall efficiency of the system under real conditions was not been studied. In this research, the efficiency of a PRO system considering various pretreatment methods was evaluated using a commercial semi permeable membrane. Also, the performance of this commercial membrane was investigated under different operating conditions in FO and PRO modes.

- While many researchers have studied the fouling phenomena and cleaning methods in FO membranes, very few publications have addressed the foulant identification and membrane cleaning methods in PRO processes. In this research, PRO membrane foulants including organic and inorganic are identified to determine the type of fouling in order to control and clean the PRO membrane.

Based on the type of fouling two physical and chemical cleaning methods are used to investigate their roles in reduction and control of PRO membrane fouling.

## References


Abbasi-Garravand, E., C.M. Mulligan, C.B. Laflamme and Clairet, G., 2015. Using ultrafiltration and sand filters as two pretreatment methods for improvement of the osmotic power (Salinity Gradient Energy) generation process. in 4th Climate Change Technology Conference. Montreal, Canada: 12 pages.

Abbasi-Garravand, E. and C.N. Mulligan, 2014. Using micellar enhanced ultrafiltration and reduction techniques for removal of Cr(VI) and Cr(III) from water. Separation and Purification Technology, 132: 505–512.

Abbasi-Garravand, E., C.N. Mulligan, C.B. Laflamme and G. Clairet, 2016. Role of two different pretreatment methods in osmotic power (salinity gradient energy) generation. Renewable Energy, 96: 98-119.

Achilli, A., T.Y. Cath and A.E. Childress, 2009. Power generation with pressure retarded osmosis: An experimental and theoretical investigation. Journal of Membrane Science, 343: 42–52.

Achilli, A. and A.E. Childress, 2010. Pressure retarded osmosis: From the vision of Sidney Loeb to the first prototype installation — Review. Desalination, 261: 205–211.

Agashichev, S.P., 2006. Enhancement of concentration polarization due to gel accumulated at membrane surface. Journal of Membrane Science, 285: 96–101.

Alhadidi, A., A.J.B. Kemperman, J.C. Schippers, M. Wessling and W.G.J. Van der Meer, 2011. The influence of membrane properties on the silt density index. The Journal of Membrane Science, 384: 205-218.

Alsvik, I.L. and M. Hägg, 2013. Pressure retarded osmosis and forward osmosis membranes: materials and methods. Polymers, 5: 303-327.

Altaee, A. and A. Sharif, 2015. Pressure retarded osmosis: advancement in the process applications for power generation and desalination. Desalination, 356: 31–46.

Álvarez-Silva, O., A. Osorio, S. Ortega and P. Agudelo-Restrepo, 2011. Estimation of the electric power potential using pressure retarded osmosis in the Leon River's Mouth: a First step for the harnessing of saline gradients in Colombia. IEEE: 7 pages.

Ambashta, R.D. and M.E.T. Sillanpää, 2012. Membrane purification in radioactive waste management: A short review. Environmental Radioactivity, 105: 76-84.

Amini, M., M. Jahanshahi and A. Rahimpour, 2013. Synthesis of novel thin film nanocomposite (TFN) forward osmosis membranes using functionalized multi-walled carbon nanotubes. Journal of Membrane Science, 435: 233-241.

Applied Membranes Inc, 2015. Am-11 Specifications. 1-1.

Arkhangelsky, E., F. Wicaksana, S. Chou, A.A. Al-Rabiah, S.M. Al-Zahrani and R. Wang, 2012. Effects of scaling and cleaning on the performance of forward osmosis hollow fiber membranes. Journal of Membrane Science, 415-416: 101–108.

Arthanareeswaran, G., D. Mohan and M. Raajenthiren, 2007. Part I. preparation and performance of polysulfone-sulfonated poly(ether ether ketone) blend ultrafiltration membranes. Applied Surface Science, 253: 8705–8712.

ASTM, S.D.-. 2007. Standard test method for silt density index (SDI) of water, D19.08 on membranes and ion exchange materials.

Baoxia, M.I. and M. Elimelech, 2010. Gypsum scaling and cleaning in forward osmosis: Measurements and mechanisms. Environmental Science and Technology, 44: 2022–2028.

Belfort, G., 1984. Synthetic membrane processes: Fundamentals and water applications. Academic Press Inc.

Beolchini, F., F. Pagnanelli, I. Demichelis and F. Veglio, 2006. Micellar enhanced ultrafiltration for arsenic(v) removal: Effect of main operating conditions and dynamic modelling. Environmental Science and Technology 40: 2746-2752.

Berrouche, Y. and P. Pillay, 2012. Determination of salinity gradient power potential in Québec, Canada. Journal of Renewable and Sustainable Energy 4: 0531131-05311319.

Bilgen, S. and K. Kaygusuz, 2004. Renewable energy for a clean and sustainable future. Energy Sources, 26: 1119–1129.

Blandin, G., A.R.D. Verliefde, C.Y. Tang, A.E. Childress and P. Le-Clech, 2013. Validation of assisted forward osmosis (AFO) process: Impact of hydraulic pressure. Journal of Membrane Science 44: 1-11.

Bolton, G., D. LaCasse and R. Kuriyel, 2006. Combined models of membrane fouling: Development and application to microfiltration and ultrafiltration of biological fluids. Journal of Membrane Science, 277: 75–84.

Bolton, G.R., A.W. Boesch and M.J. Lazzara, 2006. The effects of flow rate on membrane capacity: Development and application of adsorptive membrane fouling models. Journal of Membrane Science, 279: 625–634.

Boo, C., M. Elimelech and S. Hong, 2013. Fouling control in aforward osmosis process integrating seawater desalination and waste water reclamation. Journal of Membrane Science, 444: 148–156.

Brauns, E., 2008. Towards a worldwide sustainable and simultaneous large-scale production of renewable energy and potable water through salinity gradient power

by combining reversed electrodialysis and solar power? Desalination 219: 312–323.

Brião, V.B. and C.R.G. Tavares, 2012. Pore blocking mechanisms for the recovery of milk solids from dairy wastewater by ultrafiltration. Brazilian Journal of Chemical Engineering, 29: 393 - 407.

Brogioli, D., 2009. Extracting renewable energy from a salinity difference using a capacitor. The American Physical Society Physical Review Letters, 103 0585011-0585014.

Bui, N. and J.R. McCutcheon, 2014. Nanofiber supported thin-film composite membrane for pressure- retarded osmosis. Environmental Science and Technology, 48: 4129−4136.

Burheim, O.S., F. Liu, B.B. Sales, O. Schaetzle, C.J.N. Buisman and H.V.M. Hamelers, 2012. Faster time response by the use of wire electrodes in capacitive salinity gradient energy systems. The Journal of Physical Chemistry, 116: 19203−19210.

Cath, T.Y., A.E. Childress and M. Elimelech, 2006. Forward osmosis: Principles, applications, and recent developments. Journal of Membrane Science, 281: 70–87.

Cath, T.Y., M. Elimelech, J.R. McCutcheon, R.L. McGinnis, A. Achilli, D. Anastasio, A.R. Brady, A.E. Childress, I.V. Farr, N.T. Hancock, J. Lampi, L.D. Nghiem, M. Xie and N. Yin Yip, 2013. Standard methodology for evaluating membrane performance in osmotically driven membrane processes. Desalination, 312: 31-38.

Chen, S.C., C.F. Wan and T. Chung, 2015. Enhanced fouling by inorganic and organic foulants on pressure retarded osmosis (PRO) hollow fiber membranes under high pressures. Journal of Membrane Science, 479: 190–203.

Chen, Y., L. Setiawan, S. Chou, X. Hub and R. Wang, 2016. Identification of safe and stable operation conditions for pressure retarded osmosis with high performance hollow fiber membrane. Journal of Membrane Science, 503: 90–100.

Chesters, S.P. and M.W. Armstrong, 2013. RO membrane cleaning-explaining the science behind the art. The International Desalination Association World Congress on Desalination and Water Reuse (IDA), Tianjin, China.

Choi, Y., S. Vigneswaran and S. Lee, 2016. Evaluation of fouling potential and power density in pressure retarded osmosis (PRO) by fouling index. Desalination, 389: 215–223.

Choi, Y.J., S.H. Kim, S. Jeong and T.M. Hwang, 2014. Application of ultrasound to mitigate calcium sulfate scaling and colloidal fouling. Desalination, 336: 153–159.

Chou, S., L. Shi, R. Wang, C.Y. Tang, C. Qiu and A.G. Fane, 2010. Characteristics and potential applications of a novel forward osmosis hollow fiber membrane. Desalination 261: 365–372.

Chou, S., R. Wang, N. Anthony and G. Fane, 2013. Robust and high performance hollow fiber membranes for energy harvesting from salinity gradients by pressure retarded osmosis. Journal of Membrane Science, 448: 44–54.

Chou, S., R. Wang, L. Shi, Q. She, C. Tang and A.G. Fane, 2012. Thin-film composite hollow fiber membranes for pressure retarded osmosis (PRO) process with high power density. Journal of Membrane Science, 389: 25–33.

Chun, Y., F. Zaviska, E. Cornelissen and L. Zou, 2015. A case study of fouling development and flux reversibility of treating actual lake water by forward osmosis process. Desalination, 357: 55–64.

Chung, T., S. Zhang, K.Y. Wang, J. Su and M.M. Ling, 2012. Forward osmosis processes: yesterday, today and tomorrow. Desalination 287: 78–81.

Ding, J. and A. Somani, 2010. Reduction of green house gas emission by clean power trading. . U.S. Government: pp: 4588-4592.

Dlugolecki, P., A. Gambier, K. Nijmeijer and M. Wessling, 2009. Practical potential of reverse electrodialysis as process for sustainable energy generation. Environmental Science and Technology 43: 6888–6894.

Duong, P.H.H., J. Zuo and T. Chung, 2013. Highly crosslinked layer-by-layer polyelectrolyte FO membranes: Understanding effects of salt concentration and deposition time on FO performance. Journal of Membrane Science, 427: 411–421.

Elazher, N., B. Gourich, C. Vial, M.B. Soulami and M. Ziyad, 2008. Study of ferrous iron oxidation in Morocco drinking water in an airlift reactor. Chemical Engineering and Processing, 47: 1877-1886.

Environment Canada, 2007. National inventory report 1990–2005: Greenhouse gas sources and sinks in Canada. Inquiry Centre, Environment Canada, Gatineau, Quebec.

Environment Canada, 2008. Environment Canada 2007-2008, report on plans and priorities.

EPA, 1986. Quality criteria for water. U.S. Government printing office superintendent of documents N. capital and H street N.W., Washington, D.C., 20401.

Erdinc, O. and M. Uzunoglu, 2012. Optimum design of hybrid renewable energy systems: Overview of different approaches. Renewable and Sustainable Energy Reviews, 16: 1412-1425.

Esmaili, E., N. Mahinpey and C.J. Lim, 2013. Modified equilibrium modelling of coal gasification with in situ $CO_2$ capture using sorbent CaO: assessment of approach temperature. Chemical Engineering Research and Design, 91: 1361–1369.

Farkova, J., 1991. The pressure drop in membrane module with spacers. Journal of Membrane Science, 64: 103-111.

Fei, L., 2010. Application of environmental management on energy saving and green house gas reduction in Beijing. . Management and Service Science 1-6.

Fell, C.J.D., R.D. Noble and S.A. Stern, 1995. Membrane separations technology: Principles and applications (chapter 4). Oxford, UK.

Fernandez-Álvarez, G., G. Garralón, F. Plaza, A. Garralón, J. Pérez and M.A. Gómez, 2010. Autopsy of SWRO membranes from desalination plant in Ceuta after 8 years in operation. Desalination, 263: 264–270.

Forster, P., V. Ramaswamy, P. Artaxo, T. Berntsen, R. Betts, D.W. Fahey, J. Haywood, J. Lean, D.C. Lowe, G. Myhre, J. Nganga, R. Prinn, G. Raga, M. Schulz and R. Van Dorland, 2007. Changes in atmospheric constituents and in radiative forcing. In: Climate change 2007: The physical science basis. Contribution of working group i to the fourth assessment report of the intergovernmental panel on climate change [Solomon, S., D. Qin, M. Manning, Z. Chen, M. Marquis, K.B. Averyt, M.Tignor and H.L. Miller (eds.)]. Cambridge, United Kingdom and New York, NY, U.S.A.: Cambridge University Press.

Guo, Y.P., Y.Y. Hu, R.R. Gu and H. Lin, 2009. Characterization and micellization of rhamnolipidic fractions and crude extracts produced by Pseudomonas aeruginosa mutant mig-n146. Journal of Colloid and Interface Science, 331: 356–363.

Hach Company, 2007. Methods for the examination of water, and waste water.

Hajibabai Dizaji, L. and P.M. Feniosky, 2009. Visualizing green house gas emissions during the construction phase of infrastructure projects using geo-spatial information systems. . International Workshop on Computing in Civil Engineering American Society of Civil Engineers: 299-307.

Han, G., S. Zhang, X. Li and T. Chung, 2013. High performance thin film composite pressure retarded osmosis (PRO) membranes for renewable salinity-gradient energy generation. Journal of Membrane Science, 440: 108–121.

Hancock, N.T. and T.Y. Cath, 2009. Solute coupled diffusion in osmotically driven membrane processes. Environmental Science and Technology, 43: 6769-6775.

Hayashi, H. and T. Okumura, 2016. Macro and nano behavior of salt water in pressure retarded osmosis membrane. Desalination, 389: 155–161.

Heo, J., K.H. Chu, N. Her, J. Im, Y. Park, J. Cho, S. Sarp, A. Jang, M. Jang and Y. Yoon, 2015. Organic fouling and reverse solute selectivity in forward osmosis: Role of working temperature and inorganic draw solutions. Desalination: 1-9.

Hermans, P.H. and H.L. Bredée, 1935. Zur kenntnis der filtrationsgesetze. Recueil des Travaux Chimiques des Pays-Bas, doi: 10.1002/recl.19350540902, 54(9): 680-700.

Hermans, P.H. and H.L. Bredée, 1935. Zur kenntnis der filtrationsgesetze. Recueil des Travaux Chimiques des Pays-Bas, 54: 680-700.

Hermia, J., 1982. Constant pressure blocking filtration laws—application to power-law non-Newtonian fluids. Transactions of the Institution of Chemical Engineers, 60(3): 183–187.

Herzberg, M. and M. Elimelech, 2007. Biofouling of reverse osmosis membranes: role of biofilm-enhanced osmotic pressure. Journal of Membrane Science, 295: 11–20.

Hiroyuki, I., N. Hirotomo, K. Taichi and K. Takashi, 2011. Three-Dimensionally Arrayed and Mutually Connected 1.2-nm Nanopores for High-Performance Electric Double Layer Capacitor. American Chemical Society, 133: 1165–1167.

Hoek, E.M.V. and M. Elimelech, 2003. Cake-enhanced concentration polarization: a new fouling mechanism for salt-rejecting membranes. Environmental Science and Technology, 37: 5581–5588.

Hoek, E.M.V., A.S. Kim and M. Elimelech, 2002. Influence of crossflow membrane filter geometry and shear rate on colloidal fouling in reverse osmosis and nanofiltration separations. Environmental Science and Technology, 19: 357–372.

Hoover, L.A., J.D. Schiffman and M. Elimelech, 2013. Nanofibers in thin-film composite membrane support layers: Enabling expanded application of forward and pressure retarded osmosis. Desalination, 308: 73-81.

Huang, C., C. Hsieh, P. Kuoa and H. Teng, 2012. Electric double layer capacitors based on a composite electrode of activated mesophase pitch and carbon nanotubes. Journal of Materials Chemistry, 22: 7314-7322.

Huang, H. and S. Lo, 2011. Review and classify the GHGs-related indicators. Renewable and Sustainable Energy Reviews, 15: 594-602.

Hydro-Québec, 2013. Matériel et équipement des bancs d'essai: 1-5.

IEA, 2012. $CO_2$ emissions from fuel combustion highlights. Paris, France.

Ilias, S. and R. Govind, 1993. A study on concentration polarization in ultrafiltration. Separation Science and Technology, 28: 361-381.

Institut des Sciences de la Mer de Rimouski, I.S.M.E.R., 2012. Station aquicole de l'ISMER.

IPCC Report, 2013. Working Group I Contribution to the IPCC Fifth Assessment Report Climate Change The Physical Science Basis. Stockholm: pp: 23-26

Jarusutthirak, C., 2002. Fouling and flux decline of reverse osmosis (RO), nanofiltration (NF), and ultrafiltration (UF) membranes associated with effluent organic matter (EFOM) during wastewater reclamation/reuse. in Department of Civil, Environmental, and Architectural Engineering, University of Colorado: 322 pages.

Jia, Y., H. Li, M. Wang, L. Wu and Y. Hu, 2010. Carbon nanotube: Possible candidate for forward osmosis. Separation and Purification Technology, 75: 55-60.

Jiang, T., M.D. Kennedy, B.F. Guinzbourg, P.A. Vanrolleghem and J.C. Schippers, 2005. Optimising the operation of a MBR pilot plant by quantitative analysis of the membrane fouling mechanism. Water Science & Technology, 51(6-7): 19-25.

Karl, T.R. and K.E. Trenberth, 2003. Modern global climate change. Science, 302: 1719-1723.

Katsoufidou, K., S.G. Yiantsios and A.J. Karabelas, 2005. A study of ultrafiltration membrane fouling by humic acids and flux recovery by backwashing: Experiments and modeling. Journal of Membrane Science, 266: 40-50.

Kiehl, J.T. and K.E. Trenberth, 1997. Earth's annual global mean energy budget. American Meteorological Society. National Center for Atmospheric Research, Boulder, Colorado, U.S.

Kim, G., M.E. Lee, K.S. Lee, J. Park, W.M. Jeong, S. Kang, J. Soh and H. Kim, 2012. An overview of ocean renewable energy resources in Korea. Renewable and Sustainable Energy Reviews 16: 2278– 2288.

Kim, H., J.S. Choi and S. Lee, 2012. Pressure retarded osmosis for energy production: membrane materials and operating conditions. Water Science & Technology, 65.10: 1789-1794.

Kim, J., S. Kim and D. Kim, 2013. Energy harvesting from salinity gradient by reverse electrodialysis with anodic alumina nanopores. Energy, 51: 413-421.

Kim, J., M.J. Park, M. Park, H.K. Shon, S. Kim and J.H. Kim, 2016. Influence of colloidal fouling on pressure retarded osmosis. Desalination, 389: 207–214.

Kim, K.J., A.G. Fanea, C.J.D. Fell and D.C. Joy, 1992. Fouling mechanisms of membranes during protein ultrafiltration. Journal of Membrane Science, 68: 79-91.

Kim, Y.C. and M. Elimelech, 2013. Potential of osmotic power generation by pressure retarded osmosis using seawater as feed solution: Analysis and experiments. Journal of Membrane Science, 429: 330-337.

Kim, Y.C., Y. Kim, D. Oh and K.H. Lee, 2013. Experimental investigation of a spiral-wound pressure-retarded osmosis membrane module for osmotic power generation. Environmental Science and Technology, 47: 2966−2973.

Kim, Y.C., J.H. Lee and S. Park, 2015. Novel cross flow membrane cell with asymmetric channels: Design and pressure-retarded osmosis performance test. Journal of Membrane Science, 476: 76–86.

Kimura, K., S. Okazaki, T. Ohashi and Y. Watanabe, 2016. Importance of the co-presence of silica and organic matter in membrane fouling for RO filtering MBR effluent. Journal of Membrane Science, 501: 60–67.

Kurniawan, T.A., G.Y.S. Chan, W.H. Lo and S. Babel, 2006. Physico–chemical treatment techniques for wastewater laden with heavy metals. Chemical Engineering Journal of Colloid and Interface Science, 118: 83-98.

Kwona, O., H. Yang, Y. Choi and S. Noh, 2008. Fouling control of a submerged membrane module (yef) by filtration modes. Desalination 234: 81-88.

La Mantia, F., M. Pasta, H.D. Deshazer, B.E. Logan and Y. Cui, 2011. Batteries for efficient energy extraction from a water salinity difference. American Chemical Society Nano Letters, 11: 1810–1813.

Labrecque, R., 2009. Exergy as a useful variable for quickly assessing the theoretical maximum power of salinity gradient energy systems. Entropy, 11: 798-806.

Lacey, R.E., 1980. Energy by reverse electrodialysis. Ocean Energy, 7: 1-47.

Laflamme, C.B., 2013. Énergie osmotique – potentiel au Québec, rapport LTE-RT-2013-diffusion Hydro-Québec. 1-58.

Le, N.L., N.M.S. Bettahalli, S.P. Nunes and T. Chung, 2016. Outer-selectivethin film composite (TFC) hollow fiber membranes for osmotic power generation. Journal of Membrane Science, 505: 157–166.

Le Treut, H., R. Somerville, U. Cubasch, Y. Ding, C. Mauritzen, A. Mokssit, T. Peterson and M. Prather, 2007. Historical overview of climate change. In: Climate change 2007: The physical science basis. Contribution of working group i to the fourth assessment report of the intergovernmental panel on climate change [Solomon, S., D. Qin, M. Manning, Z. Chen, M. Marquis, K.B. Averyt, M. Tignor and H.L. Miller (eds.)]. United Kingdom and New York, NY, USA.: Cambridge University Press, Cambridge.

Lee, J., B. Kim and S. Hong, 2014. Fouling distribution in forward osmosis membrane process. Journal of Environmental Science, 26: 1348–1354.

Lee, J., Y. Kim, S. Shim, B. Im and W. Kim, 2015. Numerical study of a hybrid multi-stage vacuum membrane distillation and pressure-retarded osmosis system. Desalination, 363: 82–91.

Lee, J.Y., Y. Wang, C.Y. Tang and F. Huo, 2015. Mesoporous Silica Gel-Based Mixed Matrix Membranes for Improving Mass Transfer in Forward Osmosis: Effect of Pore Size of Filler. Scientific Report, 5: 16808 -16817.

Lee, S., C. Boo, M. Elimelech and S. Hong, 2010. Comparison of fouling behavior in forward osmosis (FO) and reverse osmosis (RO). Journal of Membrane Science, 365: 34–39.

Lee, S., J. Cho and M. Elimelech, 2004. Influence of colloidal fouling and feed water recovery on salt rejection of RO and NF membranes. Desalination, 160: 1–12.

Li, X. and T. Chung, 2014. Thin-film composite P84 co-polyimide hollow fiber membranes for osmotic power generation. Applied Energy, 114: 600-610.

Ling, M.M. and T. Chung, 2011. Desalination process using super hydrophilic nanoparticles via forward osmosis integrated with ultrafiltration regeneration. Desalination 278: 194–202.

Liu, Y. and B. Mi, 2012. Combined fouling of forward osmosi smembranes: Synergistic foulant interaction and direct observation of fouling layer formation. Journal of Membrane Science, 407-408: 136–144

Liu, Y. and B. Mi, 2014. Effects of organic macromolecular conditioning on gypsum scaling of forward osmosis membranes. Journal of Membrane Science, 450: 153–161.

Londono, I.C., 2011. Assesment of causes of irreversible fouling in powdered activated carbon/ultrafiltration membrane (PAC/UF) systems. M.A.Sc. Thesis in Civil Engineering. The University of British Columbia: Vancouver.

Lonsdale, H.K. and H.E. Podall, 1972. Reverse osmosis membrane research. New York, United States of America: Plenum Press.

López , J.M., Á. Gómez, F. Aparicio and F.J. Sánchez, 2009. Comparison of ghg emissions from diesel, biodiesel and natural gas refuse trucks of the city of madrid. Applied Energy, 86: 610–615.

Ma, B., W. Yu, H. Liu and J. Qu, 2014. Comparison of iron (III) and alum salt on ultrafiltration membrane fouling by alginate. Desalination, 354: 153–159.

Maisonneuve, J., 2015. Osmotic power for remote communities in Quebec. PhD Thesis. Concordia University, Montreal, Quebec, Canada.

Malaviya, P. and A. Singh, 2011. Physicochemical technologies for remediation of chromium-containing waters and wastewaters. Environmental Science and Technology, 41: 1111-1172.

Manzini, F., J. Islas and M. Martinez, 2001. Reduction of greenhouse gases using renewable energies in Mexico 2025. International Journal of Hydrogen Energy, 26: 145-149.

Mattaraj, S., C. Jarusutthirak, C. Charoensuk and R. Jiraratananon, 2011. A combined pore blockage, osmotic pressure, and cake filtration model for crossflow nanofiltration of natural organic matter and inorganic salts. Desalination, 274: 182–191.

Mi, B. and M. Elimelech, 2010. Organic fouling of forward osmosis membranes: Fouling reversibility and cleaning without chemical reagents. Journal of Membrane Science, 348: 337–345.

Mi, B. and M. Elimelech, 2013. Silica scaling and scaling reversibility in forward osmosis. Desalination, 312: 75–81.

Millero, F.J. and H.L. Wing, 1976. The thermodynamics of seawater at one atmosphere. American Journal of Science, 276: 1035-1077.

Mosqueda-Jimenez, D.B. and P.M. Huck, 2006. Characterization of membrane foulants in drinking water treatment. Desalination, 198: 173-182.

Mulder, M., 1991. Basic principales of membrane technology. Dordrecht, The Netherlands: Kluwer Academic Publishers.

MWH, 2005. Water treatment principles and design. Hoboken, New Jersey: John Wiley & Sons, Inc.

Nazarenko, O. and R. Zarubina, 2013. Application of sakhaptinsk zeolite for improving the quality of ground water. Energy and Environmental Engineering Journal, 1(2): 68-73.

Nghiem, L.D. and S. Hawkes, 2007. Effects of membrane fouling on the nanofiltration of pharmaceutically active compounds (PhACs): Mechanisms and role of membrane pore size. Separation and Purification Technology, 57: 176–184.

Nishihara, H., H. Itoi, T. Kogure, P.-X. Hou, H. Touhara, F. Okino and T. Kyotani, 2009. Investigation of the ion storage/transfer behavior in an electrical double-layer capacitor by using ordered microporous carbons as model materials. Chemistry a European Journal, 15: 5355 – 5363.

O'Toole, G., L. Jones, C. Coutinho, C. Hayes, M. Napoles and A. Achilli, 2016. River-to-sea pressure retarded osmosis: Resource utilization in a full-scale facility. Desalination: 13 pages.

Olsson, M., G.L. Wick and J.D. Isaacs, 1979. Salinity gradient power: utilizing vapour pressure differences. Science, 206: 452-454.

Park, M., J. Lee, C. Boo, S. Hong, S.A. Snyder and J.H. Kim, 2013. Modeling of colloidal fouling in forward osmosis membrane: Effects of reverse draw solution permeation. Desalination, 314: 115–123.

Patel, S., 2010. Norway inaugurates osmotic power plant. Power: 1.

Peiris, R.H., H. Budman, C. Moresoli and R.L. Legge, 2010. Understanding fouling behaviour of ultrafiltration membrane processes and natural water using principal component analysis of fluorescence excitation-emission matrices. Journal of Membrane Science, 357: 62-72.

Phillip, W.A., J.S. Yong and M. Elimelech, 2010. Reverse draw solute permeation in forward osmosis: modeling and experiments. Environmental Science and Technology, 44: 5170–5176.

Porifera Inc., 2014. High rejection, high flux forward osmosis membranes. FOMEM-0513 FAQ. 1-2.

Porifera Inc., 2014. Specification Sheet: FOMEM-0513 July. 1.

Post, J.W., J. Veerman, H.V.M. Hamelers, G.J.W. Euverink, S.J. Metz, K. Nymeijer and C.J.N. Buisman, 2007. Salinity-gradient power: Evaluation of pressure-retarded osmosis and reverse electrodialysis. Journal of Membrane Science 288: 218–230.

Professional Water Technologies Inc, 2011. Lavasol 7 liquid membrane cleaner. 1-2.

Quebec Government, 2012. Quebec and Climate change: A Greener Environment. Quebec.

Ramon, G.Z., B.J. Feinberg and E.M.V. Hoek, 2011. Membrane-based production of salinity-gradient power. Energy and Environmental Science, 4: 4423–4434.

Reis, R.V. and A. Zydney, 2007. Bioprocess membrane technology. Journal of Membrane Science, 297 (1-2): 16-50.

Rezaei, H., F. Zokaee Ashtiani and A. Fouladitajar, 2011. Effects of operating parameters on fouling mechanism and membrane flux in cross-flow microfiltration of whey. Desalination, 274: 262–271.

Saito, K., M. Irie, S. Zaitsu, H. Sakai, H. Hayashi and A. Tanioka, 2012. Power generation with salinity gradient by pressure retarded osmosis using concentrated brine from SWRO system and treated sewage as pure water. Desalination and Water Treatment, 41: 114–121.

Sarp, S., Z. Li and J. Saththasivam, 2016. Pressure retarded osmosis (PRO): Past experiences, current developments, and future prospects. Desalination, 389: 2–14.

Schafer, A.I., 2001. Natural organics removal using membranes: Principles, performance and cost. Technomic Publishing Company, Inc.

Schock, G. and A. Miquel, 1987. Mass transfer and pressure loss in spiral wound modules. Desalination, 64: 339-352.

Seidel, A. and M. Elimelech, 2002. Coupling between chemical and physical interactions in natural organic matter (NOM) fouling of nanofiltration membranes: Implications for fouling control. Journal of Membrane Science, 203: 245–255.

She, Q., D. Hou, J. Liu, K.H. Tan and C.Y. Tang, 2013. Effect of feed spacer induced membrane deformation on the performance of pressure retarded osmosis (PRO): Implications for PRO process operation. Journal of Membrane Science, 445: 170–182.

She, Q., X. Jin, Q. Li and C.Y. Tang, 2012. Relating reverse and forward solute diffusion to membrane fouling in osmotically driven membrane processes. Water Research, 46: 2478-2486.

She, Q., X. Jin and C.Y. Tang, 2012. Osmotic power production from salinity gradient resource by pressure retarded osmosis: Effects of operating conditions and reverse solute diffusion. Journal of Membrane Science, 401-402: 262–273.

She, Q., R. Wang, A.G. Fane and C.Y. Tang, 2016. Membrane fouling in osmotically driven membrane processes: A review. Journal of Membrane Science, 499: 201-233.

She, Q., J. Wei, N. Ma, V. Sim, A.G. Fane, R. Wang and C.Y. Tang, 2016. Fabrication and characterization of fabric-reinforced pressure retarded osmosis membranes for osmotic power harvesting. Journal of Membrane Science, 504: 75–88.

She, Q., W.W. YewKong, Z. Shuaifei and Y.T. Chuyang, 2013. Organic fouling in pressure retarded osmosis: Experiments, mechanisms and implications. Journal of Membrane Science, 428: 181-189.

Shi, W., 2010. Renewable energy: finding solutions for a greener tomorrow. Environmental Science and Bio/Technology, 9: 35-37.

Shi, X., G. Tal, N.P. Hankins and V. Gitis, 2014. Fouling and cleaning of ultrafiltration membranes: A review. Journal of Water Process Engineering, 1: 121–138.

Sivertsen, E., T. Holt, W. Thelin and G. Brekke, 2013. Pressure retarded osmosis efficiency for different hollow fibre membrane module flow configurations. Desalination, 312: 107–123.

Song, L., 1998. Flux decline in crossflow microfiltration and ultrafiltration: mechanisms and modeling of membrane fouling. Journal of Membrane Science, 139: 183-200.

Statkraft, 2011. Salinity Gradients: Stable Energy from The Ocean: Osmotic power harnesses the potential of the world`s great rivers to deliver stable and emissions-free energy. Norway, Access Year: 2014, Access Date: August 28th, URL: http://statkraft.com/Statkraft/Documents/en/2011_10_12%20Position%20Paper%20-%20Osmotic%20Power%20-%20final_tcm9-19270.pdf.

Tanaka, S., H. Nakao, T. Mukai, Y. Katayama and Y. Miyake, 2012. An Experimental Investigation of the Ion Storage/Transfer Behavior in an Electrical Double-Layer Capacitor by Using Monodisperse Carbon Spheres with Microporous Structure. The Journal of Physical Chemistry, 116: 26791−26799.

Tang, C.Y., Q. She, W.C.L. Lay, R. Wang and A.G. Fane, 2010. Coupled effects of internal concentration polarization and fouling on flux behavior of forward osmosis membranes during humic acid filtration. Journal of Membrane Science, 354: 123–133.

Tanioka, A., K. Saito, M. Irie, S. Zaitsu, H. Sakai, H. Hayashi, A. Kumano, Tokyo Institute of Technology - Japan, L.-J. Kyowakiden Industry Co., Nagasaki University - Japan and L.-J. Toyobo Co., 2012. Power generation by pressure retarded osmosis using concentrated brine from sea water desalination. Desalination and Water Treatment, 41(1-3): 114-121.

Thelin, W.R., E. Sivertsen, T. Holt and G. Brekke, 2013. Natural organic matter fouling in pressure retarded osmosis. Journal of Membrane Science, 438: 46–56.

Touati, K., F. Tadeo, C. Ha¨nel and T. Schiestel, 2016. Effect of the operating temperature on hydrodynamics and membrane parameters in pressure retarded osmosis. Desalination and Water Treatment, 57: 10477–10489.

Valladares Linares, R., Z. Li, M. Abu-Ghdaib, C.H. Wei, G. Amy and J.S. Vrouwenvelder, 2013. Water harvesting from municipal waste water via osmotic gradient: an evaluation of process performance. Journal of Membrane Science, 447: 50–56.

Valladares Linares, R., Z. Li, V. Yangali-Quintanilla, Q. Li and G. Amy, 2013. Cleaning protocol for a FO membrane fouled in waste water reuse. Desalination and Water Treatment, 51: 4821–4824.

Veerman, J., J.W. Post, M. Saakes, S.J. Metz and G.J. Harmsen, 2008. Reducing power losses caused by ionic shortcut currents in reverse electrodialysis stacks by a validated model. Journal of Membrane Science 310: 418–430.

Wan, C.F. and T. Chung, 2015. Osmotic power generation by pressure retarded osmosis using seawater brine as the draw solution and wastewater retentate as the feed. Journal of Membrane Science 479: 148–158.

Wan, C.F. and T. Chung, 2016. Energy recovery by pressure retarded osmosis (PRO) in SWRO–PRO integrated processes. Applied Energy, 162: 687–698.

Wei, C., S. Laborie, R.B. Aim and G. Amy, 2012. Full utilization of silt density index (SDI) measurement for seawater pretreatment. The Journal of Membrane Science, 405-406: 212-218.

Wei, X., Z. Wang, F. Fan, J. Wang and S. Wang, 2010. Advanced treatment of a complex pharmaceutical wastewater by nanofiltration: Membrane foulant identification and cleaning. Desalination, 251: 167–175.

Wijmans, J.G., S. Nakao, J.W.A. Van den berg, F.R. Troelstra and C.A. Smolders, 1985. Hydrodynamic resistance of concentration polarization boundary layers in ultrafiltration. Journal of Membrane Science, 22: 117-135.

Xin, Y., M.W. Bligh, A.S. Kinsela and T.D. Waite, 2016. Effect of iron on membrane fouling by alginate in the absence and presence of calcium. Journal of Membrane Science, 497: 289–299.

Xiong, J.Y., Z.L. Cheng, C.F. Wan, S.C. Chen and T. Chung, 2016. Analysis of flux reduction behaviors of PRO hollow fiber membranes: Experiments, mechanisms, and implications. Journal of Membrane Science, 505: 1-14.

Xu, Y., X. Peng, C.Y. Tang, Q.S. Fu and S. Nie, 2010. Effect of draw solution concentration and operating conditions on forward osmosis and pressure retarded osmosis performance in a spiral wound module. Journal of Membrane Science, 348: 298–309.

Yiantsios, S.G. and A.J. Karabelas, 2002. An assessment of the Silt Density Index based on RO membrane colloidal fouling experiments with iron oxide particles. Desalination, 151: 229-238.

Yip, N.Y. and M. Elimelech, 2013. Influence of natural organic matter fouling and osmotic backwash on pressure retarded osmosis energy production from natural salinity gradients. Environmental Science and Technology, 47: 12607–12616.

Zhan, H., J. Zhang, D. Luo and X. Li, 2004. Reducing concentration polarization in hollowfibre hollowfibre. Membrane Technology: 5-9.

Zhang, S., K.Y. Wang, T. Chung, H. Chen, Y.C. Jean and G. Amy, 2010. Well-constructed cellulose acetate membranes for forward osmosis: Minimized internal concentration polarization with an ultra-thin selective layer. Journal of Membrane Science, 360: 522–535.

Zhang, Z., V.M. Bright and A.R. Greenberg, 2006. Use of capacitive microsensors and ultrasonic time-domain reflectometry for in-situ quantification of concentration polarization and membrane fouling in pressure-driven membrane filtration. Sensors and Actuators, 117: 323–331.

Zhao, S., L. Zou, C.Y. Tang and D. Mulcahy, 2012. Recent developments in forward osmosis: Opportunities and challenges. Journal of Membrane Science, 396: 1– 21.

Zheng, X., M. Ernst and M. Jekel, 2009. Identification and quantification of major organic foulants in treated domestic wastewater affecting filterability in dead-end ultrafiltration. Water Research, 43: 238-244.

Zularisam, A.W., A.F. Ismail and R. Salim, 2006. Behaviours of natural organic matter in membrane filtration for surface water treatment — a review. Desalination, 194: 211–231.

# Appendix

Results for Water Quality:

- Color in River Water

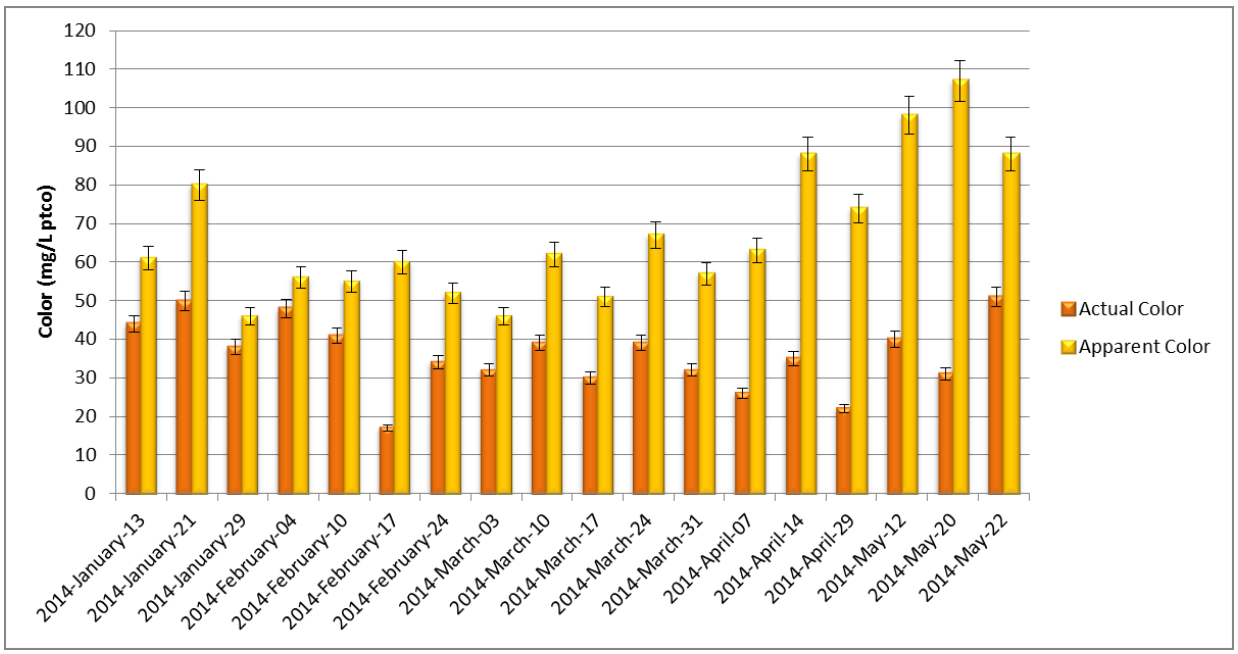


- Iron Concentration in River Water

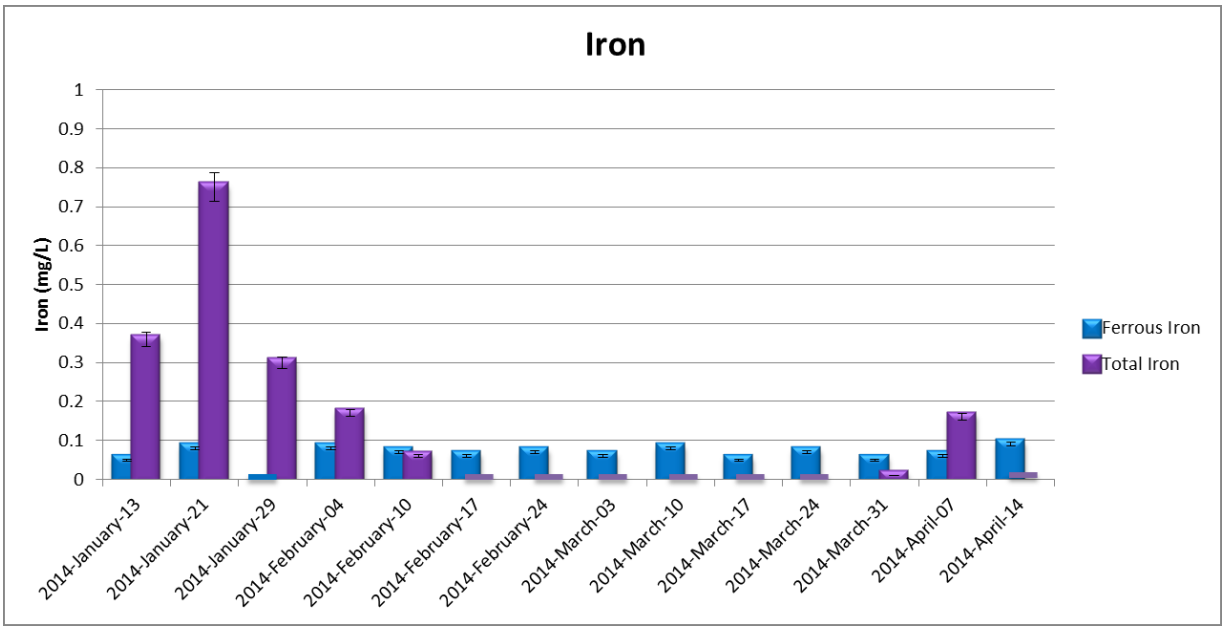

- Silica Concentration in River Water

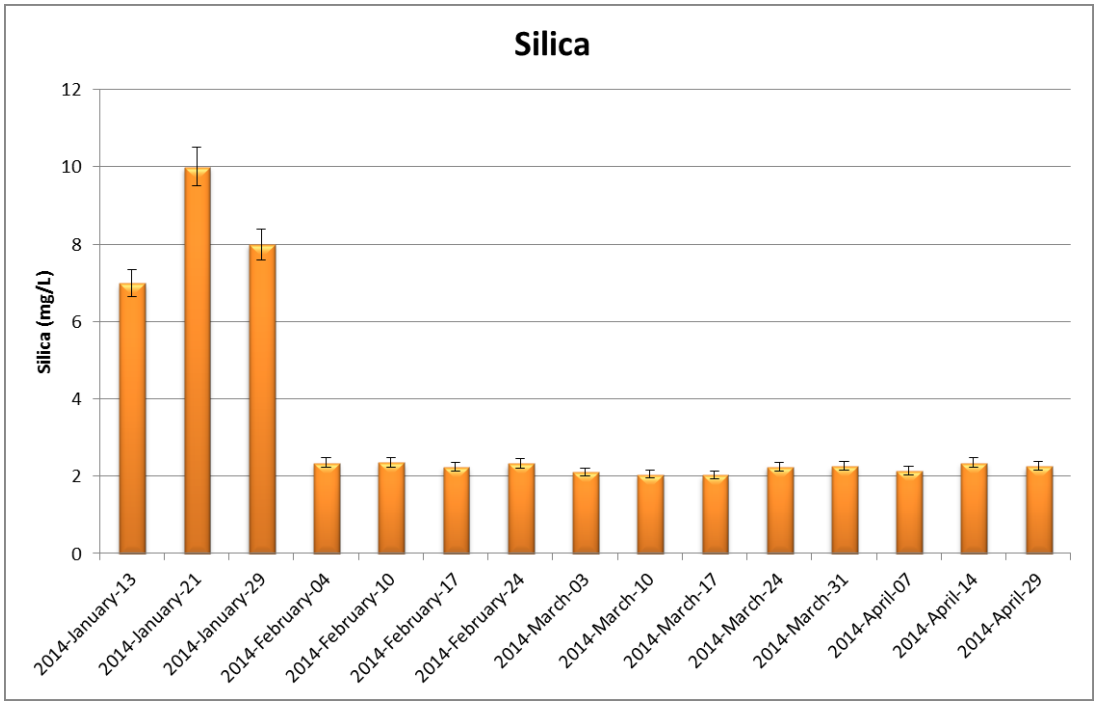


- Suspended Solids Concentration in River Water

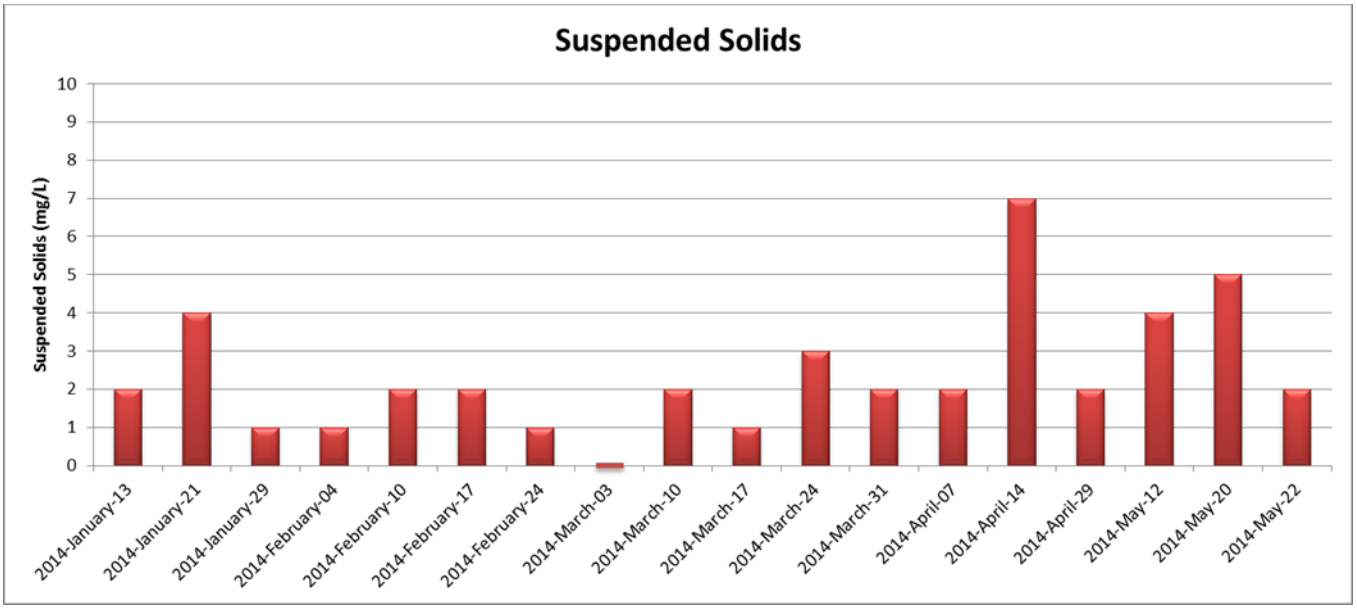

- Particle Size Distribution in River Water

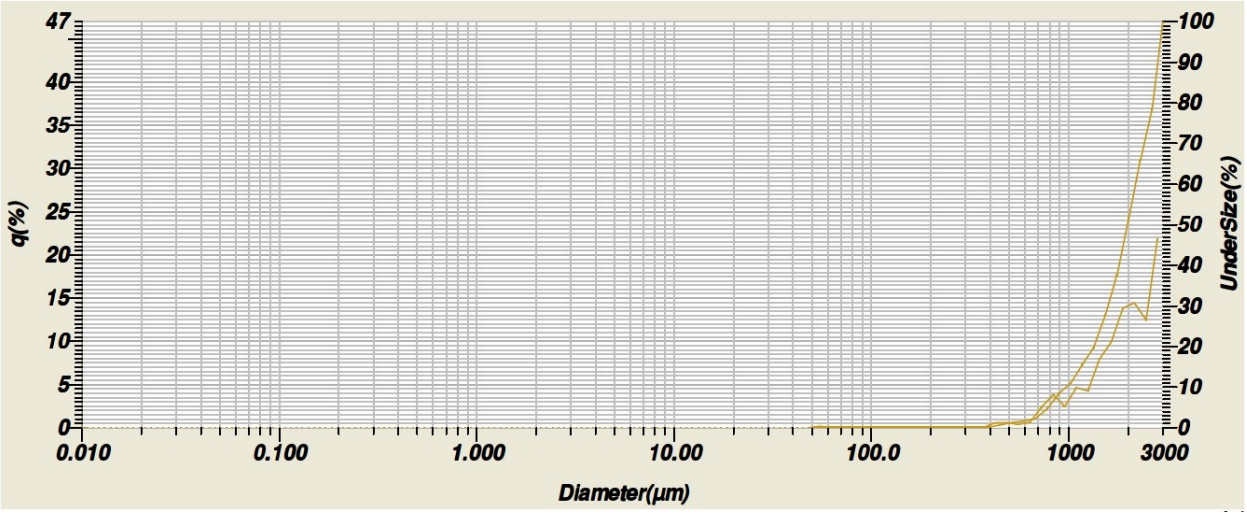


- Alkalinity in River Water

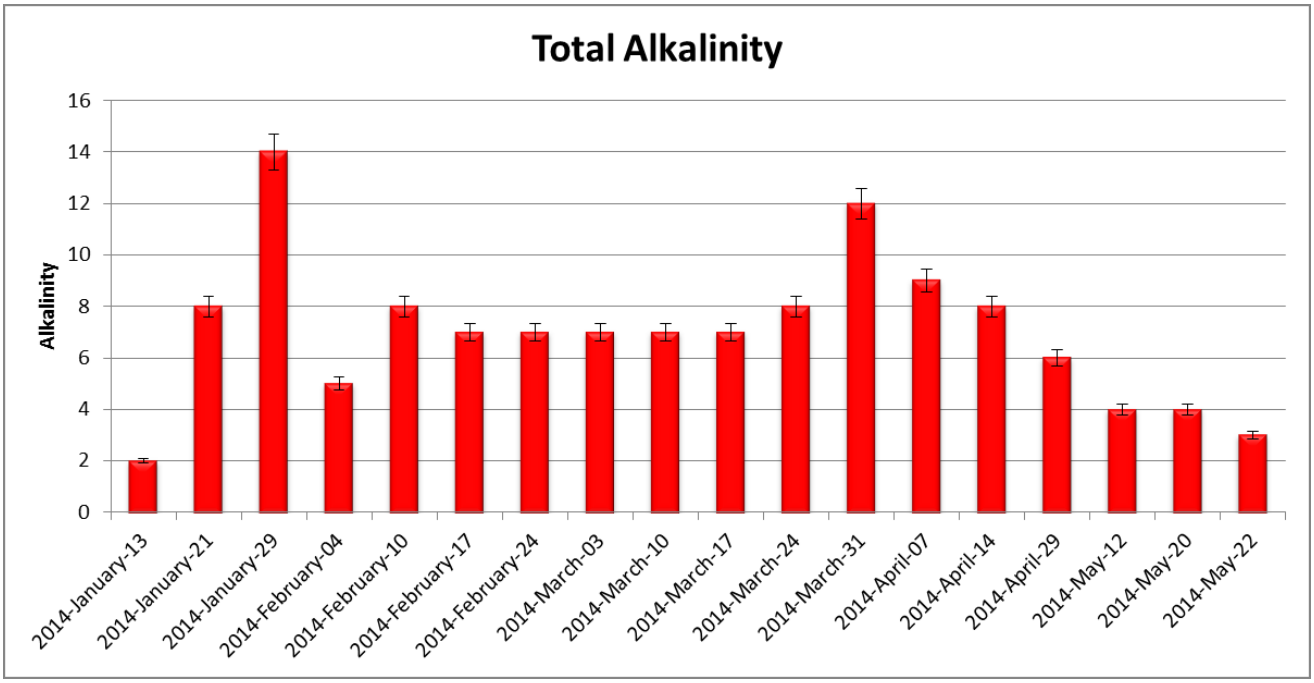

- pH in River Water

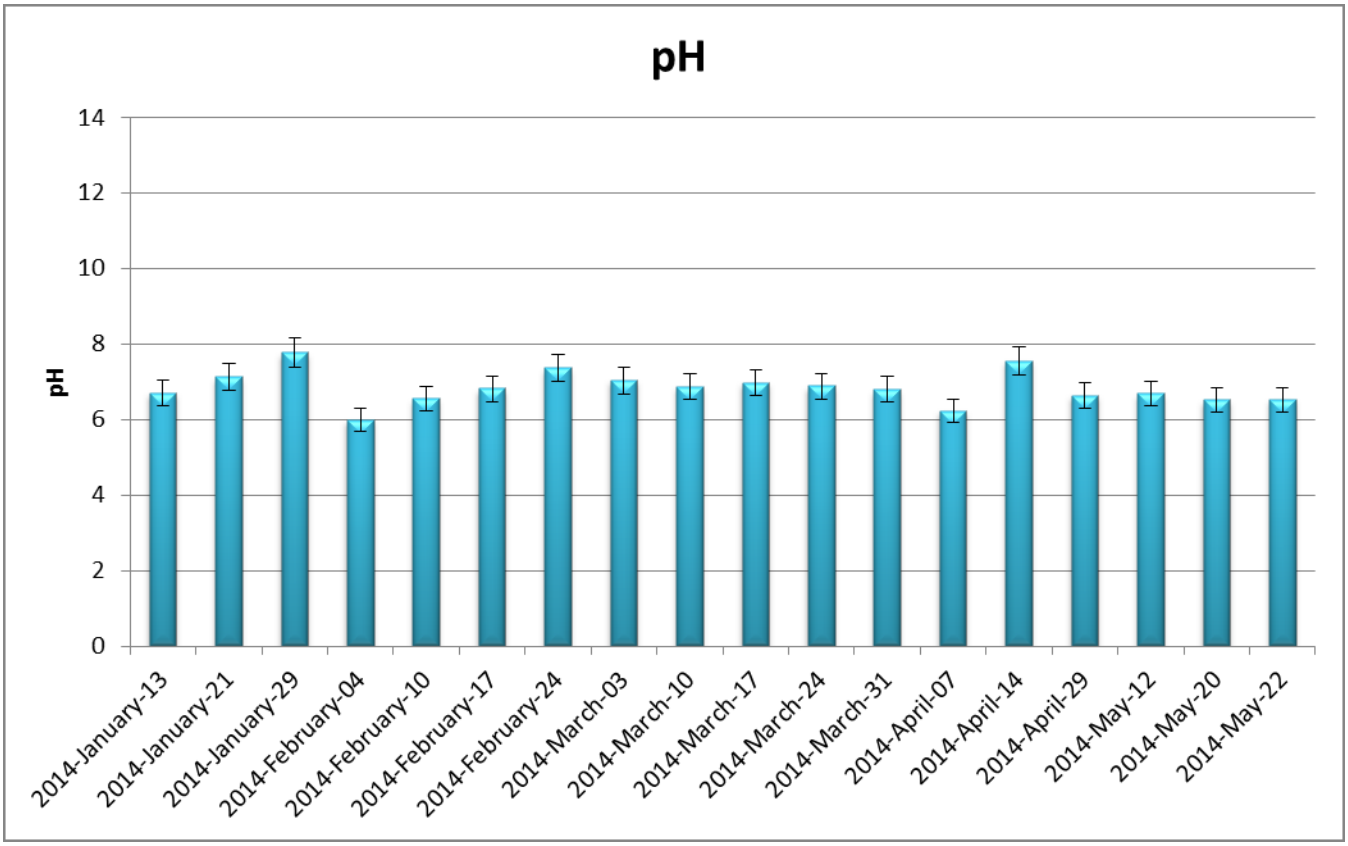


- Salinity in River Water

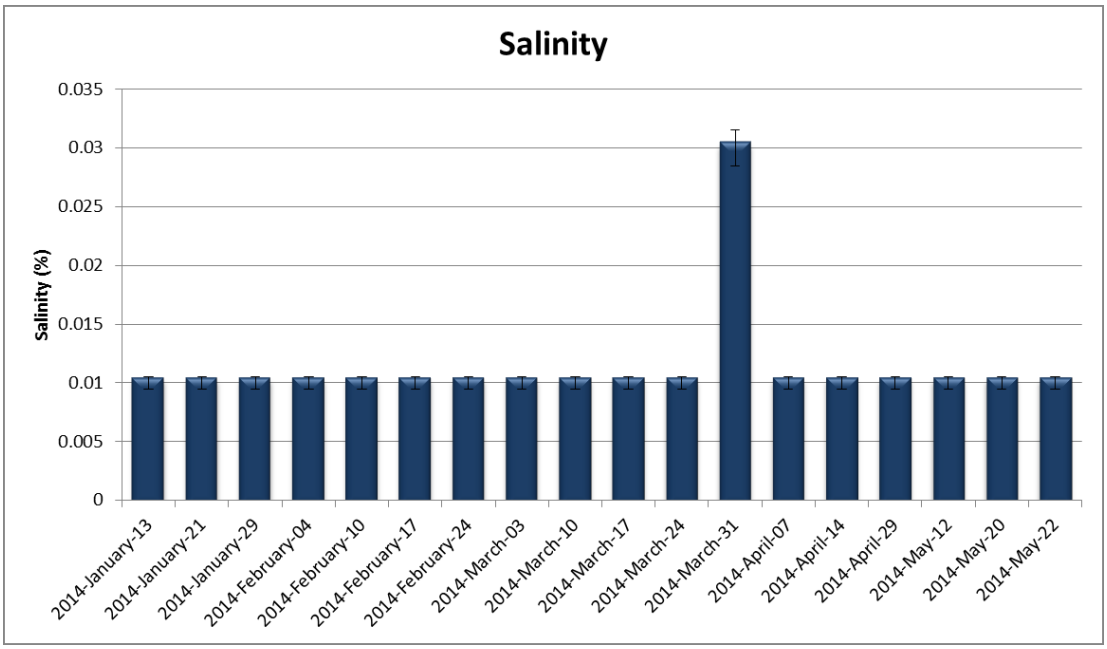

- Conductivity in River Water

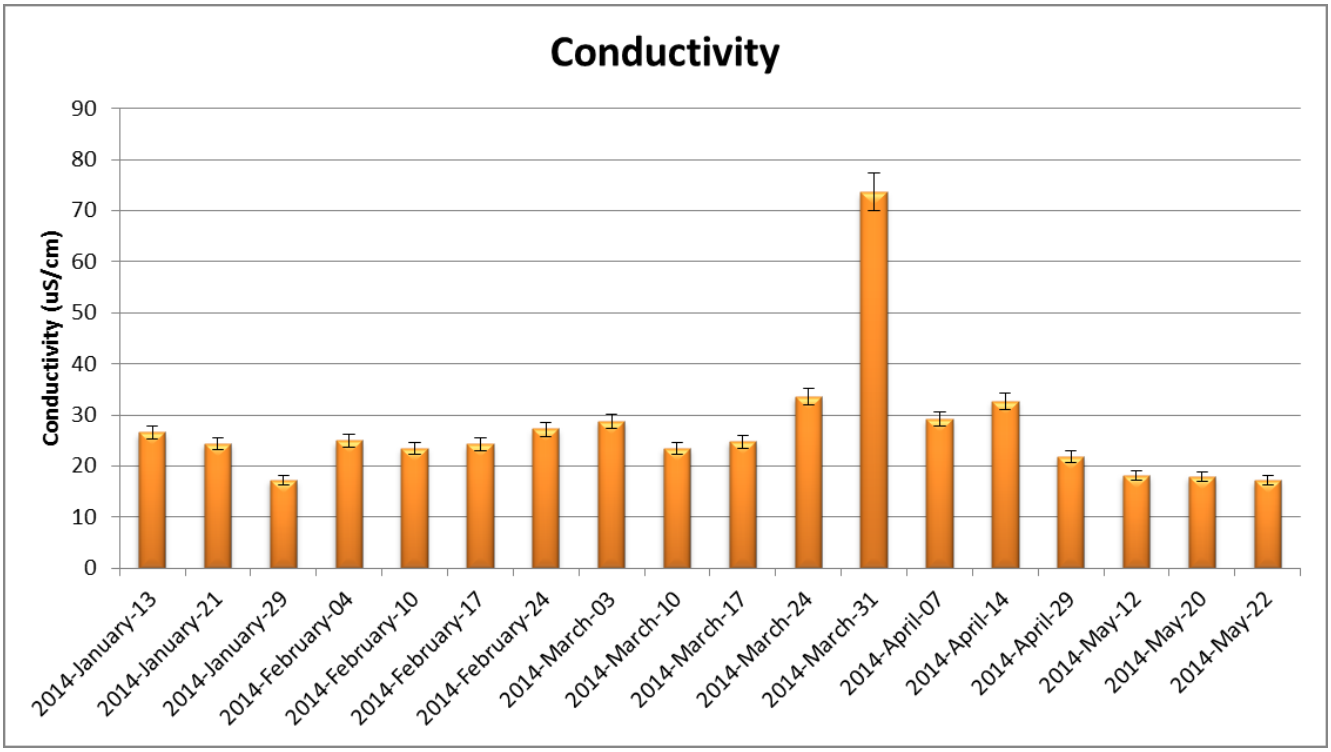


- Dissolved Solids Concentration in River Water

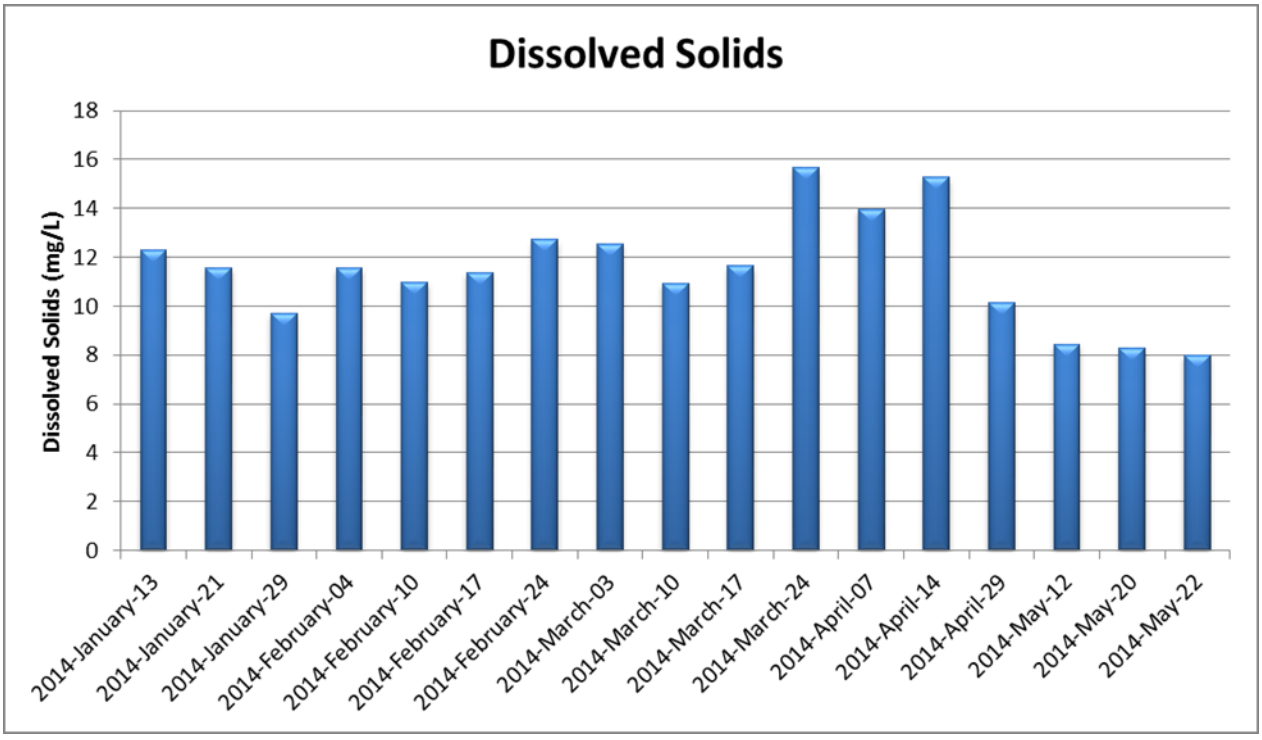

- Sodium Concentration in River Water

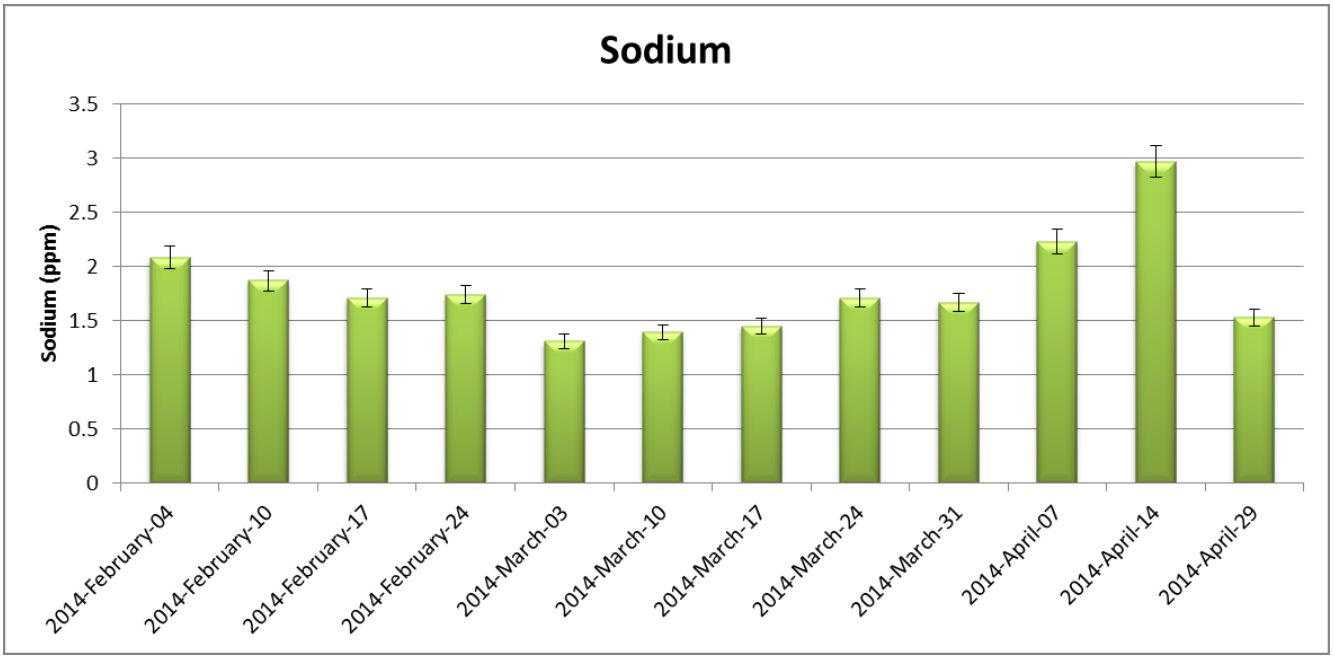


- Calcium Concentration in River Water

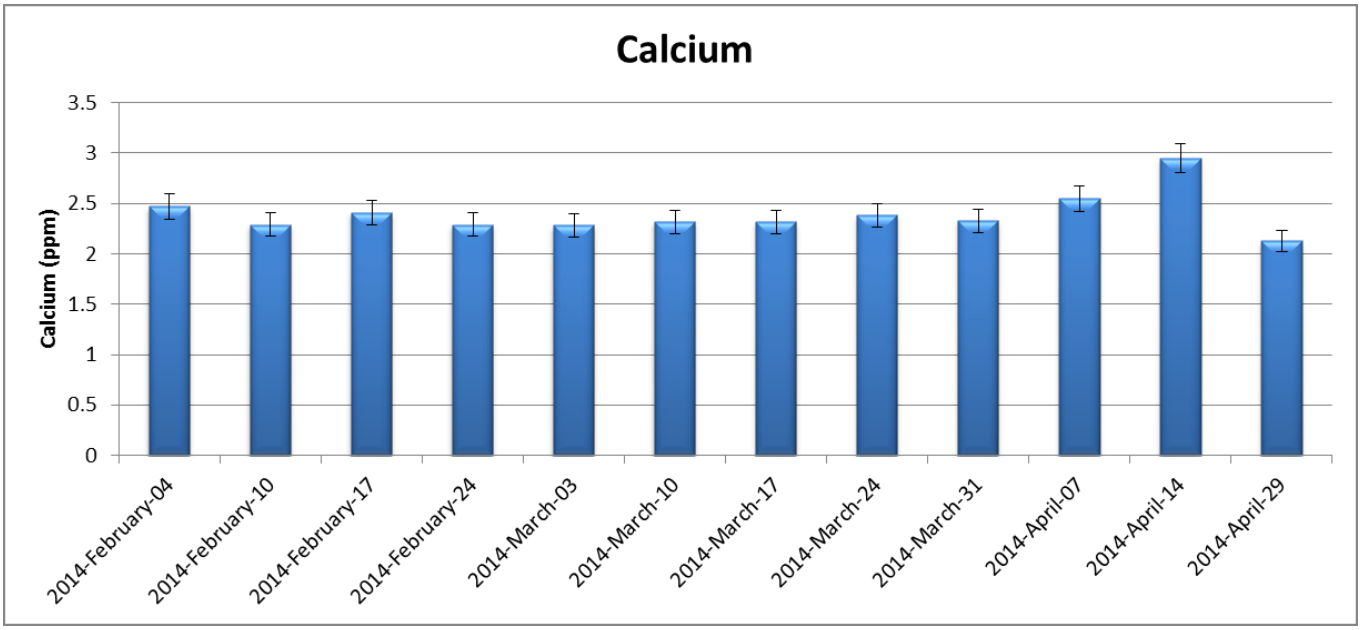

- Magnesium Concentration in River Water

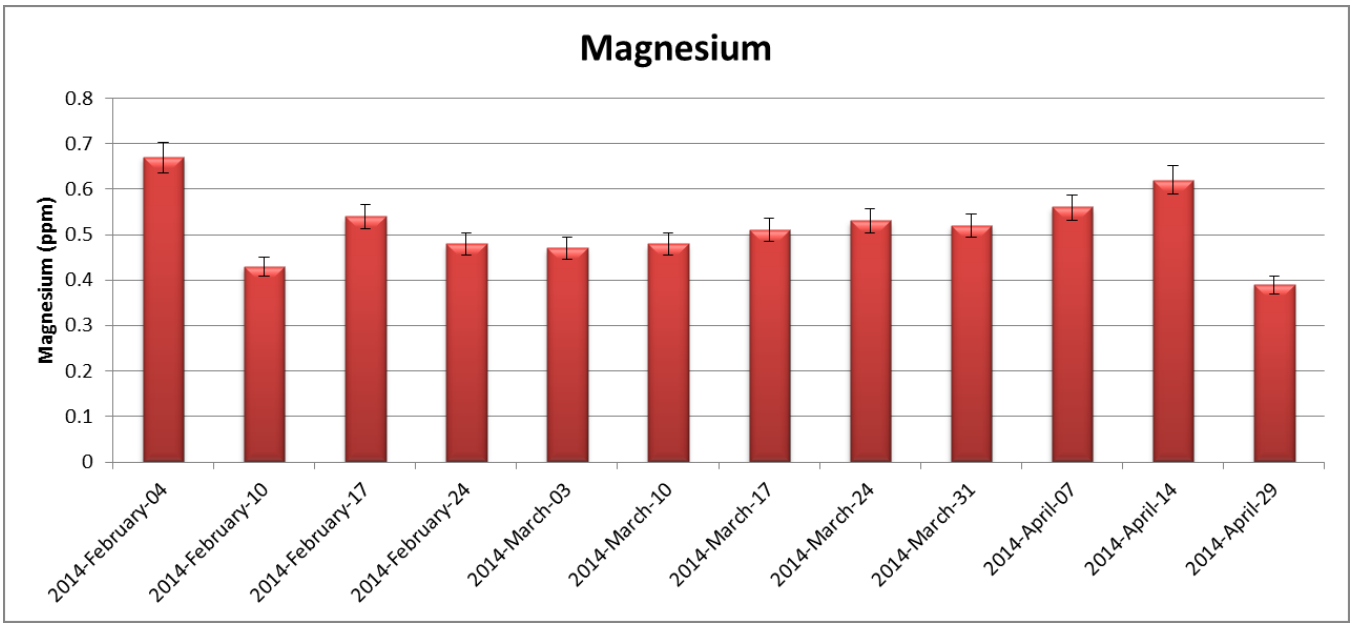


- Potassium Concentration in River Water

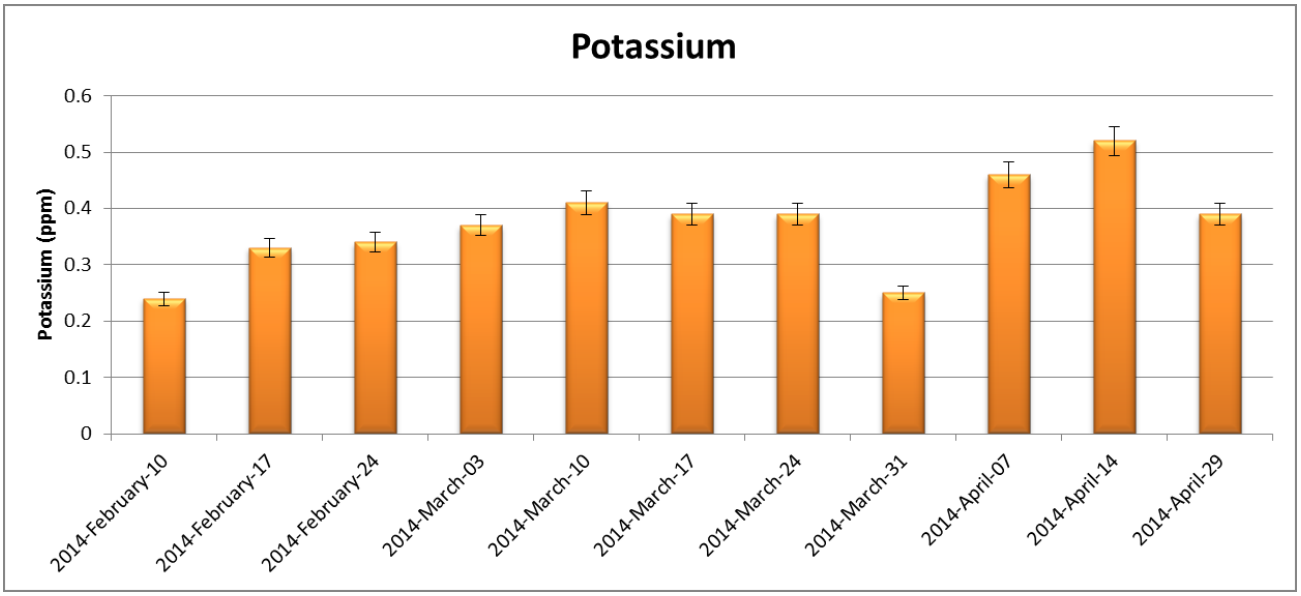

- Silt Density Index (SDI) in River Water

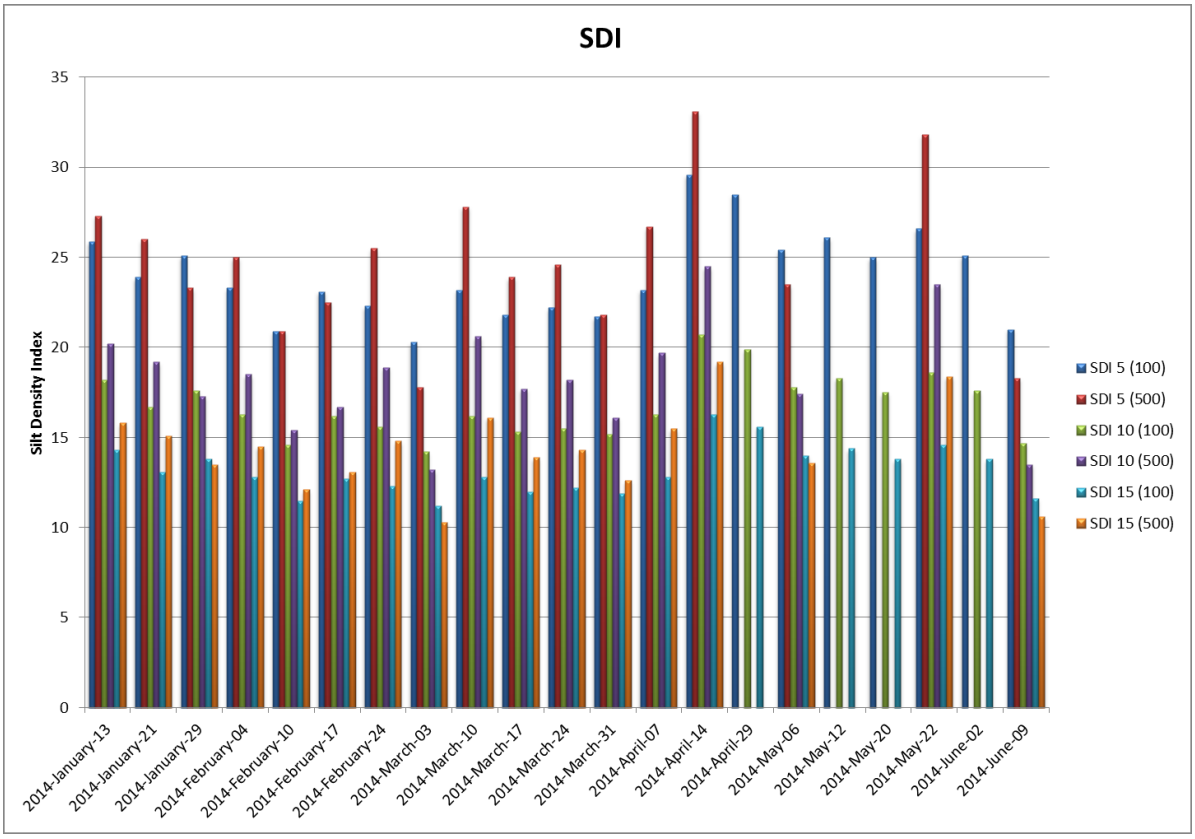


- Temperature in Saint-Maurice River: